INVESTIGATIONS ON THE PREPARATION AND PROPERTIES OF REACTIVELY EVAPORATED LEAD SULPHIDE AND TIN TELLURIDE THIN FILMS

Thesis submitted by
PALSON T. I.

In partial fulfilment of the
requirements for the Degree of
Doctor of Philosophy

SOLID STATE PHYSICS LABORATORY
DEPARTMENT OF PHYSICS
Cochin University of Science and Technology

1987

To my parents

CERTIFICATE

Certified that this thesis is based on the work done by Mr. PALSON, T.I. under my guidance in the Department of Physics, Cochin University of Science and Technology and no part of this has been presented by him for any other degree.

Cochin-22,
February 16, 1987.
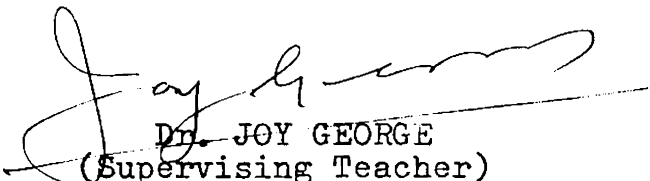
Dr. JOY GEORGE
(Supervising Teacher)
PROFESSOR IN INDUSTRIAL PHYSICS
DEPARTMENT OF PHYSICS
COCHIN UNIVERSITY OF SCIENCE AND
TECHNOLOGY.

DECLARATION

Certified that the work presented in this thesis is based on the original work done by me under the guidance of Prof. JOY GEORGE in the Department of Physics, Cochin University of Science and Technology and has not been included in any other thesis submitted previously for the award of any degree.

Cochin-22,
February 16, 1987.

PALSON, T.I.

SYNOPSIS

INVESTIGATIONS ON THE PREPARATION AND PROPERTIES
OF REACTIVELY EVAPORATED LEAD SULPHIDE AND TIN
TELLURIDE THIN FILMS

IV-VI compounds such as sulphides, selenides
and tellurides of lead and tin and their alloys have
attracted much attention for a long time. Suitably
prepared polycrystalline films of lead salts have been
used as photoconductive detectors in the near infrared.
More recently solid solutions of SnTe in PbTe, and SnSe
in PbSe have been used to construct photoconductive and
photovoltaic detectors for longer wavelengths. The con-
struction of p-n junction injection lasers of lead salts,
and of solid solutions with their tin analogs has been
an important technological development.

The work reported in this thesis is the preparat-
ion, and the structural, electrical and optical properties
of reactively evaporated lead sulphide and tin telluride
thin films. The three temperature method had been used
for the preparation of these semiconductor thin films.
In this preparation technique constituent elements are
evaporated from separate sources with the substrate kept
at a particular temperature. When one of the constituent

element is a gas near room temperature, the method is often called reactive evaporation. It has been found for many materials that a stoichiometric interval exists with a limited range of flux and substrate temperature. Usually this technique is used for the preparation of thin films of high melting point compounds or of materials which decompose during evaporation. Tin telluride and lead sulphide are neither high melting point materials nor do they decompose on melting. But even then reactive evaporation offers the possibility of changing the ratios of the flux of the constituent elements within a wide range and studying its effect on the properties of the films.

A variety of physical and chemical deposition techniques have been developed for the deposition of thin films of lead sulphide. Nobody has yet reported the preparation of PbS thin films by the reactive evaporation technique. Stoichiometric as well as sulphur rich films can be prepared by this technique. To get stoichiometric films the sulphur source was baffled, so that the sulphur vapour beam did not strike the substrate as such. The number of sulphur molecules striking the substrate surface per unit area in unit time in this case will be that due to the partial pressure of the sulphur vapour in the chamber. In the case of sulphur rich films, the sulphur source was not baffled and more sulphur molecules will strike the substrate surface.

It has been found that the following parameters give good stoichiometric films of PbS:

Pb atom flux : 1.3×10^{15} to 2.6×10^{15} atoms $cm^{-2}s^{-1}$

S_2 molecule flux : 2.2×10^{16} to 1.1×10^{17} molecules $cm^{-2}s^{-1}$

Substrate temperature : 300 - 650K.

Unless otherwise stated lead sulphide films refer hereafter to stoichiometric lead sulphide films. X-ray diffraction studies of the PbS films indicated that films prepared below the substrate temperature of 325K were amorphous in nature. As the substrate temperature was increased polycrystalline PbS films were obtained. Further increase in the substrate temperature gave a preferred orientation to the grains with (100) planes parallel to the substrate surface.

Electrical measurements were made and d.c. conductivity, Hall mobility, carrier concentration and thermoelectric power were studied in the temperature range 100 - 400K on polycrystalline films prepared at different substrate temperatures. Hall effect measurements showed that the films obtained were p-type. A typical PbS film prepared at 400K had a carrier concentration of $\simeq 6 \times 10^{17}$ cm^{-3} and Hall mobility of $\simeq 30$ cm^2 $V^{-1}s^{-1}$ at 300K. Thermoelectric power was as high as 500 $\mu V/K$ at 300K. This is around 1.7 times the single crystal value. Films prepared at substrate

temperature $\sim$ 600K gave a maximum mobility of $\simeq$ 125 cm^{2}V^{-1}s^{-1} at 300K.

Amorphous films of PbS had been characterised optically and electrically. Optical characterisation showed that amorphous PbS films had an optical band gap of 1.6 eV and a refractive index of 2.5. Crystalline PbS is having a band gap of 0.39 eV and refractive index of 4.5. This large deviation was explained in terms of the difference in coordination of the amorphous and crystalline environments. Sulphur rich amorphous PbS films had a still higher optical band gap of 1.8 eV and show no optical absorption before the onset of band to band transitions, whereas stoichiometric amorphous PbS films showed an absorption which was decreasing with the photon energy before the onset of band to band transition.

Electrical measurements of amorphous PbS films showed a room temperature resistivity of 1.7 x 10^4 ohm cm. The films crystallised when heated beyond 330K and the resistivity of the films decreased by three orders of magnitude. Sulphur rich amorphous films were more resistive ($\sim$ 4 x 10^6 ohm cm) and these films crystallised at around 330K and resistivity decreased by five orders of magnitude.

SnTe films were usually prepared from p-type SnTe ingots prepared by fusing stoichiometric proportions

of Sn and Te. In the work reported here, SnTe thin films were prepared for the first time by the three temperature method to avoid incongruent evaporation from a single source and the consequent lack of stoichiometry.

It had been found that good stoichiometric films of SnTe were obtained with the following parameters:

tin flux $= 4.1 \times 10^{14}$ to 2.4×10^{15} atoms $cm^{-2} s^{-1}$

tellurium flux $= 7.4 \times 10^{15}$ to 2.2×10^{16} atoms $cm^{-2} s^{-1}$

substrate temperature $= 568 - 598K$.

The structural characterisation of these films were done by x-ray diffraction technique. These films had grains oriented such that (111) planes were parallel to the substrate surface. Optical micrographs of the films before and after annealing showed that annealing at the preparation temperature had no effect on the grain size. The temperature dependences of the electrical conductivity, the Hall coefficient and Hall mobility of these films were studied in the temperature range 100-450K. As prepared thin films of SnTe, had got the following electrical characteristics at room temperature:

Conductivity $\simeq 6.5 \times 10^{3}$ (ohm cm)$^{-1}$

Hall coefficient $\simeq 1.55 \times 10^{-2}$ cm^{3} coulomb^{-1}

Hall mobility $\simeq 100$ $cm^{2} v^{-1} s^{-1}$

The effect of annealing on the electrical propert-
ies had also been investigated. The carrier concentration
and conductivity decreased after annealing whereas the
Hall mobility increased.

Due to the low chemical diffusion constant of tin,
which results in the freezing of the equilibrium tin vacancy
concentration, SnTe is always a p-type extrinsic semicond-
uctor. Because of the heavy carrier concentration and the
consequent repulsion between the carriers, the mobility of
charge carriers in SnTe films are low. The mobility can be
increased by reducing the carrier concentration. This can
be achieved by filling the tin vacancies by an appropriate
cation which is having a high mobility in the SnTe matrix.
It has been possible to obtain mobilities better than
1000 $cm^2V^{-1}S^{-1}$ at room temperature by doping SnTe films
with germanium.

A setup for testing IR detectors had been fabri-
cated and is also reported in this thesis. A cell which
could be evacuated and cooled to LN_2 temperature with pro-
visions for detector mounting and illumination had been
fabricated as part of this setup. A light chopper also was
designed and fabricated in house, for this purpose. This
chopper can produce light pulses from 10 Hz to 2000 Hz
using two chopping blades and had an accuracy better than
0.1% and negligible temperature drift.

CONTENTS

INTRODUCTION

Two dimensional materials created by the process of condensation of atoms, molecules, or ions are called thin films. Thin films have got unique properties significantly different from the corresponding bulk materials, because of their small thicknesses, large surface-to-volume ratios, and unique physical structures which are direct consequences of the growth processes. The characteristic features of thin films can be drastically modified to obtain the desired and required physical characteristics. These features form the basis of development of a lot of thin film device applications in the last two decades.

The first evaporated metal film was prepared by Faraday in 1857 when he exploded metal wires in an inert atmosphere. Vacuum deposition of thin films was first carried out by Nahrwold in 1887. In the following decades evaporated thin films remained in the domain of academic interest until the development of vacuum equipment had progressed far enough to permit large scale applications and control of film properties. Evaporated thin films have found industrial usages for an increasing number of purposes. Examples are antireflection coating, front surface mirrors, interference filters, sun glasses, decorative coatings on plastics and textiles, in the

manufacture of cathode ray tube, in electronic circuits and most recently in solar cells for photovoltaic conversion and in semiconductor hetro-junction lasers. Almost all sophisticated modern optical and electronic devices contain thin film components.

In the earlier period semiconductor thin films were deposited in elemental form for applications in electronics. Germanium, silicon and selenium were the then known and most used elemental semiconductors. Interest in compound semiconductor thin films began with the realization of the fact that optimum material properties in device applications, which cannot be achieved in the case of a single element, can easily be achieved using a combination of two or more elements. Therefore germanium, silicon and selenium had to make way for the semiconducting II-VI, III-V, and IV-VI compounds.

Relatively few inorganic compounds, alloys, or mixtures evaporate congruently using single source evaporation technique because the constituents which are present in the solid or liquid state usually differ in their vapour pressures and often a large fraction of the compound dissociate when heated. When the compound dissociates in vacuum, the volatile component will be given off first.

Consequently, the composition of the vapour and hence
the condensate is not the same as that of the source
material. Deposition of the high melting point carbides
and nitrides is another area where single source evapor-
ation is not practicable because of the lack of suitable
support materials for evaporation which can withstand
the high temperatures needed for evaporation. Special
techniques such as 'three temperature method' and 'flash
evaporation' have been developed to overcome these diffi-
culties.

The preferential condensation of compounds from
binary vapours has been analysed by Gunther and developed
into an experimental technique known as the 'three tem-
perature method'. This method is based on the fact that
continuous condensation of a given vapour at a given de-
position rate is possible only if the substrate temperat-
ure drops below a critical value.

The work reported in this thesis is the preparat-
ion, and the structural, electrical and optical properties
of thin films of lead sulphide and tin telluride in which
the constituent elements have widely different vapour
pressures.

In the first chapter of this thesis, the relevant

semiconductor principles are described. Different
methods of thin film preparation, and reactive evaporat-
ion technique (a variant of 'three temperature method')
in particular, are described in chapter 2. Third chapter
contains the experimental techniques employed in the
present work. Chapters 4, 5 and 6 deal with the pre-
paration and characterisation of lead sulphide thin films.
Preparation and characterisation of tin telluride thin
films is given in chapter 7. In chapter 8 is reported
the preparation and characterisation of Ge doped tin
telluride (SnTe:Ge) thin films. In chapter 9 is described
the fabrication of a setup for the testing of IR detectors.

Part of the work reported in this thesis has been
published/communicated and is listed below:

1) Electrical measurements in co-evaporated SnTe
   thin films.
   Thin Solid Films, 127 (1985) 233.

2) Polycrystalline films of PbS prepared by reactive
   evaporation.
   Solid state commun. 58 (1986) 605.

3) A variable speed light chopper using a feedback
   controlled DC motor.
   Int. J. Electronics, 54 (1983) 361.

4) Amorphous films of PbS
   Phil. Mag. Letters, 55 (April 1987)

5) SnTe thin films prepared by three temperature method
   Proceedings of the "Solid State Physics Symposium",
   Vol.27C (1984) p.202.

6) Structural and electrical properties of reactively
   evaporated PbS films.
   Proceedings of the "Solid State Physics Symposium",
   Vol.28C (1985) p.336.

7) Lead sulphide (PbS) films prepared by co-evaporation.
   Proceedings of the XVIIth National seminar on
   crystallography, (1985) p.29.

8) High mobility polycrystalline SnTe:Ge films.
   (Communicated).

9) Electrical properties of co-evaporated PbS thin
   films.
   (Communicated).

CHAPTER I

SEMICONDUCTOR PRINCIPLES

1.1. BAND STRUCTURE

The motion of electrons in solids has been a
matter of discussion for a long time. The concept that
electronic properties may be described in terms of free
electrons was developed long before the invention of
wave mechanics. According to A. Sommerfeld's /1/ quantum
free electron theory, the valance electrons of tne con-
stituent atoms of the metals are free to move throughout
the entire volume of tne specimen (fig.1.1a). The poten-
tial energy exerted by all nuclei and all other electrons
were considered to be constant everywhere inside the metal
except at the boundary of the solid.

According to this free electron theory, tne
energy of the free electron as a function of wave vector
is given by

$$E = \frac{\hbar^2 k}{2m}$$ (1.1.1)

where wave vector $k = \frac{2\pi}{\lambda} = P/\hbar$. Here λ is the wave-
length associated with the electron and P is the momentum.

In this case there is no upper limit for the

(a)

Fig.1.1(a) : Sommerfeld model for potential energy V(x)
of electrons in a crystalline solid.
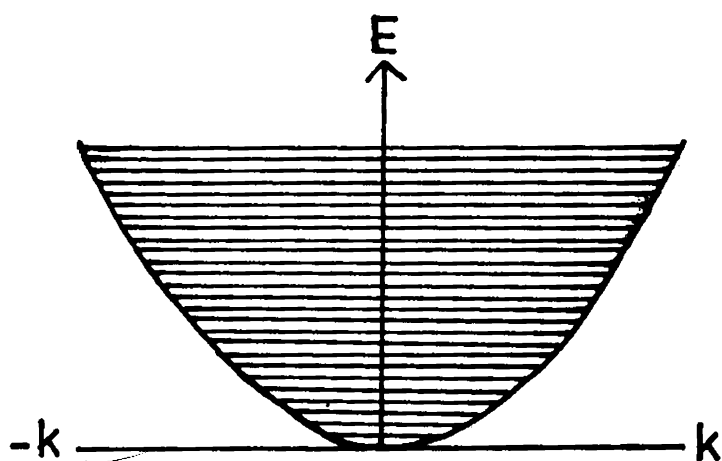
(b)

Fig.1.1(b) : Energy (E) versus wave vector (k) for a
free electron.

energy; ie. the energy spectrum is quasi continuous (fig.1.1b).

This theory enabled to explain the phenomena like heat capacity and magnetic susceptibility.

Most of the electronic properties were explained by the free electron theory. However the fact that some solids are conductors of electricity while others are not, cannot be explained on the basis of free electron theory. In order to explain this, the motion of electrons in a periodic potential produced by the periodic array of atoms was considered (fig.1.2). In this model tne electron-electron interaction was neglected. The motion of electrons in such a periodic potential was discussed by F. Block /2/. In this theory, it was assumed that the nuclei in the crystalline solids are at rest. The total wave function for tne system is given by the combination of wave functions, each of which involves the coordinate of only one electron. The field seen by a given electron is assumed to be that of the fixed nuclei plus some average field produced by the charge distribution of all other electrons.

By considering the motion of electrons in a periodic potential we reach at the following conclusions:

$V(x)$

Fig.1.2 : Periodic potential due to the atomic core in a
crystalline solid.

E

Forbidden
bands

Allowed
bands

$\frac{-2\pi}{a}$ $\frac{-\pi}{a}$ $\frac{\pi}{a}$ $\frac{2\pi}{a}$ k
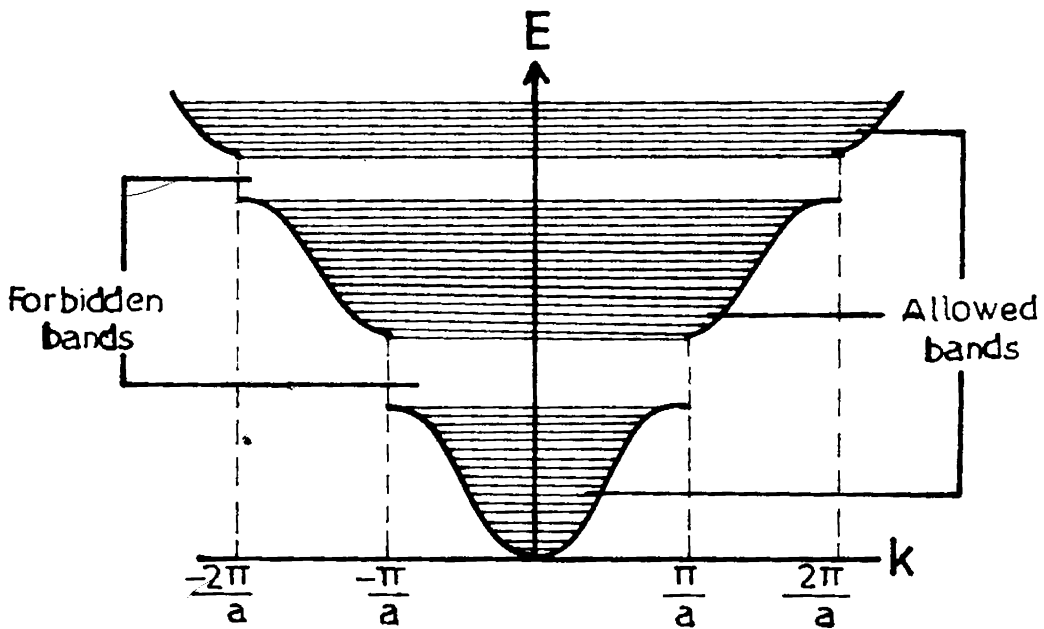
Fig.1.3 : Energy (E) versus wave vector (k) for a periodic
lattice of lattice constant, a.

1) The energy spectrum of an electron in a periodic
   potential consists of a number of allowed energy
   bands separated by forbidden bands (fig.1.3).

2) The energy, E is a period function in wave vector k
   (fig.1.3).

The discontinuities in the curve occur for
$k = \frac{n\pi}{a}$, where n = 1,2,3, ... and a is the lattice
constant. These k values define the boundaries of the
first, second etc. Brillouin Zones.

The concept of band theory put forward the idea
of effective electron mass. It was given by the ex-
pression,

$$m^* = \hbar^2 / \frac{d^2E}{dk^2} \qquad (1.1.2)$$

Using band theory the electrical conduction can
be explained as follows. A solid for which a certain
number of energy bands are completely filled, while the
others being completely empty is an insulator. On the
other hand, a solid containing an energy band which is
partly filled has metallic character. The ideal case
of an insulator occur only at absolute zero, where the
crystal is in its lowest energy state and the upper

filled band and lower empty band are separated by a
forbidden energy gap Eg. At temperatures different
from zero some electrons from the upper filled band
will be excited to the next empty band and conduction
becomes possible. For a small band gap, the number of
thermally excited electrons may become appreciable and
in this case one speaks of a semiconductor. The distin-
ction between semiconductors and insulators are only
quantitative; all semiconductors are insulators at
absolute zero, whereas all insulators may be considered
as semiconductors at temperatures above absolute zero.

1.2. INTRINSIC AND EXTRINSIC SEMICONDUCTORS

· Conductivity in semiconductors are usually
brought about by thermal excitation, impurities or
lattice defects.

There are generally two type of semiconductors,
intrinsic semiconductors and extrinsic semiconductors.

Intrinsic semiconductors: Semiconductors in which
conductivity is controlled by valence electrons are
known as intrinsic semiconductors. The intrinsic tem-
perature range is that in which the electrical properties
of a semiconductor are not essentially modified by impu-
rities in the crystal.

At absolute zero we postulate a vacant cond-
uction band, separated by an energy gap Eg from a filled
valence band. As the temperature is increased, electrons
are thermally excited from the valence band to the con-
duction band. In an intrinsic semiconductor at temperat-
ures above zero, a certain number of electrons may be
excited thermally from upper filled band into the conduct-
ion band. Thus some of the states in the normally filled
band are unoccupied. These unoccupied states lie near
the top of the filled band (valence band). These are
known as 'holes'. A 'hole' has got a positive charge
numerically equal to the electronic charge. Both the
electrons in the conduction band and the holes left behind
in the valence band will contribute to the electrical con-
ductivity.

According to the earlier definitions
conductivity is given by,

$$\sigma = |e| \; (n_e \mu_e + n_h \mu_h) \tag{1.2.1}$$

If we assume that the temperature dependence
of mobility of electrons and holes is less, the conduct-
ivity σ is of the form,

$$\sigma = \sigma_0 \; e^{(-Eg/2KT)} \tag{1.2.2}$$

where Eg is the energy gap between valence band and
conduction band.

Using the Fermi-Dirac distribution function, in an intrinsic semiconductor, concentration of electrons in the conductor band is given by,

$$n_i = 2 \left(\frac{2 \pi m_e KT}{h^2} \right)^{3/2} \exp \frac{E_F - Eg}{KT} \qquad (1.2.3)$$

where m_e is the effective mass of an electron in the conduction band and E_F is the Fermi energy level.

Concentration of holes in the valence band is given by

$$P_i = 2 \left(\frac{2 \pi m_h KT}{h^2} \right)^{3/2} \exp \frac{-E_F}{KT} \qquad (1.2.4)$$

where m_h is the effective hole mass.

On multiplying together the expression for n_i and P_i we have the useful equilibrium relation,

$$n_i P_i = 4 \left(\frac{2 \pi KT}{h^2} \right)^{3} (m_e m_h)^{3/2} \exp \frac{-Eg}{KT} \qquad (1.2.5)$$

From this relation we get the important fact that the product of the electron and hole concentrations is a constant for a given material at a given temperature.

For an intrinsic semiconductor, $n_i = P_i$, as the thermal excitation of an electron from the valence

band leaves behind a hole, we get the equation of the form,

$$n_i = p_i = 2 \left(\frac{2\pi KT}{h^2} \right)^{3/2} (m_e m_h)^{3/4} \exp \frac{-Eg}{2KT} \qquad (1.2.6)$$

Extrinsic semiconductors: Semiconductors in which conductivity is controlled by impurities and imperfections are called extrinsic semiconductors.

Semiconductors, no matter how pure they are, always contain some impurity atoms, which create their own energy levels termed as 'impurity levels'. These levels may occupy positions both inside the allowed and forbidden bands of the semiconductor at various distances from the top of the valence band and from the bottom of the conduction band. Frequently the impurities are introduced intentionally to impart specific properties to the semiconductor. This process is known as 'doping'.

There are two types of impurity levels; donor and acceptor levels (fig.1.4). The impurities which supply electrons are known as donors and the energy levels of these impurities are donor levels. The semiconductors doped with donor impurities are termed as n-type semiconductors. The impurities that trap electrons from the valence band are termed as acceptors and
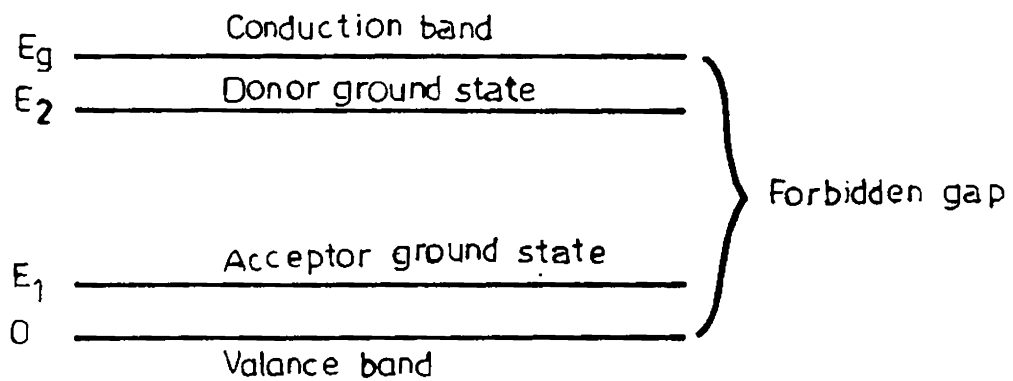
Fig.1.4 : Energy level diagram of an extrinsic semiconductor.

the energy levels of such impurities are acceptor
levels. The semiconductors doped with acceptor impuri-
ties are known as p-type semiconductors.

The density of the free electrons in the
conduction band due to donor levels is given by the
relation,

$$n = (2 n_d)^{1/2} (\frac{2 \pi m_e KT}{h^2})^{3/4} \exp \frac{-E_d}{2KT} \qquad (1.2.7)$$

where n_d is the donor density and $E_d = Eg - E_2$, the
donor ionisation energy.

This shows that $n \propto n_d^{1/2}$

Identical results hold for acceptors.

1.3. THE HALL EFFECT /3/

When a conductor is placed in a magnetic field
perpendicular to the direction of current flow, a volt-
age is developed across the specimen in the direction
perpendicular to both the current and magnetic field.
This effect is known as Hall effect and the voltage is
called Hall voltage. It is developed because the moving
charge carriers making up the current are forced to one
side by the magnetic field. The charges accumulate at
one face of the specimen until the electric field

associated with the accumulated charge is large enough
to cancel the force exerted by the magnetic field. The
Hall voltage measurement is an important tool, especi-
ally in semiconductor research, as it provides a direct
estimate of the concentration of charge carriers.

Let us consider an infinite semiconductor having
an electric current density J in the x-direction and a
magnetic field in the z-direction. If we consider the
effect of the magnetic field on the drift velocity of
electrons in an electric field in the x-y plane, we see
that there must be a component of the field at right
angles to the current flow to balance the transverse
force due to the magnetic field (fig.1.5). The drift
velocity V_x is equal to -J/ne. The average transverse
force on an electron in the y-direction is then eBV_x and
the balancing field E_y is given by

$$e \, E_y = e \, BV_x = -BJ/n \qquad (1.3.1)$$

where B is the magnetic induction. The component of
electric field E parallel to the current is given by
the equation

$$J = ne \, \mu_e \, E_x \qquad (1.3.2)$$
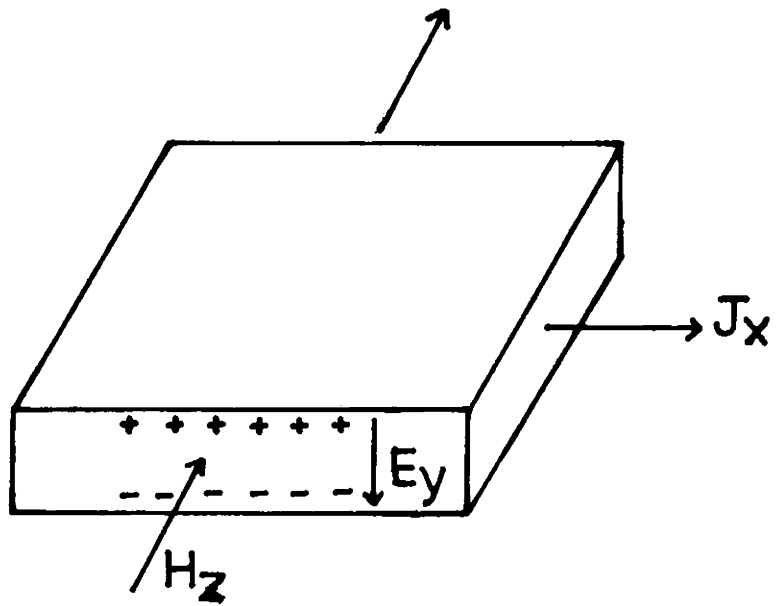
Fig.1.5 : Hall effect. Electrons flowing in the
x-direction in the presence of magnetic field
Hz are deflected towards the y-direction.
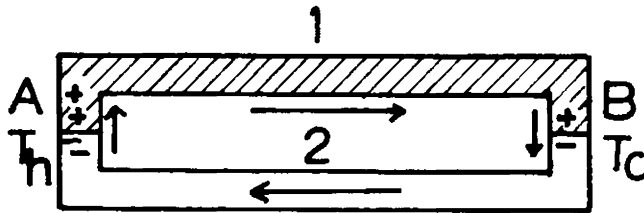
Fig.1.6 : Junctions A and B at temperatures T_h and T_c
between the conductors 1 and 2.

The angle Θ between the current and resultant field is then given by

$$\tan \Theta = E_y/E_x = -B \, \mu_e \qquad (1.3.3)$$

Angle Θ is known as Hall angle.

The Hall effect is described by the Hall constant R_H defined in terms of the current density J by the equation

$$E_H = R_H \, J \, B \qquad (1.3.4)$$

where E_H is the Hall field. If t is the thickness of the film, V_H is the Hall voltage and I the current,

$$V_H = R_H \, I \, B/t \qquad (1.3.5)$$

therefore

$$E_H = R_H \, ne \, \mu_e = -B \, \mu_e \, E_x \qquad (1.3.6)$$

so that

$$R_H = -1/ne \qquad (1.3.7)$$

This equation holds exactly, only when relaxation time is not a function of the velocity. We generally have to include a numerical factor 'r' which varies between 1 and 2 according to the type of scattering which predominates. Apart from this uncertainity, we may obtain

from a measurement of the Hall constant the important quantity n_e giving the electron concentration in the conduction band. The sign of the Hall constant tells whether we have a n-type or p-type semiconductor. Since $\sigma = ne\mu$, by measuring the conductivity of the sample alongwith the Hall constant, we can determine μ, the mobility of the carriers.

1.4. THERMO-ELECTRIC EFFECT /4/

In 1823, T. Seebeck discovered that an electromotive force V appears in a circuit composed of two dissimilar conductors 1 and 2 if the junctions A and B between the conductors are held at different temperatures T_h and T_c respectively (fig.1.6). This emf is known as a thermal emf. As shown by experiment, in a relatively narrow temperature range this emf is proportional to the temperature difference between the junction A and B.

$$V = \alpha(T_h - T_c) \qquad (1.4.1)$$

The proportionality factor, $\alpha = \dfrac{dV}{dT}$ $\qquad$ (1.4.2)

and this is known as the thermoelectric power and it depends on the nature of the conductors in contact and temperature.

There are two main sources of origin of thermal emf: a change in the contact potential difference with

temperature (a contact component V_c) and a directional
carrier flow that emerges in the conductor under the
action of a temperature gradient (volume component V_v).
Contact component of thermal emf: In metals and n-type
semiconductors, an increase in temperature tends to lower
the Fermi level. A change in the position of the Fermi
level causes a change in the thermodynamic work function.
If there is a change in the work function in the two con-
ductors forming the junction, or if the Fermi levels in
the conductors are at different heights, there will be
disturbance of equilibrium at the junction. A new equili-
brium state is setup by virtue of the flow of electrons
from the first to the second conductor until the Fermi
levels are at the same height. Thus a temperature increase
at one of the junctions changes the contact potential
difference across it and gives rise to the potential
difference V_c between the hot and cold junctions, which
is the contact component of the thermal emf. Volume com-
ponent of thermal emf: The carrier concentration in a
conductor is temperature dependent. In metals this
dependence is very weak and determined by thermal expans-
ion causing variation in the conductor volume. In semi-
conductors, however, the carrier concentration can grow
quite heavily with temperature. For this reason the
carrier concentration at the hot end of a semiconductor
may be higher than that at the cold end. A diffusion

flow then appears, which moves from the hot to the cold end, thereby building up the negative space charge at the cold end and the positive space charge at the hot end of the n-type semiconductor. These charges produce a potential difference V_v which is the volume component of the thermal emf.

1.5. AMORPHOUS SEMICONDUCTORS /5/

The ideal, infinite crystal is characterised by the regular arrangement of the atoms in its lattice. Concerning this there are two aspects: short-range order and long-range order. By short-range order we mean the regular arrangement of lattice atoms in the immediate vicinity of the particular atom considered. Long-range order is the strict periodicity and hence the translational invariance of the crystal lattice. Long-range order connects the regions of short-range order in such a way that atoms at equivalent lattice sites have the same surroundings in the same orientation.

The theory of band model is depending on the long-range order. But it must be noted that strict long-range order scarcely influences the physical properties of a solid. The unperturbed, infinite lattice is an idealisation, and in reality a crystal is always perturbed.

A lattice can be referred as ordered if it is possible to explain its characteristics by starting with an infinite lattice with ideal long-range order as the zeroth approximation and to include the dynamic and static perturbations by perturbation theory. We shall call an arrangement of atoms disordered when this approximation is not meaningful.

To understand the order-disorder phenomena let us consider the fig.1.7. The two dimensional cubic point lattice of fig.1.7a has three important signs of order. All lattice atoms are equal, the neighbours arranged in a geometrically fixed short-range order and the number of nearest neighbours is the same for all atoms. In fig.1.7b two sorts of atoms are statistically distributed over the available lattice sites. This type of disorder is called compositional. In fig.1.7c, all the lattice atoms are the same as in the ordered lattice, but it is statistically disturbed. This type of disorder is known as positional disorder. Positional disorder is the characteristic of amorphous phases of a solid. A further type of disorder can be added to positional disorder, namely topological disorder (fig. 1.7d). Here the topology of the lattice is perturbed. In addition to the four atom rings which are characteristic for the cubic net, fig.1.7d shows the appearance of rings with five and six atoms.
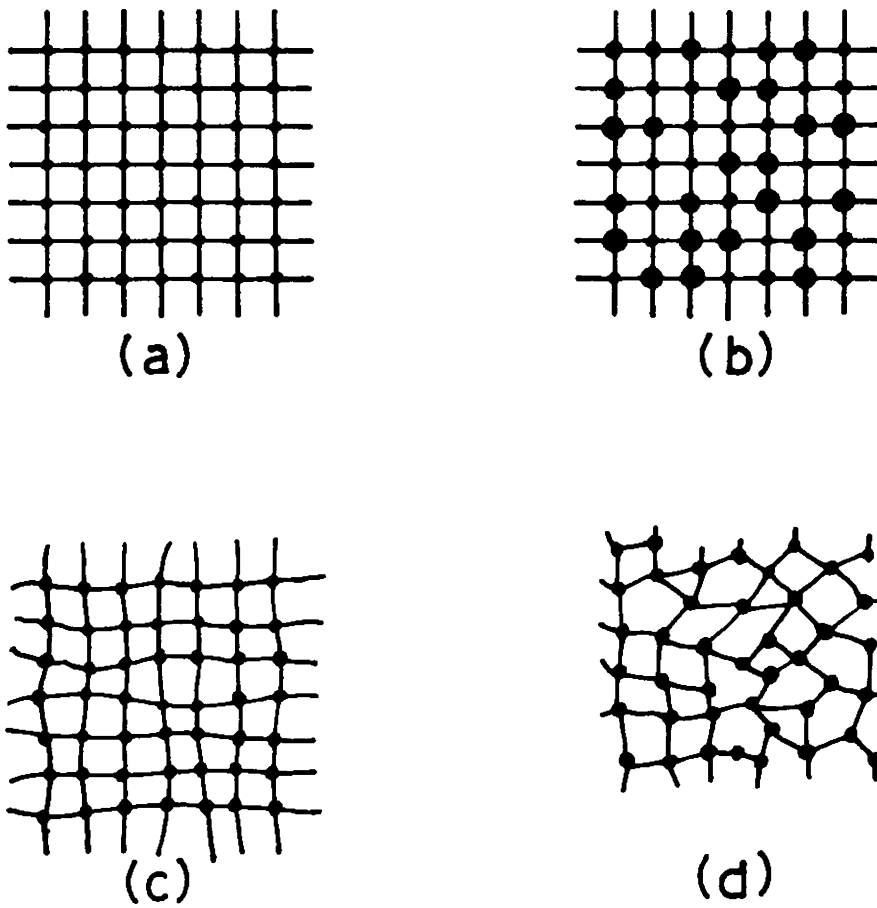
Fig.1.7 : Possible types of lattice disorder: (a) ordered lattice, (b) compositional disorder, (c) positional disorder and (d) topolotical disorder.

In the disordered solid, in contrast to cry-
stalline infinite medium, localized states can occur. In
crystalline media a single imperfection leads to the
splitting-off and simultaneous localization of a state
from the band edge. With increasing number of imperfect-
ions the number of localized states outside the band
increases. The defect levels combines into a band
(impurity band) which can overlap with the bands of the
delocalized states if the defect concentration is suffi-
ciently high. We can imagine that the same phenomena
occurs with increasing disorder of the lattice. The
state at the edge of an energy band become localized
first, and simultaneously shift into the energy gap.
The band thus acquires tails with localized states at
the top and bottom edges as in fig.1.8. With growing
disorder, the limits E_c and $E_{c'}$ approach one another
from either side and meet in the middle of the band.
When they meet, all band states are localized.

The distinct energy E_c separate localized and
delocalized states. If one approaches from the delocal-
ized state side, the mean-free-path become smaller. But
mean-free-path cannot become smaller than a lattice-
constant, a minimum conductivity remains. At absolute
zero conductivity σ_E at the localized regions is zero.
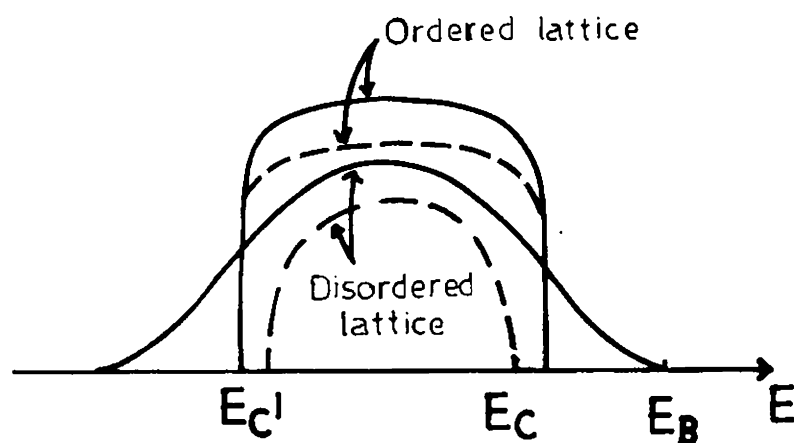
Fig. 1.8 : Density of states (solid curve) and distribution
of the extended states (dashed lines) for an
energy band of an ordered and disordered lattice.
E_B - band edge; E_c, $E_{c'}$ - limits between localized
and extended states.

At E_c an abrupt step occurs in σ_E and hence in mobility. Hence E_c is referred to in the literature as mobility edge.

For a disordered lattice, wave vector k is no longer a good quantum number and concepts like effective mass, crystal momentum etc. does not hold. A concept which is valid as long as one electron states E_i can be defined, is the density of states g(E) and is given by

$$g(E) = \frac{1}{V_g} \sum_i \delta(E-E_i) \qquad (1.5.1)$$

Fig.1.9 shows the density of states in amorphous semiconductors. Fig.1.9a shows the band edges of the conduction and valence bands, containing localized states, which are separated from the extended states by mobility edges. As in fig.1.9b the band tails can overlap (pseudogap). Further local defects (dangling bonds, etc.) can cause impurity bands or levels to appear in the gap or pseudogap (fig.1.9c).

1.5.1. Conductivity in Amorphous Semiconductors:

Conductivity in amorphous semiconductors can be classified into four parts.

(1) Conductivity at the delocalized states, where $E_F \ll E_c$

$$\sigma = \sigma_{E_c} \exp -(E_c - E_F)/KT \qquad (1.5.2)$$

where σ_{E_c} is the conductivity at the mobility edge.
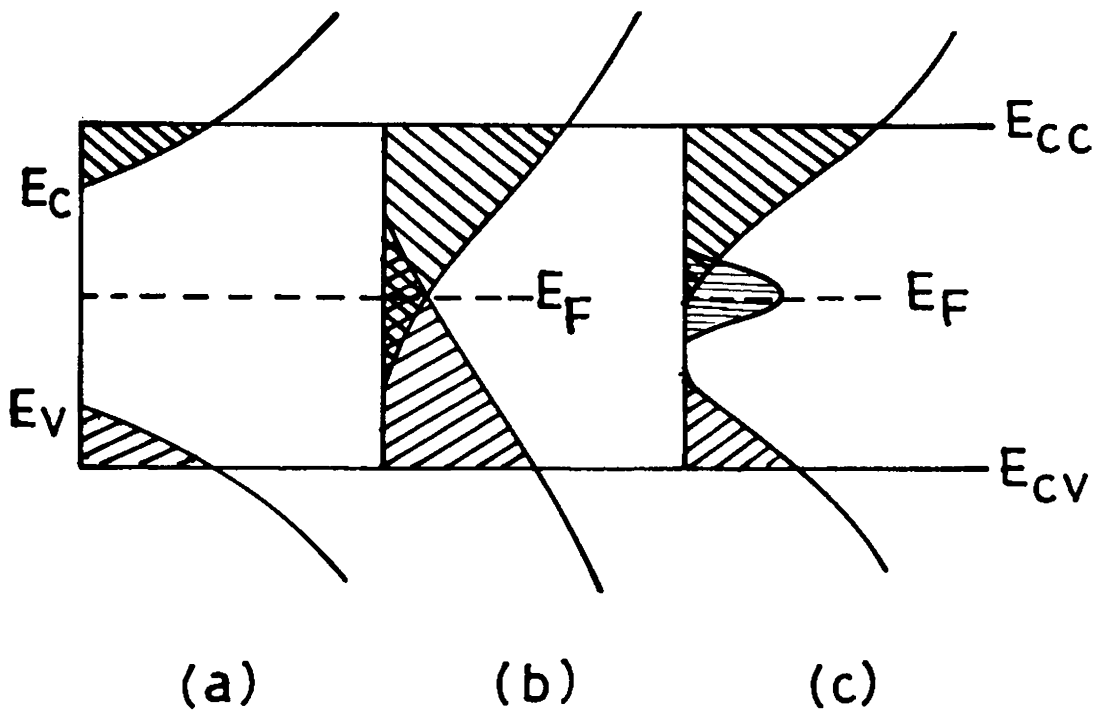
Fig.1.9 : Possible density of states in amorphous
semiconductors (a) localized states at the
edges of the valence and conduction bands,
(b) overlap of the tails of the localized
states, (c) additional impurity bands of
local defects.

(2) Conduction due to carriers at the localized states near the mobility edge.

Here, $E_c > E_i \gg E_F$

$$\sigma = \sigma_1 \exp \; -(E_i - E_F + W)/KT \qquad (1.5.3)$$

where W is the mean hopping energy.

(3) Conductivity in the localized states near the Fermi energy at high temperature:

$$\sigma = \sigma_2 \exp \; (-W/KT) \qquad (1.5.4)$$

(4) Conductivity in the localized states near the Fermi energy at low temperature:

$$\sigma = \sigma_3 \exp \; -(T_o/T)^{1/4} \qquad (1.5.5)$$

Here $T_o = \dfrac{5/2}{9 \pi \lambda^3 K g}$ and λ is a measure of the extend of the state (localization length).

This is Mott's $T^{1/4}$ law.

1.5.2. Optical Absorption in Amorphous Semiconductors

In disordered solids we can distinguish three characteristically different regions of absorption (fig.1.10 and fig.1.11) /6/.

The transition from localized into localized states are important in explaining the shape of the curve for small photon energies. This region is very
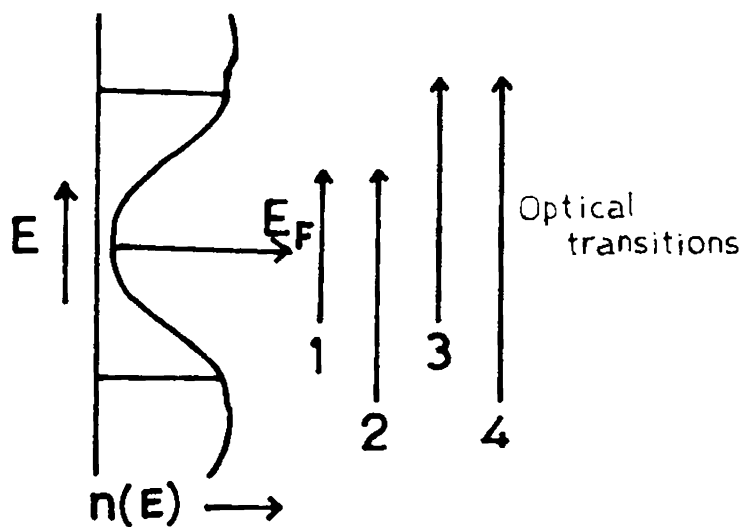
Fig.1.10 : Optical transitions in disordered materials.
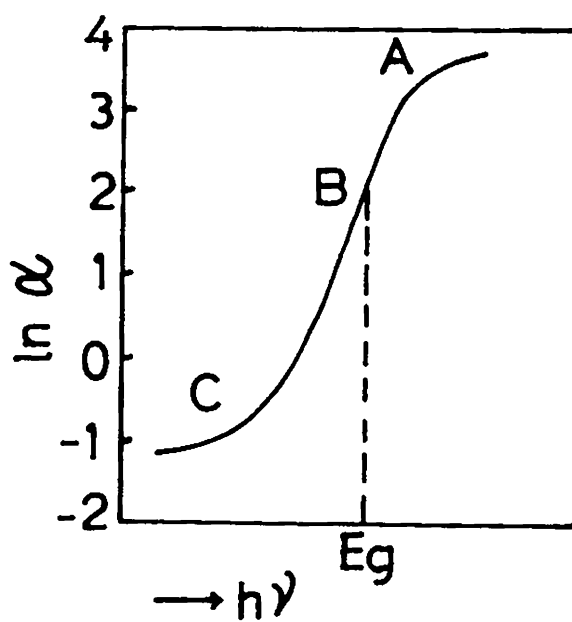
Fig.1.11 : Shape of the optical edge of disordered material.

difficult to treat theoretically and experimentally.
Using exponential valence and conduction band tails
one can estimate the absorption coefficient.

$$\omega \, \alpha \, (\omega) \sim \exp \, (\omega / E_1) \qquad (1.5.6)$$

where E_1 is some characteristic temperature dependent
parameter, $(E_1 \approx 0.1 \; eV)$ and α is the absorption coeffi-
cient. For transitions between localized and delocalized
states (and vice versa) one can also derive an exponential
law, by using exponential density of states for the local-
ized states and a free election density of states for the
extended states.

$$\omega \, \alpha(\omega) \sim \exp \, (\omega / E_2) \qquad (1.5.7)$$

For transitions between extended valence states
and extended conduction states we can assume a power law
to hold. i.e.

$$n_v(E) \sim (E_v - E)^{r_v}$$

$$n_c(E) \sim (E - E_c)^{r_c}$$

Then with constant matrix elements,

$$\omega \, \alpha \, (\omega) \sim (E - Eg)^{r_v + r_c + 1} \qquad (1.5.8)$$

With a phenomenological optical energy gap Eg.
For $r_v = r_c = 1/2$ we obtain

$$\omega \, \alpha(\omega) \sim (E - Eg)^2$$

This is the so called non-direct transition law.

REFERENCES

1. A. Sommerfeld, Z. Phys., 47 (1928) 1.

2. F. Bloch, Z. Phys., 52 (1928) 555.

3. R.A. Smith, Semiconductors (Cambridge University Press, Cambridge, 1978) p.104.

4. G.I. Yepifanov and Yu. A. Moma, Introduction to Solid State Electronics (Mir Publishers, Moscow, 1984) p.409.

5. O. Madelung, Introduction to Solid-State Theory, (Springer-Verlag, Berlin, 1978) p.435.

6. B. Kramer, Physics of Structurally Disordered Solids; Ed. S.S. Mitra, (Plenum Press, New York, 1976) p.374.

CHAPTER II

METHODS OF PREPARATION OF THIN FILMS

Thin films can be prepared on metallic or non-metallic substrates by several different techniques /1-6/. These techniques can in general, be classified into two methods, namely physical and chemical.

2.1. CHEMICAL METHODS

The deposition of thin films by chemical methods depends on chemical reactions. Chemical methods may be broadly classified into: (1) Electrodeposition, (2) Chemical vapour deposition.

2.1.1. ELECTRODEPOSITION

a. Electrolytic Deposition

In this method the metallic ions in the electrolyte migrate towards the cathode under the influence of the applied electric field, which can be very high ($\sim 10^7$V/cm) between the cathode surface and the ions in the double layer, and deposit on the substrate. By this method it is possible to deposit films only on metallic substrates and the films may be contaminated by the electrolyte.

b. Electroless deposition

In this process of preparation the material is deposited from the solution by electrochemical processes without the presence of an externally applied field. The rate of deposition depends on the temperature of the bath and in some cases the deposition needs to be stimulated by a catalyst.

c. Anodic oxidation

Anodic oxidation is used mainly in the formation of films of the oxides of certain metals. By anodic polarization of these metals in a suitable aqueous solution (which does not dissolve the oxide), a protective high resistance film can be grown. For anodic oxidation it is possible to use either the constant current or constant voltage method. Growth rate of an anodic film depends on the current density and the temperature of the electrolyte. The quality of the oxide films and their adhesion to the parent metal depend much on the surface of the metal. A smooth, electrolytically polished surface is essential for obtaining adherent, pinhole free film.

2.1.2. CHEMICAL VAPOUR DEPOSITION

When a volatile compound of the substance to be deposited is vaporized, and the vapour is thermally decomposed or reacted with other gases, vapours, or liquids at

the substrate to yield non-volatile reaction products
which deposit atomistically on the substrate, the pro-
cess is called chemical vapour deposition. This is a
widely used method in thin film technology for the
preparation of pure metals, semiconductors and insulators.

Several type of reactions are classified under
the chemical vapour deposition technique.

a. Pyrolysis

The thermal decomposition of a compound to yield
a deposit of the stable residue is called pyrolysis.

$$AB \rightarrow A + B$$

Electron-beam-bombardment heating is best suited
for pyrolysis of metal compounds. Epitaxial films of
silicon and germanium have been prepared by the pyrolysis
of silane (SiH_4) and germane (GeH_4).

b. Hydrogen Reduction

Hydrogen reduction is a variant of pyrolysis
reaction which is facilitated by the removal of one or
more of the gaseous products of decomposition. Hydrogen
reduction of metal halide is frequently used for deposit-
ing metal films. The reaction temperature is lowered by
several hundred degrees below that needed in the absence
of hydrogen.

c. Transfer Reactions

Deposition can be obtained in a heterogeneous chemical reaction system at equilibrium by setting up a temperature differential in the system to disturb the equilibrium. Among the more useful applications of this method are the epitaxial growth of III-V compounds such as GaAS.

d. Polymerization

Polymer films can be prepared from the monomer vapour by the use of electron beam, ultraviolet radiation or glow discharge. The polymerization process probably results in loss of hydrogen or dissociation by breaking the carbon chain in a hydrocarbon.

2.1.3. LIQUID PHASE EPITAXY (LPE)

LPE growth is a method of depositing semiconducting epitaxial films based on crystallization of semiconducting materials dissolved in a suitable metal. A saturated solution is prepared at a high temperature (1000°C), then gradually cooled. The solution becomes super saturated and crystalline phase begins to grow over a given substrate. By this process monocrystalline films with a low number of crystal defects may be prepared.

2.1.4. LANGMUIR-BLODGETT TECHNIQUE

This technique is used for depositing monolayer films of fatty acids. A small amount of a high molecular-weight substance which has polar molecules (e.g. fatty acids or higher alcohols) is dissolved in a volatile solvent and one drop of the solution is sprinkled on the surface of the water. The solvent evaporates and the molecules of the substance diffuse over the surface of water, all oriented in the same manner due to their polarity. Such a film can be lifted up and put upon a plate.

2.2. PHYSICAL METHODS

Physical method depends on the evaporation or ejection of the material from the source and the most important physical methods for the preparation of thin films are sputtering and vacuum evaporation. Both methods require low pressure in the working space and hence a vacuum system is needed.

2.2.1. SPUTTERING

In sputtering, the target surface (cathode) is bombarded by energetic particles which cause ejection of the surface atoms. Ejected atoms can then be condensed on a substrate to form a thin film. Thin films of refractory materials may be deposited by sputtering without high source temperature sucn as required by evaporation and, alloy films can be prepared by this method without the fractionisation of the components.

a. Glow-Discharge Sputtering

The material to be sputtered is used as a
cathode in a system in which a glow discharge is esta-
blished in an inert gas at a pressure between 10^{-1} and
10^{-2} torr and the discharge gives the energetic ions
that are needed for the ejection. The factors influenc-
ing this sputtering technique are the pressure of the
system, the current and the voltage dependence and the
cathode area. As a consequence of the relatively high
pressure used in this system the surface is also bom-
barded by the residual gas molecules and these are
embedded in the growing film. Hence it is not possible
to obtain films of high purity. However, several modi-
fications were developed which made it possible to grow
films of high purity.

(1) Bias Sputtering

A small negative bias is given to the substrate
with respect to the anode so that it is subjected to steady
ion bombardment throughout its growth, a process which
effectively cleans the film of adsorbed gases otherwise
trapped in it as impurities.

(2) Ion Plating

The effect of sputter cleaning is utilized in

this system. It is a combination of evaporation from
a heated wire and use of a discharge. The films are
obtained by evaporation from a filament and the deposit
is simultaneously bombarded with accelerated gas ions.

(3) Getter Sputtering

In getter sputtering, two cathodes of the
material to be sputtered are symmetrically located with
respect to the anode. The bell jar is divided into two
parts, the gettering and the working region, in such a
way that the gas which enter the working region has to
pass through the gettering region and is thus to a con-
siderable degree deprived of active admixtures.

b. Low-Pressure Sputtering

In the glow-discharge sputtering, useful sputter-
ing rate can be got only in the 2×10^{-2} to 10^{-1} torr argon
pressure range, since the density of ions required for
sputtering falls rapidly with decreasing pressure. Notable
merits of low-pressure sputtering are the decreasing influ-
ence of gas atoms, the lower concentration of trapped gas
atoms, and the higher mean free path of the ejected atoms
striking the substrate owing to smaller collision losses.
Efforts to lower the working pressure, while keeping the
same current density, have resulted in systems employing

various means to enhance the ionization effect with simultaneous decrease in the working pressure.

(1) Magnetic Field

The ionising efficiency may be increased by increasing the path length of the ionising electrons by the utilization of a magnetic field of appropriate configuration.

(2) Triode Sputtering

In this system, a secondary electron gun has been used to increase the concentration of the ionising electrons. The length of the electron mean-free-path is enhanced by using a magnetic field.

(3) RF Sputtering

Enhanced ionization can be achieved by using a r.f. field so that it is possible to sputter at pressures at least an order lower than those of ordinary glow discharges. A significant development employing r.f. sputtering was that, it can be used to sputter from insulators. It may be used additionally in any one of the above described sputtering arrangements to obtain increased sputtering rates at lower pressures.

(4) Ion Beam Sputtering

A specific ion source is used instead of using a discharge system and this enables to grow films sputtered

from targets in a residual pressure as low as 10^{-5} torr.

c. Reactive Sputtering

In this system a partial pressure of reactive gas such as oxygen or nitrogen is deliberately introduced, and films of oxides or nitrides etc. of the target metals are obtained. This is a very useful system particularly for materials that would normally dissociate on evaporation.

2.2.2. EVAPORATION

Vacuum evaporation is the most widely used method for the preparation of thin films. The method is comparatively simple and films of high purity can be obtained under proper experimental conditions. A vast number of materials can be evaporated in vacuum and caused to condense on cooled surfaces.

The process of film formation by evaporation consists of several physical stages:

(1) transformation of the material to be deposited by evaporation or sublimation into the gaseous state;

(2) transfer of atoms/molecules from the evaporation source to the substrate;

(3) deposition of these particles on the substrate;

(4) rearrangement or modifications of their bindings on the surface of the substrate.

Rates of evaporation and condensation can vary over a very wide range depending upon the type and temperature of the source and the material used.

During evaporation a fraction of the vapour atoms will be scattered due to the collision with the ambient gas atoms. Pressures lower than 10^{-4} torr are necessary to ensure a straight line path for most of the emitted vapour atoms.

The rate of free evaporation of vapour atoms from a clean surface of unit area in vacuum is given by the Langmuir expression

$$m_e = 5.83 \times 10^{-2} \; P_e \; \left(\frac{M}{T} \right)^{1/2} \; gm \; cm^{-2} s^{-1} \qquad (2.2.1)$$

where P_e is the equilibrium vapour pressure (in torr) of the evaporant under saturated vapour conditions at a temperature T and M is the molecular weight of the evaporant material.

Number of molecules ejecting per unit area per unit time is given by

$$N_e = 3.513 \times 10^{22} \; \frac{P_e}{(MT)^{1/2}} \; molecules \; cm^{-2} s^{-1} \qquad (2.2.2)$$

Deposition of the vapour on a substrate depends on the source geometry, its position relative to the

substrate and the condensation coefficient. For the ideal case of deposition from a clean, uniformly emitting point source onto a plane substrate, the rate of deposition varies as $\text{Cos}\,\theta/r^2$ (Knudsen Cosine law), where r is the radial distance of the substrate from the source and θ is the angle between the radial vector and the normal to the substrate plane.

a. Evaporation Methods

(1) Resistive heating

In this method the material to be evaporated is heated with a resistively heated filament or boat made of refractory metals such as W, Mo, Ta, Nb etc. Crucibles of quartz, graphite, alumina, beryllia and zirconia are used with indirect heating. The source material is primarily determined by the evaporation temperature and the resistance to chemical reaction of the evaporant.

(2) Flash Evaporation

Here there is instant evaporation of a small amount of material which is dropped onto hot surface of the source. This technique is well suited for multicomponent compounds or mixtures, from which thin films can be prepared that have the same composition as the parent material. The evaporant should be in the form of a powder which is dispensed from a reservoir in small quanta with the help of a mechanical or ultrasonic vibrator.

(3) Arc Evaporation

Refractory materials such as Nb and Ta can be evaporated using sufficiently high temperature by striking an arc between two electrodes of a conducting material. This method is widely used for the evaporation of carbon for electron-microscope specimens.

(4) Exploding - Wire technique

Using this method a very rapid evaporation of a given amount of metal can be achieved by the passage of a strong current pulse through a thin wire. The pulse is obtained by rapid discharge of a capacitor charged to a sufficiently high voltage.

(5) Laser Evaporation

The enormous intensity of a laser may be used to heat and vaporise materials by keeping the laser source outside the vacuum system and focussing the beam onto the surface of the material to be evaporated. The laser beam penetrates to the depth of only ≤ 100 nm and the evaporation take place only on the surface.

(6) R.F. Heating

R.F. or induction heating can be provided to the material by suitable arrangement of R.F. coils. This avoids the contamination of the film by the support material to a greater extent.

(7) Electron Beam Evaporation

An electron beam of sufficient intensity is ejected from a cathode, accelerated and focussed onto an evaporant material, which is heated at the site of incidence to the temperature required for evaporation. The method enables us to attain a very high temperature and to evaporate materials which would otherwise evaporated with difficulty or cannot be evaporated at all. The possibility of deflecting the electron beam by an electric or magnetic field allows the use of the same gun for subsequent evaporation of various materials.

b. Reactive Evaporation

Reactive evaporation is a variant of Günther's /7/ three temperature method (TTM). Günther analysed the condensation of multicomponent vapours on the basis of nucleation theory, according to which a critical flux exists for every substrate temperature (and vice versa) at which spontaneous nucleation occurs.

For a given vapour on a given substrate, the condensation flux N_K exceeds zero only if the ratio P/P_e of the actual vapour pressure P and equilibrium pressure P_e exceeds a critical value q_c.

$$\text{i.e.} \quad N_K > 0, \text{ if } (P/P_e) > q_c \qquad (2.2.3)$$

For a given substrate temperature, it can be written as,

$$N_K = 0 \quad \text{if } N_+ \leqslant N_{+C} \text{ (T)} \qquad (2.2.4)$$

$$N_K > 0 \quad \text{if } N_+ > N_{+C} \text{ (T)} \qquad (2.2.5)$$

where N_+ is the incident flux and N_{+C} is the critical value of the incident flux. If the flux exceeds N_{+C}, the condensation flux rises rapidly and approaches its maximum value given by

$$N_{K \text{ max}} = \alpha (N_+ - N_e) \qquad (2.2.6)$$

where α is the condensation coefficient and N_e is the reevaporation flux from the substrate. This behaviour is shown in fig.2.1. $(P/P_e)^*$ corresponds to the beginning of nucleation due to surface diffusion.

Assuming a constant incident flux N_+ for vapour particles on a substrate, the condition for progressive condensation can be expressed in terms of a critical temperature T_c:

$$N_K = 0 \quad \text{if } T \geqslant T_c \text{ (N}_+) \qquad (2.2.7)$$

$$N_K > 0 \quad \text{if } T < T_c \text{ (N}_+) \qquad (2.2.8)$$

Thus by analogy with fig.2.1, the condensation can be represented schematically as a function of substrate temperature in the manner of fig.2.2; after dropping below
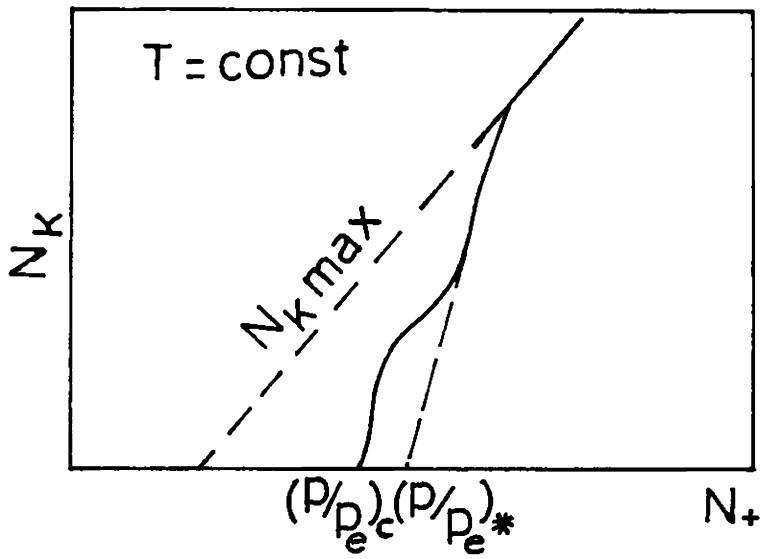
Fig.2.1 : Variation of condensation flux N_k with flux N_+ of incident particles.
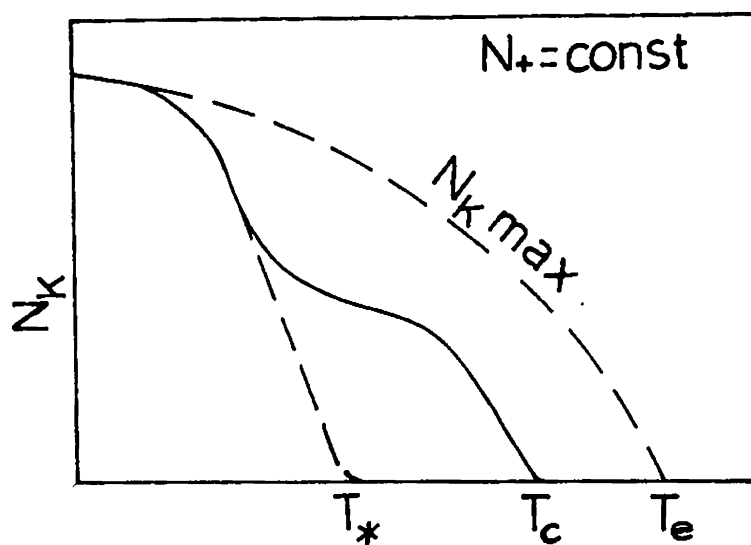
Fig.2.2 : Variation of condensation flux N_k with
substrate temperature T.

the critical temperature T_c, the condensation sets in
spontaneously and quickly approaches a maximum. T_e
indicates the equilibrium temperature corresponding to
N_+ and T^* indicates the beginning of nucleation by sur-
face diffusion.

Suppose the vapour phase consists of two compo-
nents A and B and both being incident on the substrate
under consideration. As in all cases of high vacuum
deposition, the vapour density may be low enough to negl-
ect collision between particles of the components A and B
in the vapour phase. However, interaction can take place
between such particles which are adsorbed on the substrate
surface. These interactions, due to the strong attractive
forces between particles A and B, may lead to the formation
of molecules.

$$A + B \rightarrow AB \qquad\qquad (2.2.9)$$

where AB stands for all possible compounds of A and B.
A rough estimate of interaction probability on the surface
gives a density

$$n_{AB} = \text{Const. } x \ n_A \ n_B \ \bar{D} \qquad\qquad (2.2.10)$$

where n_A and n_B are the number of adsorbed atoms A and B
and $\bar{D}$, the mean diffusion coefficient.

Since the number of adsorbed atoms is proportional
to actual vapour pressure P, or the incident flux N_+ of the

particular vapour, the density n_{AB} should also be proportional to the product of incident fluxes (N_{+A} N_{+B}) or vapour pressures ($P_A P_B$).

In order to estimate the critical values which now apply, the equilibrium pressures P_{eA}, P_{eB} of the components and P_{eAB} of the compound must be considered. P_{eAB} usually corresponds to the dissociation pressure of the compound and is equivalent to the pressure of the more voltaile component (say, A) in equilibrium with the compound. In most cases, this value is much lower than the equilibrium pressure P_{eA} of the pure component A. Thus the critical values of one component A in the presence of the other component B shall vary as follows:

$$N_{+CA} \ (B) \ll N_{+cA} \qquad (2.2.11)$$

$$T_{CA} \ (B) > T_{CA} \qquad (2.2.12)$$

This means that it will be possible to condense A (in combination with B) at a lower critical flux in the presence of B for a given substrate temperature. Or in terms of substrate temperature, it means that, a higher substrate temperature may be used to deposit A in combination with B for a given flux of A.

Fig.2.3 shows the condensation flux as a function of temperature with two given incident components N_{+A} and N_{+B}.
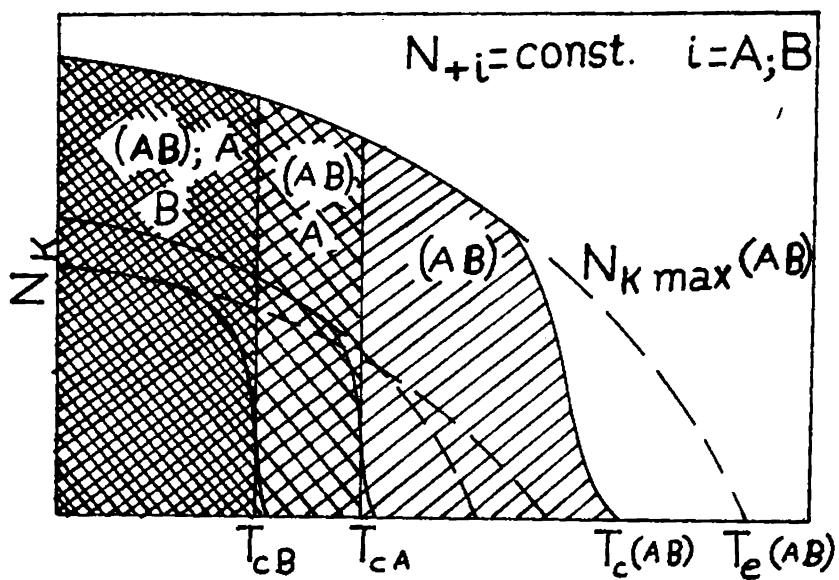
Fig.2.3 : Condensation flux as a function of
temperature with two incident components
A and B.

Fig.2.4 shows the condensation diagram for two incident components A and B for a given substrate temperature.

The advantages of reactive evaporation are as follows:-

(a) There is no need to go through tedious and some times expensive metallurgy to prepare the material in bulk before evaporation.

(b) Although high temperatures $(T \approx 2000^{\circ}C)$ are frequently needed to evaporate a compound (eg., a rare earth compound) the constituent elements have vapour pressures that are high enough at low temperatures $(50 < T < 1500^{\circ}C)$.

(c) The stoichiometry can be adjusted by simply varying the individual evaporation rates and thus the number of current carriers and the type of conductivity of the compound can be controlled.

(d) The decomposition of the compound on heating in vacuum and subsequent loss of the original composition in the films are inherently not present.

(e) The lowest substrate temperature possible is dictated by the condensation temperature of the more volatile component and is usually low (eg. O_2, S_2 and Se_2) and consequently this method can be used as an efficient technique for the preparation of amorphous films.
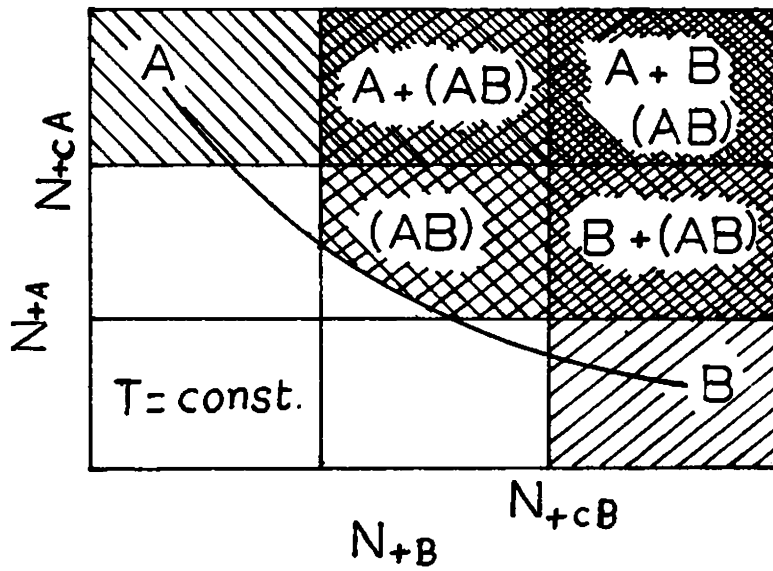
Fig.2.4 : Condensation diagram for two incident
components A and B.

(f) Dopants can be directly introduced in their elemental form and the doping level can be easily controlled.

This technique has got the following draw backs:

(a) The use of large volatile flux and consequent wastage of the volatile element.

(b) High volatile partial pressure in the vacuum system reduces the mean free path and also scatters the non-volatile beam away from the substrate surface.

(c) Because of the high volatile elemental pressure, some unreacted volatile flux may get entrapped in the growing film which will have drastic effects in the film properties.

In reactive evaporation technique, chemical reaction rate can be increased by increasing the kinetic energy of the particles. The most versatile way of increasing the kinetic energy of particles is by ionising them with electron beams or suitable radiations and accelerating them in electric fields. Bunshah and Raghuram /8/ introduced this technique to increase the chemical reaction rate and is known as the activated reactive evaporation (ARE). In this technique, electron from an electron gun ionise the reactive gas atoms generating a thick plasma. Because of the presence of this plasma the chemical reaction rate will be very much high.

REFERENCES

1. K.L. Chopra, "Thin Film Phenomena", (Robert E. Kringer Publishing Company, Inc., New York, 1979).

2. R.W. Berry, P.M. Hall and M.T. Harris, "Thin Film Technology", (Van Nonstrand, New York, 1968).

3. L. Holland, "Vacuum Deposition of Thin Films", (Chopman and Hall, London, 1956).

4. J.C. Anderson (Ed.), "The Use of Thin Films in Physical Investigations" (Academic Press, London, 1966).

5. R. Glang, "Hand Book of Thin Film Technology", Ed. by L.I. Maissel and R. Gland (McGraw-Hill, New York, 1970) p.1-3.

6. D.S. Campbell, "Physics of Non-metallic Thin Films", Ed. by C.H.S. Dupuy and Cachard, (Plenum press, New York, 1976) p.9.

7. K.G. Gunther, "The use of Thin Films in Physical Investigations", Ed. by J.C. Anderson, (Academic Press, London, 1966) p.213.

8. R.F. Bunshah and A.C. Raghuram, J. Vac. Sci. Tech., 9 (1972) 1389.

CHAPTER III

EXPERIMENTAL TECHNIQUES

3.1. PREPARATION OF COMPOUND THIN FILMS BY REACTIVE
EVAPORATION

For the preparation of lead sulphide and tin
telluride thin films, reported in this thesis, reactive
evaporation technique was used. In the case of lead
sulphide, lead was evaporated in an atmosphere of sulphur.
By adjusting the temperature of sulphur source, it was
possible to maintain an atmosphere of sulphur vapour
inside the chamber. This had been made possible because
sulphur vapour will not stick onto a clean substrate or
bell jar even at room temperature at the ordinary sulphur
vapour partial pressure needed ($\sim 10^{-4}$ torr). That is,
sulphur vapour behaves almost like a gas. Here because
of the excess sulphur molecules, usually the most sulphur
rich phase is formed. Usually for the preparation of sul-
phides by reactive evaporation technique, H_2S has been used
as the reactive gas. But H_2S is a poisonous gas and by
using this gas, sulphur deficient phase may be formed. In
the case of tin telluride, tellurium atoms were unable to
stick onto the substrate independently at the elevated
temperature (>425K), and a tellurium partial pressure
is formed inside the chamber.

For the kinetics of reactive evaporation, it is important that the mean free path at 10^{-4} torr is of the order of 50 cms. Hence the probability of forming the compound molecule through collision in the gas phase is very small. Instead, the recombination take place on the substrate surface, which is exposed to high incidence rate of metal and chalcogen particles.

The rate of evaporation Γ from a surface at a temperature T is given by the Langmuir expression,

$$\Gamma \; = \; m \; \frac{dNe}{A_e dt} \; = \; \left(\frac{M}{2 \pi RT} \right)^{1/2} P \qquad\qquad (3.1.1)$$

where m is the mass of a molecule of the material, dN_e is the number of molecules evaporating from a surface area A_e during the time dt, M is the molecular weight of the material, R is the universal gas constant and P is the vapour pressure.

In the reactive evaporation technique, the suitable temperature for evaporation is that at which the vapour pressure of the material is $\sim 10^{-2}$ torr. Fig.3.1 shows the variation of vapour pressure of tin and lead with temperature /1/.

For the purpose of reactive evaporation, the rate at which metal atoms arrive at the substrate is best expressed in terms of the deposition rate as obtained
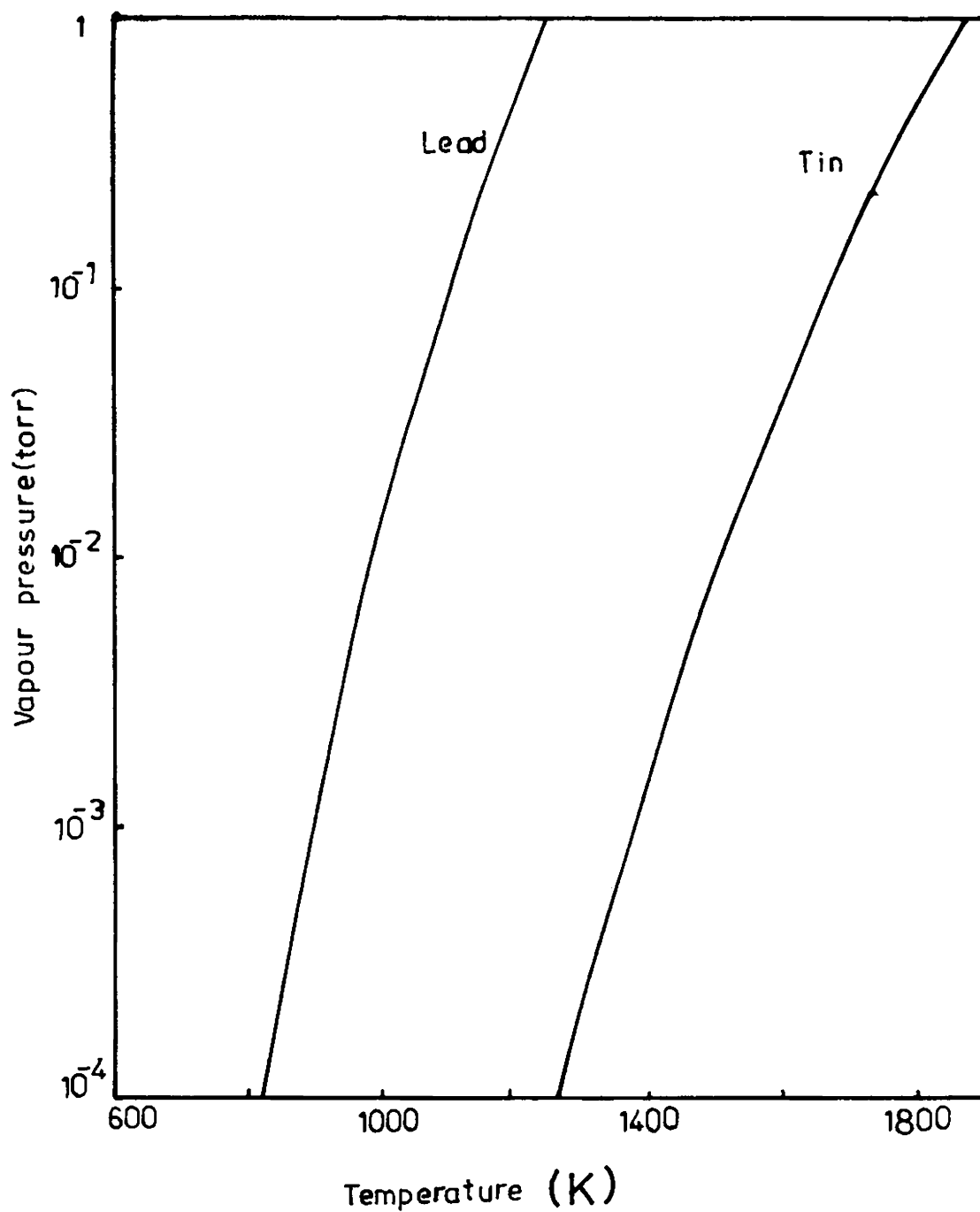
Fig.3.1 : Variation of vapour pressure with temperature
for lead and tin.

from the same source at the same temperature and substrate to source distance, but in the absence of chalcogen /2/:

$$\frac{dNm}{A_r dt} = N_a \frac{\rho_m}{M_m} \; d \; \text{atoms cm}^{-2}\text{s}^{-1} \qquad (3.1.2)$$

where ρ_m is the density of the metal film in g. cm^{-3}, M_m is the molar mass of the metal in g. cm^{-3}, d is the pure metal condensation rate in cm. S^{-1} and A_r is the receiving surface area in cm^2.

The impingement rate of chalcogen molecules is given by

$$\frac{dN_c}{A_r dt} = 3.513 \times 10^{22} \; (M_c T)^{-1/2} \; P_c \; \text{molecules cm}^{-2}\text{s}^{-1} \qquad (3.1.3)$$

where M_c is the molar mass of chalcogen, T is the vapour temperature and P_c is the chalcogen partial pressure in torr.

From equations (3.1.2) and (3.1.3) the impingement rate of atoms/molecules on the substrate for given deposition rate/partial pressure can be found out.

Substrate Cleaning: Substrates must be thoroughly cleaned before deposition, and a variety of procedures exist for this purpose. The following procedure was used for cleaning the substrates for the work reported in this thesis.

Optically flat glass/quartz slides of the required sizes
were first dipped in chromic acid for one hour and then
cleaned with an industrial detergent-teepole. After this
the substrates were washed in tap water followed by dist-
illed water. Then these substrates were rinsed thoroughly
in analytical reagent grade acetone followed by fifteen
minutes cleaning in doubly distilled water in an ultra-
sonic cleaner. The cleaned substrates were then dried
in a flow of hot air and loaded in the vacuum chamber.
An efficient method to remove contaminants and oxide layers
from a substrate is to sputter the surface by ionic bombard-
ment and substrates were cleaned by ion-bombardment for ten
minutes prior to the actual film deposition. This cleaning
procedure was found satisfactory and it was possible to get
films with good adhesion to the substrate.

Vacuum System: The most common type of vacuum system for
thin film deposition is the bell jar vacuum system and
this system was used for the deposition of thin films re-
ported here. This system include a diffusion pump backed
by a rotary pump. Without the use of liquid nitrogen
trap, pressure down to 9×10^{-6} torr could be achieved
with care, but routinely it was 2×10^{-5} torr. The eva-
poration chamber had provisions for three independent
resistively heated sources with two transformers capable of
supplying 200 A and one 10 A. One 200 A transformer was

used to evaporate the metal and the smaller 10 A source
was used to evaporate chalcogen. There were also pro-
visions in the chamber for ion-bombardment cleaning,
substrate heating and substrate temperature measurements.
For pressure measurements the chamber had one Pirani
gauge and one Penning gauge. The normal pumping down
time to get ultimate vacuum was around 45 minutes.

Thin Film Deposition: Prior to the evaporation, the
system was pumped to the ultimate low pressure ($\approx 10^{-5}$torr)
required, using the diffusion pump backed by the rotary
pump.

High purity materials (99,999% tin, lead and
tellurium and 99,99% sulphur) were used as evaporants.
A helical filament made of molybdenum wire was used to
evaporate tin/lead. This helical filament was covered
with stainless steel shield to minimise substrate heat-
ing. Sulphur and tellurium were evaporated from conical
glass crucibles, heated by molybdenum wire windings. The
temperatures of the sources and hence the flux could be
easily controlled by adjusting the current through the
molybdenum wire. Temperature of the sources and the
substrates were measured by chromel-alumel thermocouple
placed in contact with them. The temperature should be
controlled within an accuracy of $\pm$ 3 K. Schematic

diagram of the evaporation setup is as shown in
fig.3.2.

When the substrate had attained and stabilized
at the required temperature with the shutter placed over
the metal and chalcogen sources, the current through the
chalcogen source was switched on and it was allowed to
melt in the crucible, so that the required partial pres-
sure of chalcogen was maintained in the chamber. The
current through the metal source was then switched on
and increased to a preset value which gave the required
deposition rate of the metal film. The shutter was then
withdrawn and the deposition of the compound film allowed
to take place. The chalcogen atoms/molecules were unable
to stick to the substrate independently. The metal atoms
reaching the substrate reacted with those chalcogen atoms
present on the substrate and the compound film was de-
posited. Highly reproducible films could be produced
under these conditions.

3.2. MEASUREMENT OF FILM THICKNESS

Multiple beam interferometry, developed by
Tolansky /3/ is an accurate method available to determine
thin film thickness. Two general methods of multiple
beam interferometry are used to measure film thickness.
The first produces Fizeau fringes of equal thickness,
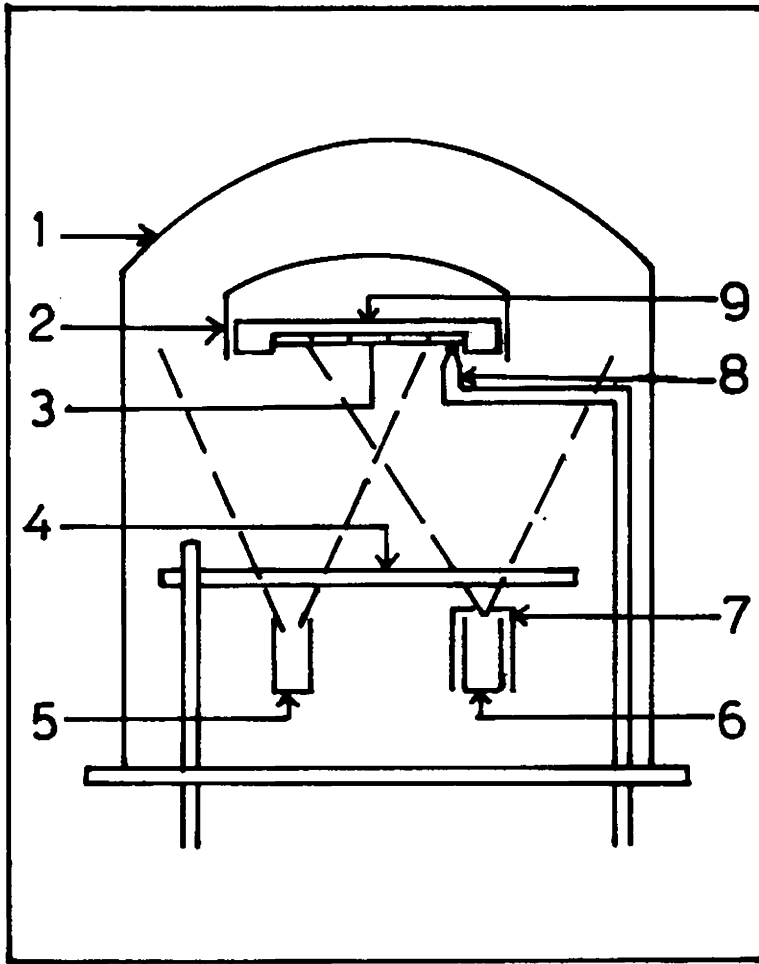
Fig.3.2 : Schematic diagram of the evaporation setup.

1. Bell jar, 2. heat shield, 3. substrates,

4. shutter, 5. chalcogen source, 6. metal source,

7. heat shield, 8. thermocouple, 9. substrate heater.

using a monochromatic light source. The second uses
a white light source and produces fringes of equal chro-
matic order. For thickness measurement of the films
reported in this thesis, the first method was used.

The procedure used to produce Fizeau fringes
of equal thickness is as follows: The film whose thick-
ness is to be measured is deposited on a glass substrate
with sharp step between the surface of the substrate and
the surface of the film. A highly reflecting opaque film
is deposited on the surface of the film and on the glass
substrate. A semi silvered glass substrate is then pre-
pared and a multiple beam interferometer is formed by
keeping both the film surfaces in contact. This is
tightly fixed using a circular jig with three tilt adjust-
ment screws. This is illuminated with collimated mono-
chromatic light, and the fringe system produced is viewed
with a microscope. A typical interferometer arrangement
for producing reflection Fizeau fringes is as shown in
Fig.3.3a. By adjusting the tilt adjustment screws the
fringes can be made to run in straight line perpendicular
to the step. The fringe spacing and the fringe displace-
ment across the step are measured and used to calculate
the film thickness. Fig.3.3b shows the fringes produced
by multiple beam interferometry across a film-substrate
step.

Filter

Beam
splitter

Multiple beam
interferometer→
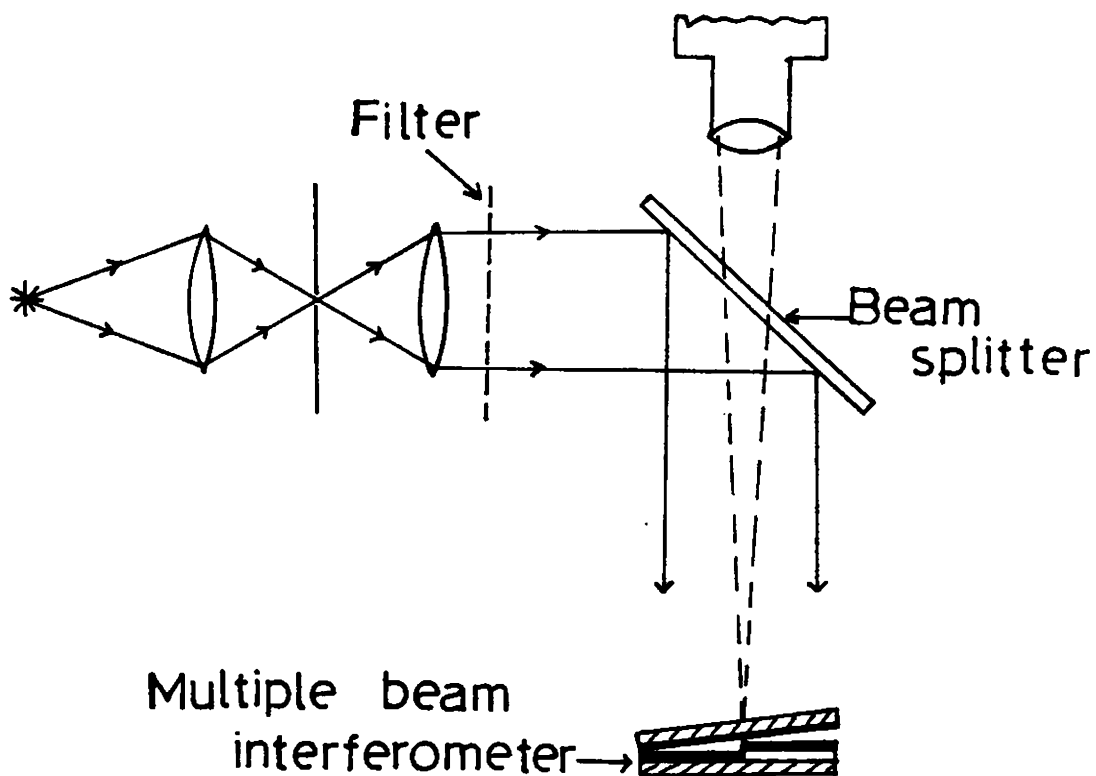
Fig.3.3(a) : Multiple beam interferometer arrangement.

D

d
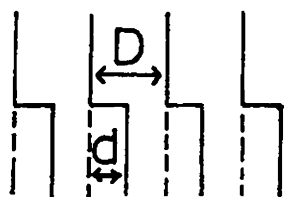
Fig.3.3(b) : Fringes with steps produced by multiple
beam interferometry.

The distance between successive fringes D corresponds to $\lambda/2$, where λ is the wavelength of the monochromatic radiation used. When a sharp step exists on the substrate, the fringe system is abruptly displaced by an amount 'd' as shown in fig.3.3b. The amount of displacement 'd' is a measure of the film thickness, t. The film thickness is given by

$$ t = \frac{d}{D} \cdot \frac{\lambda}{2} $$

For the production of sharp fringes following conditions must be taken care off:

(1) The overlayer on the step must be highly reflective. A reflectivity of 0.94 has been found to be optimum.

(2) The reflecting film must be of uniform thickness over the specimen and the distance between the plate surfaces must be as small as possible.

(3) The angular spread in the incident beam should be less than 1° to 3°.

(4) The incident light should be normal to the reference plate.

(5) The substrate should be flat. Lack of flatness causes the fringes to be curved and reduces the accuracy of the step-height measurement.

3.3. X-RAY DIFFRACTION STUDIES

It is very necessary to identify the compound thin films obtained and to know whether it is crystalline or amorphous in nature. For this, x-ray diffraction is a non-distructive technique and the film thickness here should be greater than 2000 Å. Electron diffraction is more sensitive and can be used even if the film is very thin; but suffers from the drawback that the film has to be detached from the substrate.

In usual x-ray diffractometers the Bragg-Brentano geometry is used, where the x-ray beam is incident at an angle θ to the substrate and the detector is placed at an angle 2θ. The specimen and the detector are rotated at angular frequencies ω and 2ω respectively to get the various diffracting planes. In this geometry when thin films are used, the effective thickness the x-ray beam sees at any angle of incidence will be $t/Sin\theta$, where t is the film thickness and θ is the angle of incidence of the x-ray beam. Consequently scattered intensities will be angle dependant (enhanced by a factor $t/Sin\theta$) and this must be borne in mind when comparing the intensities with ASTM cards. If proper care is taken, x-ray diffraction can yield good results and any particular compound in the binary or ternary system can be identified without difficulty.

X-ray unit used for diffraction studies was
a Philips PW 1140/90 unit fitted with a Philips
PW 1050/70 goniometer. Filtered copper K_α radiation
was used. The accelerating potential applied to the
x-ray tube was 25-30 KV and the tube current was
14-16 mA. X-ray beam was scanned from θ values of
10° to 30°. The spectra (intensity of the diffracted
beam versus 2θ) were recorded on chart recorder running
in synchronization with the goniometer.

3.4. MEASUREMENT OF ELECTRICAL RESISTIVITY

Electrical resistivity is a property of primary
interest in semiconductors. Both electrons and holes
control the electrical resistivity of a semiconductor.
As the temperature increases from absolute zero electrons
from closest donor levels will be excited to the conduct-
ion band and there will be a decrease in the resistivity.
Activation energy in this case is the gap between this
donor and conduction band. As the temperature is in-
creased all carriers from these impurity donor levels
will be excited to the conduction band. (In case of
p-type samples similar transitions will be held between
valance band and acceptor levels). At sufficiently high
temperature intrinsic conductivity starts and electron
transitions from the valance band to conduction band

take place. In this case the activation energy is the
band gap between the valence band and conduction band.
If we plot a graph between $\log \rho$ versus $1/T$, where ρ is
the resistivity and T is the temperature, we could get
the activation energy for conduction from the slope of
the straight line portions of this graph (fig.3.4).
That is, the measurement of electrical resistance as a
function of temperature can yield information regarding
the impurity levels in the forbidden band and also the
value of band gap. In semiconductor materials which
have got very high density of impurity levels the con-
ductivity will be controlled by them. In case of mater-
ials in which these impurity levels lie close to the
conduction band, the resistivity will increase with
temperature after a certain temperature. This is because,
all the carriers from the impurity levels are already
excited and any further increase in temperature will
decrease the mobility and thereby increase the resisti-
vity. Only at a very high temperature the intrinsic
conductivity will set in.

Electrical resistivity of highly resistive
samples are rather complicated and a number of problems
are associated with the electrical disturbances and
humidity. The electrical disturbances can be minimised
by enclosing leads in shielded cables and if necessary,
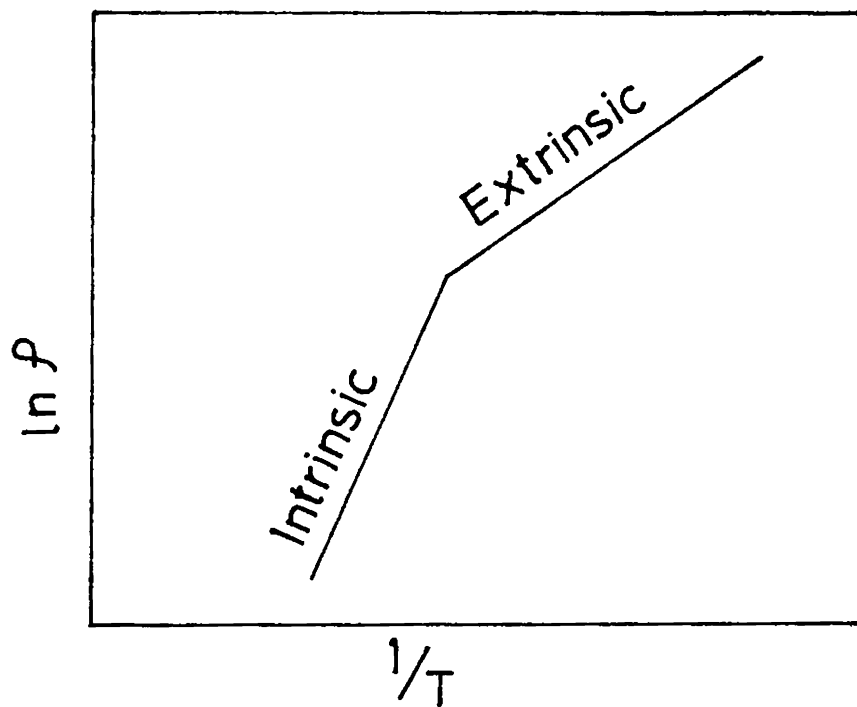
Fig.3.4 : Dependence of resistance on temperature
(lnP vs. 1/T).

by enclosing the whole setup in a shielded cabin.
Both high resistivity semiconductors and insulators
will be influenced by water vapour, which present in
the atmosphere may short circuit the specimen and give
a false low resistance. To avoid the difficulties that
arise from electrical disturbances and water vapour,
an all metal cell was fabricated, which can be eva-
cuated to a vacuum between than 10^{-2} torr. Fig.3.5a
shows the all-metal cell and a typical specimen fixed
inside it. For the measurement of small values of
current ($\sim 10^{-12}$ A) good quality electrometers have
to be used.

Current to the heater block on which the
specimen is mounted for varying the specimen temperat-
ure, should be well smoothed DC and one terminal of it
should be earthed. This is because any ripple present
in the DC will induce large currents in the film or con-
tacts which will completely mask the required signal.
When the resistance is measured as a function of tem-
perature, sufficient time should be given for the speci-
men to take up the heater block temperature.

The metal contact made to the film must be
ohmic in characteristic. Substrate on which film is
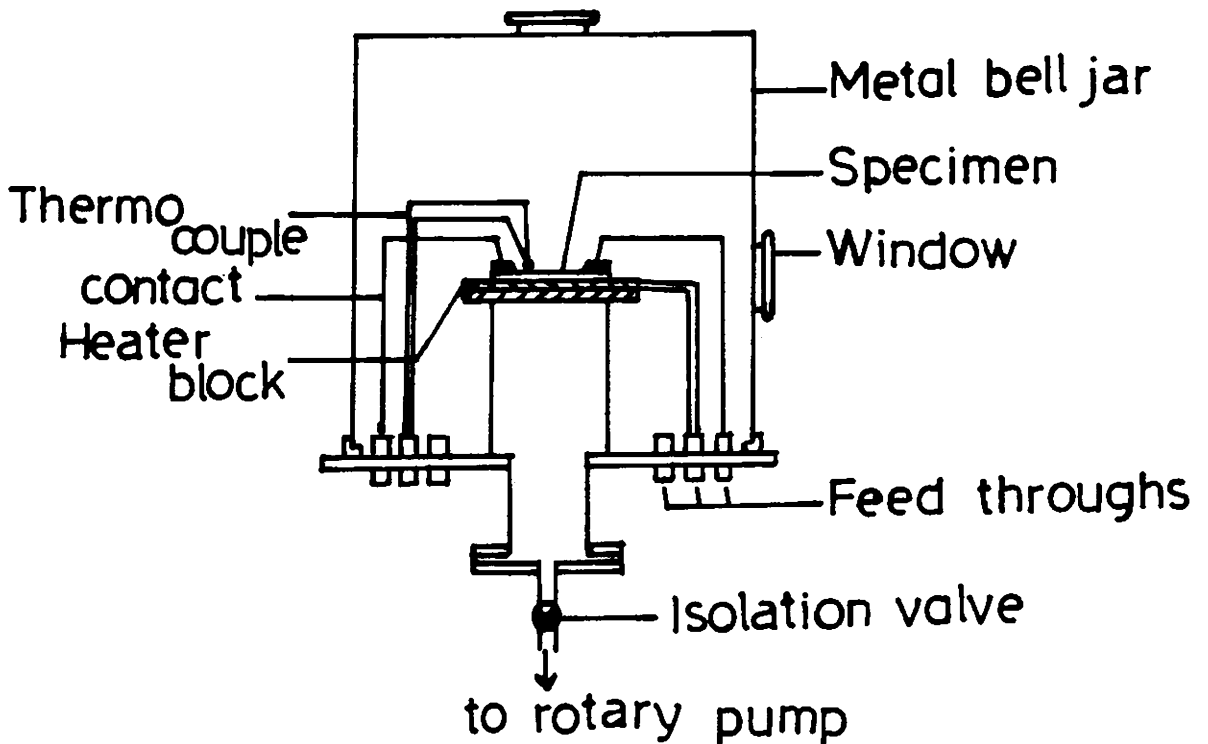
Fig.3.5(a) : High resistivity measurement setup.
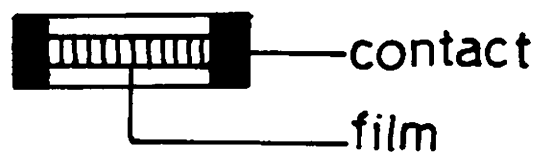
Fig.3.5(b) : Typical specimen geometry.

coated should be atleast hundred times more resistive than the film. Otherwise film will be electrically short circuited by the substrate. It must be noted that all electrical insulations in the cell should be made of teflon.

The specimen geometry is as shown in fig.3.5b. The voltage applied across the specimen was measured using a Hewlett Packard 3465A digital multimeter. The meter used for current measurement was a Keithley Model 616 - digital electrometer. The temperature was measured using a chromel-alumel thermocouple placed in contact with the specimen and which was connected to a $4\frac{1}{2}$ digit, 200 mV DPM.

3.5. HALL EFFECT MEASUREMENTS

Hall voltage measurement is one of the most powerful tool for studying the electronic properties of semiconductors. The Hall coefficient is measured using the formula,

$$R_H = \frac{V_H \cdot d}{H \cdot I} \times 10^8 \ cm^3/Coulomb.$$

where V_H the Hall voltage (Volts), d the specimen thickness (centimeters), H the magnetic field (gauss) and I the current through the sample (amperes).

Since R_H is inversily proportional to the carrier concentration, we can calculate carrier

concentration by measuring the Hall voltage. In fact
this is the standard technique for determining carrier
concentration. Hall coefficient can also be used in
calculating the Hall mobility, such that the product
of Hall coefficient and conductivity gives the mobility.
Hence the measurement of Hall voltage in conjunction with
conductivity may in principle be used for the complete
electrical characterisation of the material. Block dia-
gram of the d.c. apparatus used for measuring Hall volt-
age and conductivity is as shown in fig.3.6.

Because of the relative high conductivity of
lead sulphide and tin telluride, contacts are easily made
to the films. Satisfactory contacts have been made to
the bridge shaped samples (fig.3.6) using silver paste
and pressed indium. Current through the specimen was
kept below 5mA and was measured using a Keithley Model
No.181 digital nanovoltmeter. The magnetic field upto
5 K Gauss was applied using a magnet which have got a
pole piece separation of 2 cms. To eliminate electrical
noises an all metal cell was used /4/, which has got
provisions for cooling down to liquid nitrogen temper-
ature and heating upto 450K and can be evacuated to
10^{-2} torr. A cross section of the cell is as shown in
fig.3.7.
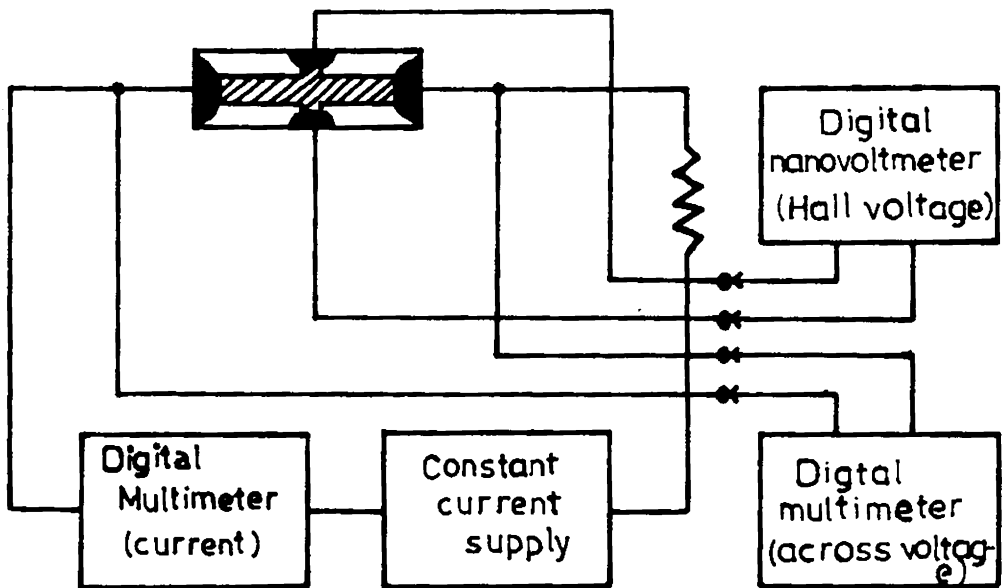
Fig.3.6 : Block diagram of the d.c. apparatus used for
measuring Hall voltage and conductivity.
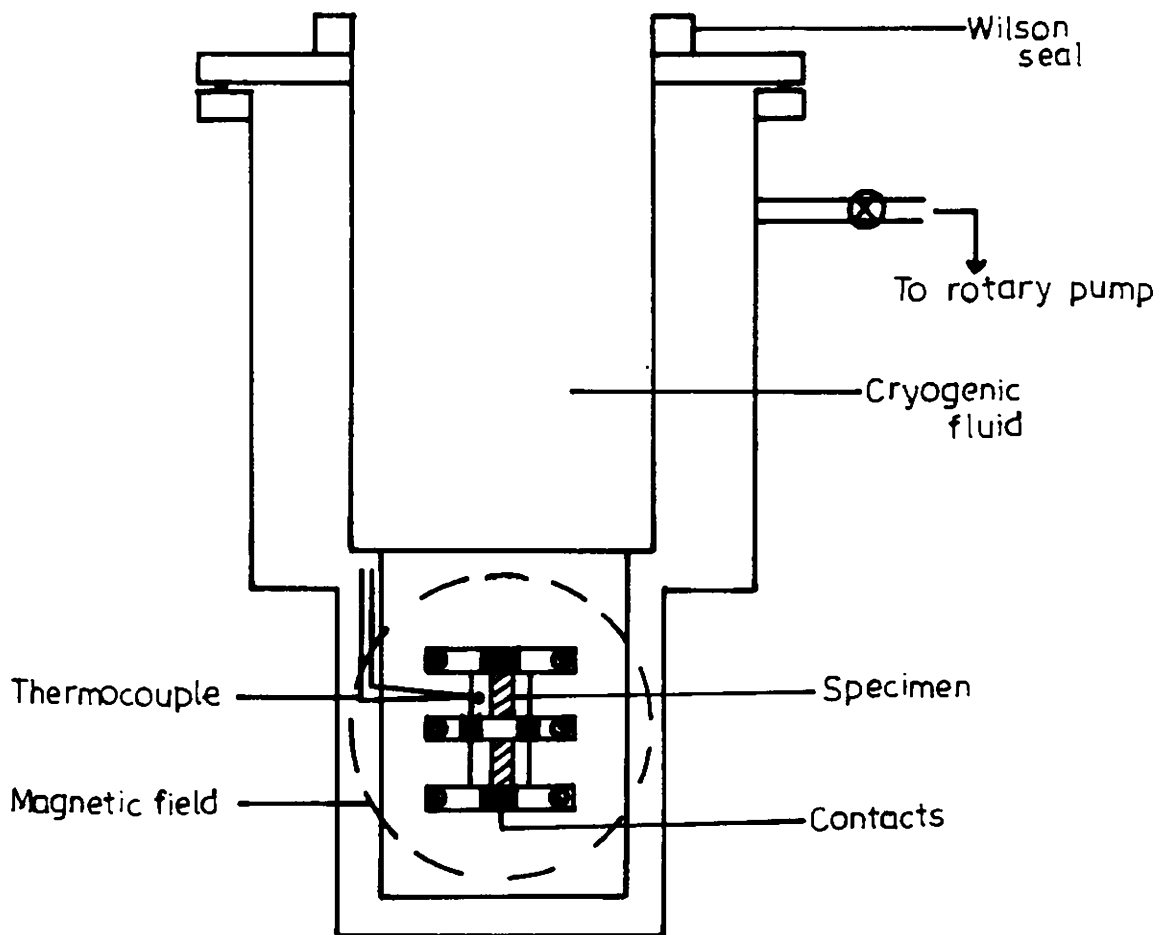
Fig.3.7 : Cross section of Hall effect measurement cell.

Films for Hall effect measurements were deposited onto 3×1 cm^2 glass substrates with the aid of suitable masks. Readings were taken with direction of the current normal and reversed and the average of two readings was taken as true Hall voltage.

The sign of the Hall voltage depends on the sign of the charge of the current carriers. Thus electrons, being negatively charged, lead to a negative Hall voltage and holes lead to a positive Hall voltage. That is, the sign of Hall coefficient indicates whether the conductivity is n-type or p-type, which is a very valuable information in the case of semiconductors.

3.6. THERMOELECTRIC POWER DETERMINATION

The measurement of the thermoelectric power requires the establishment of a temperature difference ΔT between the two junctions, the determination of ΔT (which can be measured by finding the junction temperatures T_1 and T_2) and the measurement of the voltage ΔV developed between the two junctions. Ideally, the thermoelectric power is given by the ratio $\Delta V / \Delta T$ for $\Delta T \rightarrow 0$. In practice, thermoelectric power is found as a function of temperature by using ΔT values as small as the overall accuracy of the measurement allows; the temperature difference should,

however, never be more than a few percent of the
ambient temperature of the sample.

The following considerations are essential
for the design of a suitable apparatus for the deter-
mination of the thermoelectric power: (a) the sample
and the thermocouples should be placed in vacuum,
(b) very thin electrical leads to the sample and thermo-
couples should be used to reduce errors due to thermal
conduction, (c) radiation loss should be minimised by
appropriate shielding and (d) extremely good thermal
contacts must exist between sample and thermocouples
and between sample and heat sink; thermocouple junction
must be as small as possible.

Suitably masked thin film samples for thermo-
electric measurements were prepared on glass substrates
with dimensions 2 cm x 1 cm. Electrical contacts to the
samples were made using pressed indium and silver paint.
The setup for thermoelectric power measurement is as
shown in fig.3.8. This is an all metal cell and can be
evacuated to 10^{-2} torr. This is provided with a cold
fringer which is used to cool one end of the sample down
to liquid nitrogen temperature. All electrical insulat-
ion inside the cell is of teflon. The thin film is fixed
on a stainless steel block. The bottom end of this block
is heated by a heater fixed in contact with the block

Wilson seal

To rotary pump

Cryogenic fluid

Contact leads

Thermocouples

specimen
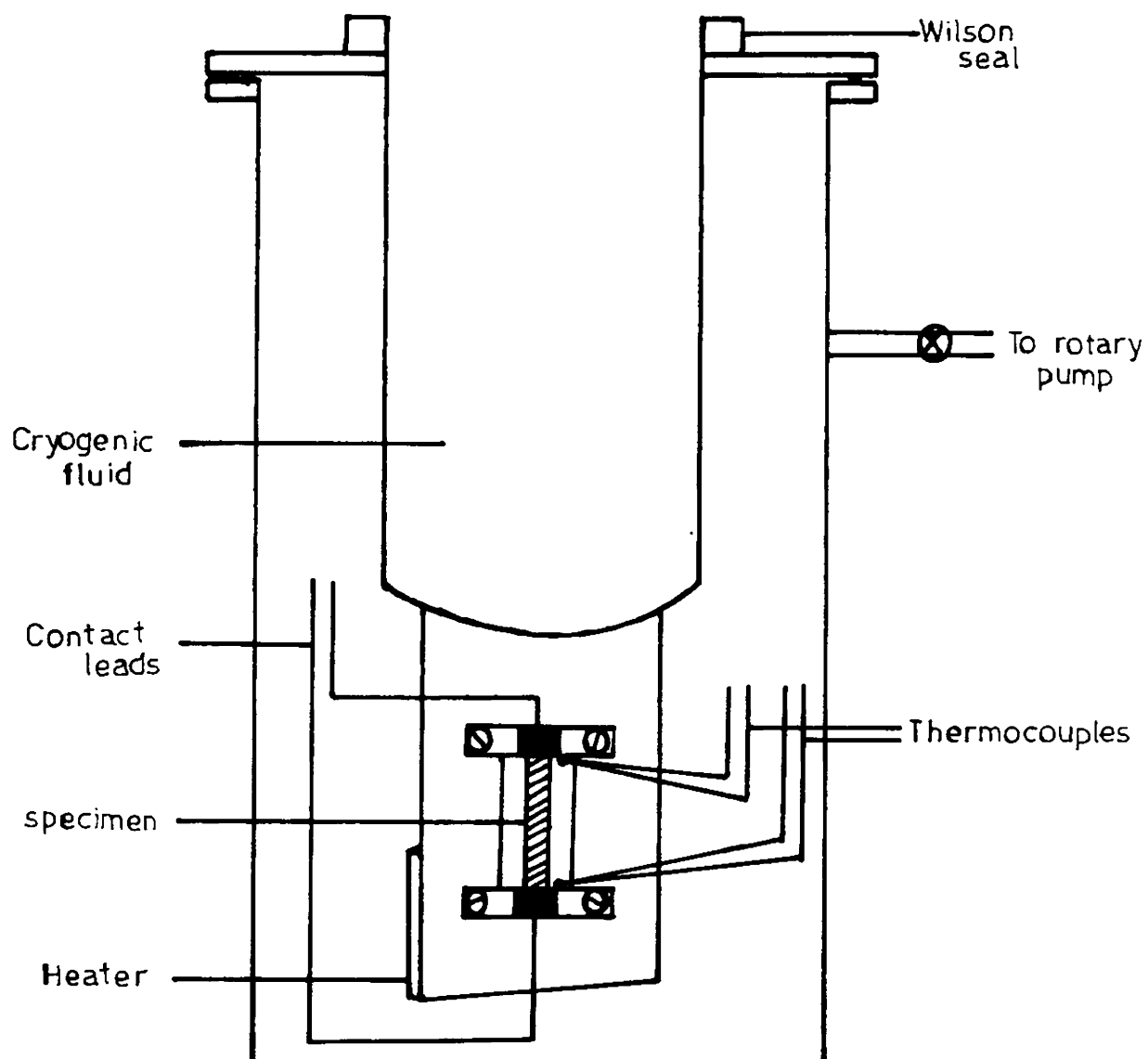
Heater

Fig.3.8 : Thermoelectric power measurement setup.

and the upper end is connected to a liquid nitrogen
reservoir. By adjusting the current through the
heater and liquid nitrogen in the reservoir we can
maintain a temperature gradient between the two ends
of the thin film sample. The temperatures of the two
ends were measured with cromel-alumel thermocouples
pressed onto the film using teflan strips and which
were connected to $4\frac{1}{2}$ digit, 200 mV, digital panel ·
meters. Voltage developed between the two ends was
measured using a Keithly Model No.181 digital Nano-
voltmeter.

A simple and convenient technique to test the
type of carriers,making use of the thermoelectric pro-
perty of the semiconductor, is known as the hot probe
method. When one end of the sample is heated by a hot
probe, carriers there get a high velocity and drift to
the cold end. This produces a disturbance in the equili-
brium distribution of carriers and sets up an electric
field which opposes the flow of carriers. This electric
field will be positive with respect to the cold end if
the carriers are electrons and negative if the carriers
are holes.

One probe of a microvoltmeter is heated with a
soldering iron for a few minutes and both the probes

(hot and cold) are touched to the sample and the deflection is observed. If the hot probe voltage is positive with respect to the cold one, the sample is n-type and if the voltage is negative, the sample is p-type.

3.7. DETERMINATION OF DIELECTRIC CONSTANT

The capacitance, C of a system with arbitrary electrode geometry is directly proportional to a characteristic property of the insulation material which is called permittivity. When normalized with respect to air or vacuum, this quantity is known as dielectric constant, $\in$ of the material

$$\in = \frac{C}{C_o}$$

where C_o is the capacitance of the system with air or vacuum instead of the material.

The dielectric measurements of amorphous lead sulphide films have been carried out using the metal-semiconductor-metal (MSM) structure as shown in fig.3.9. Gold electrode was deposited on cleaned glass substrate, with proper masking. Amorphous PbS film was then deposited above this electrode. In ordinary MIM structures another metal electrode is deposited above the film.

gold   indium   a-PbS
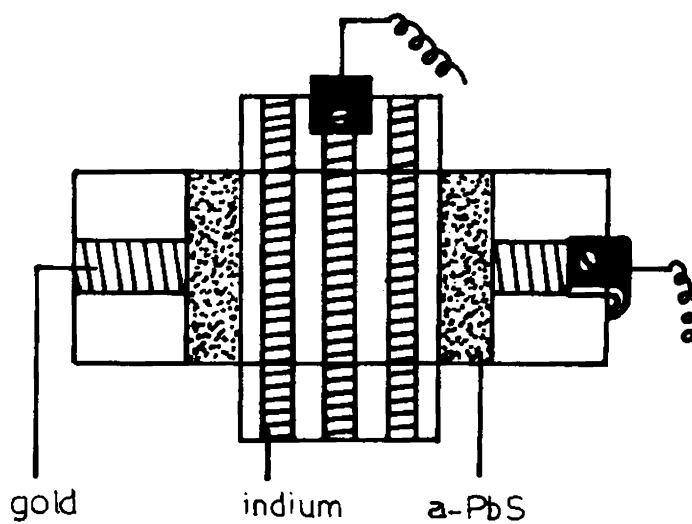
Fig.3.9 : MIM system for the measurement of dielectric
constant.
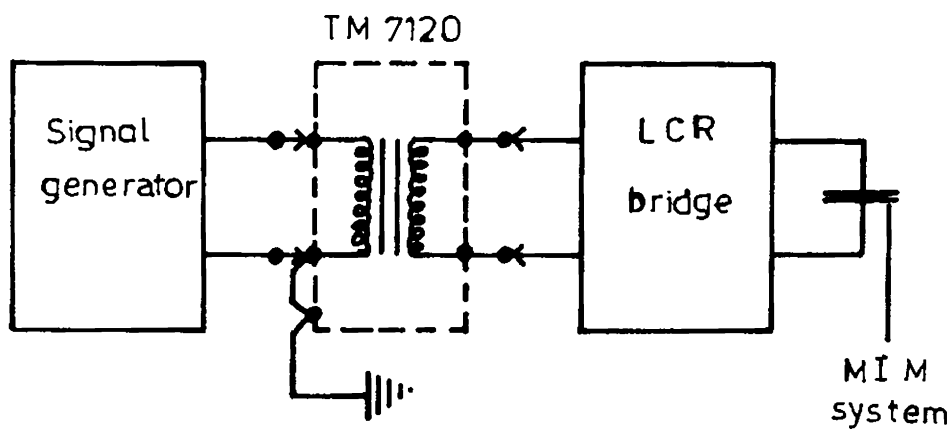
Fig.3.10 : Connection diagram of the setup for the
dielectric measurement.

But in the case of amorphous PbS films an electrode
overlayer deposition was sufficient to partly crystall-
ise the amorphous film. So, on another glass substrate
very thick Indium electrodes were deposited and these
were clamped tightly with the amorphous PbS film. The
capacitance was measured using a Marconi TF 2700 LCR
Bridge. The capacitances at different frequencies rang-
ing from 20 Hz to 20 KHz were measured using an external
signal generator in conjunction with a Marconi isolating
transformer TM 7120. The connection diagram of the setup
is as shown in fig.3.10.

From the capacitance value measured, knowing
the effective area and thickness of the film the dielectric
constant was calculated.

3.8. DETERMINATION OF OPTICAL CONSTANTS OF THIN FILMS

Determination of optical constants such as
refractive index n and extinction coefficient k, have
got much importance in solid state physics. Measurement
of these quantities as a function of wavelength can give
valuable information regarding structure and bonding.

There are different methods to measure n and k;
usual methods are spectroscopic ellipsometry, simultane-
ous measurement of transmission and reflection, and the

measurement of reflection/transmission only. Spectro-
scopic ellipsometry (which is the most precise techni-
que) has the advantage that the material need not be
transparent to the radiation used, but this method is
applicable only in the regions of wavelength where
polarizers and analysers are available. Mathematical
calculations involved in this case are also much compli-
cated. Simultaneous measurement of transmission and
reflection is the most used method for the measurement
of n and k. This method is applicable in any region of
the spectrum if suitable light sources and detector are
available and also if the material is fairly transparent.
In the highly absorbing regions of the spectra of a mater-
ial, measurement of reflectivity is the only method
available.

Recently Manifacier et. al /5/ proposed a new
calculation following traditional methods for deducing
optical constants and thickness from the fringe pattern
of the transmission spectrum of a thin transparent di-
electric film surrounded by non-absorbing media. This
method is very much simple, calculations are directly pro-
grammable, and the accuracy is of the same order as for the
other conventional methods. Because of its extreme simpli-
city and availability of commercial scanning spectrophoto-
meter in the UV-Vis-NIR regions of wavelength, this

method was used in the studies reported in this thesis.

Fig.3.11 represents a thin film with a complex refractive index $\eta = n - ik$, bounded by two transparent media with refractive indices, n_0 and n_1. Considering a unit amplitude for the incident light, in the case of normal incidence, the amplitude of the transmitted wave is given by

$$A = \frac{t_1 t_2 \exp(-2\pi i \eta t/\lambda)}{1 + r_1 r_2 \exp(-4\pi i \eta t/\lambda)} \qquad (3.8.1)$$

in which t_1, t_2, r_1, r_2 are the transmission and reflection coefficients at the front and rear faces. The transmission of the layer is given by

$$T = \frac{n_1}{n_0} |A|^2 \qquad (3.8.2)$$

In the case of weak absorption with $k^2 \ll (n-n_0)^2$ and $k^2 \ll (n-n_1)^2$

$$T = \frac{16\, n_0 n_1 n^2 \alpha_1}{c_1^2 + c_2^2 \alpha_1^2 + 2c_1 c_2 \alpha_1 \cos(4\pi nt/\lambda)} \qquad (3.8.3)$$

where $C_1 = (n + n_0)(n + n_1)$, $C_2 = (n - n_0)(n_1 - n)$ and $\alpha_1 = \exp(-4\pi kt/\lambda) = \exp(-\alpha t)$. $\qquad (3.8.4)$

α is the absorption coefficient of the thin film.

In the usual case $(n > n_1$, corresponding to a semiconducting film on a transparent non-absorbing
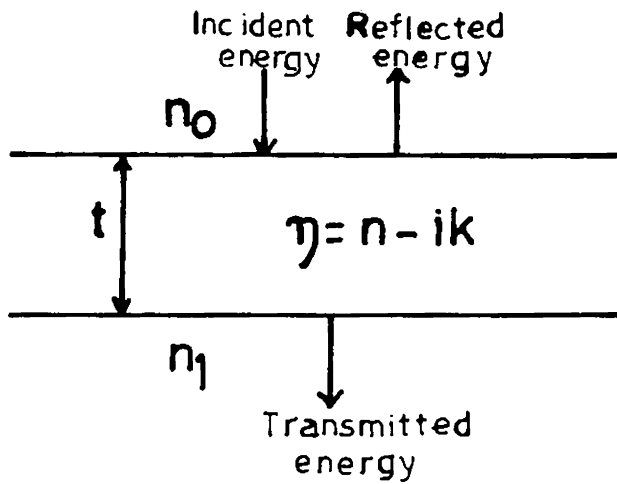
Fig.3.11 : Reflection and transmission of light by a single film.
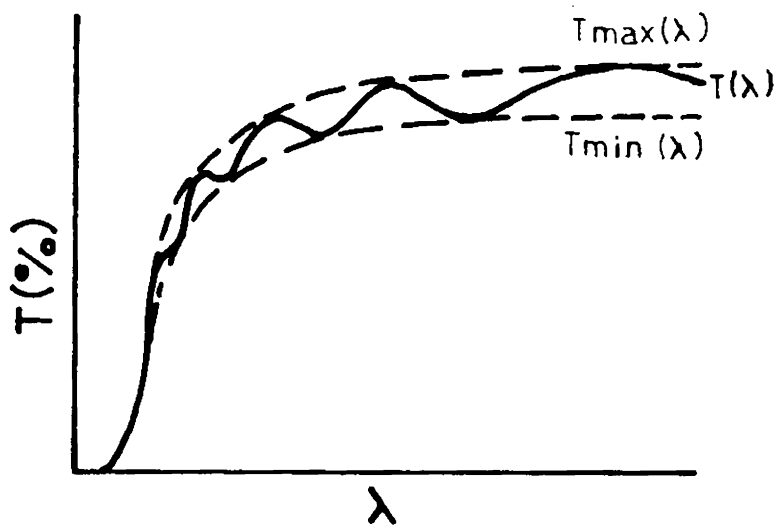
Fig.3.12 : Typical transmission spectrum for a thin film of uniform thickness.

substrate, $C_2 < 0$), the extreme values of the trans-
mission are given by the formulae

$$T_{max} = 16 \, n_o n_1 n^2 \alpha_1 / (C_1 + C_2 \alpha_1)^2 \qquad (3.8.5)$$

$$T_{min} = 16 \, n_o n_1 n^2 \alpha_1 / (C_1 - C_2 \alpha_1)^2 \qquad (3.8.6)$$

Consider T_{min} and T_{max} as continuous functions of λ
through $n \, (\lambda)$ and $\alpha_1 \, (\lambda)$. These functions which are
the envelopes of the maxima $T_{max} \, (\lambda)$ and the minima
$T_{min} \, (\lambda)$ in the transmission spectrum are shown in
fig.3.12. The equations (3.8.5) and (3.8.6) give

$$\alpha_1 = \frac{C_1 \left[1 - (T_{max}/T_{min})^{1/2}\right]}{C_2 \left[1 + (T_{max}/T_{min})^{1/2}\right]} \qquad (3.8.7)$$

Then from equation (3.2.5)

$$n = \left[N + (N^2 - n_o^2 \, n_1^2)^{1/2}\right]^{1/2} \qquad (3.8.8)$$

where

$$N = \frac{n_o^2 + n_1^2}{2} + 2 \, n_o \, n_1 \, \frac{T_{max} - T_{min}}{T_{max} \, T_{min}}$$

Thus n can be determined knowing T_{max}, T_{min}, n_1 and n_o
at the same wavelength. Using this value of n_1 we can
determine α from equations (3.8.4) and (3.8.7).

Outside the region of fundamental absorption

for higher wavelengths, the dispersion of n and k is not very large. The maxima and minima of T in equation (3.8.3) occur for

$$4\pi nt/\lambda = m\pi \qquad (3.8.9)$$

where m is the order number.

The thickness t of the layer can be calculated from two maxima or minima using above equation:

$$t = \frac{M \lambda_1 \lambda_2}{2\left[n(\lambda_1)\lambda_2 - n(\lambda_2)\lambda_1 \right]} \qquad (3.8.10)$$

where M is the number of oscillations between the two extrema (M = 1 between two consecutive maxima or minima); λ_1, $n(\lambda_1)$ and λ_2, $n(\lambda_2)$ are the corresponding wavelengths and indices of refraction. Knowing t and α_1 we are able to calculate the extinction coefficient k from equation (3.8.4).

The following conditions have to be satisfied for getting good results.

(i) To obtain good fringe pattern, which is necessary for the precise measurement of refractive index, the difference between film refractive index n and the substrate refractive index n_1 should be as great as possible.

(ii) The effective band width of the spectrophoto-
meter should be kept smaller than the half width
of the interference maximum when using a $0.2-2\mu m$
spectrophotometer, this leads to an upper limit
for the thickness of the film of the order of
$10\mu m$.

(iii) The variation of n and k with the wavelength
should be small; this condition fails in the
vicinity of the fundamental absorption short
wavelength region.

In the region of fundamental absorption,
another simpler method may be used to measure α.

Transmission through a film on a transparent
substrate in a medium of refractive index n_o is given by

$$T = \frac{16\, n_o n_1\, (n^2 + k^2)}{\left[(n_o + n)^2 + k^2\right]\left[(n_1 + n)^2 + k^2\right]}\, \exp(-\alpha t) \quad (3.8.11)$$

In weakly absorbing regions of the spectra, $n^2 \gg k^2$,
this equation approximates to

$$T = \frac{16\, n_o\, n_1\, n^2}{(n_o + n)^2\, (n_1 + n)^2}\, \exp(-\alpha t) \quad (3.8.12)$$

If we have two samples with thicknesses t_1 and t_2 and if
the samples are put in the sample and reference beam of

the spectrophotometer,

$$T_1 = \frac{16 \, n_o \, n_1 \, n^2}{(n_o + n)^2 \, (n_1 + n)^2} \exp(-\alpha t_1) \qquad (3.8.13)$$

for the specimen in the sample beam and

$$T_2 = \frac{16 \, n_o \, n_1 \, n^2}{(n_o + n)^2 \, (n_1 + n)^2} \exp(-\alpha t_2) \qquad (3.8.14)$$

for the specimen in the reference beam.

The spectrophotometer displays the log of the ratio of the two transmissions, and hence for any particular wavelength

$$\ln (T_2/T_1) = \alpha t \qquad (3.8.15)$$

where $t = t_1 - t_2$. From this equation α may be determined.

The advantage of this method is that only simple calculations are needed and one does not have to know the refractive index of the film. The only disadvantage is that a precise knowledge of film thickness is necessary as α is dependant on the difference in sample thickness, which is a small quantity.

For the optical studies a Hitachi Model No.330 UV-Vis-NIR spectrophotometer was used. This instrument can cover the wavelength range from 2500 nm to 200 nm. This instrument has got fairly high resolution and a spectral band width of 2 nm was used in the measurements.

REFERENCES

1. S. Dushman, "Scientific Foundations of Vacuum
   Technique", (John Wiley, New York, 1962) p.696.

2. R. Glang in "Hand book of Thin Film Technology",
   ed. by L.I. Maissel and R. Glang, (McGraw Hill,
   New York, 1970) p.1.

3. S. Tolansky, "An Introduction to Interferometry",
   (Longmans, London, 1955) p.170.

4. V.J. Sebastian, M.Sc. project report (Dept. of
   Physics, University of Cochin, 1982).

5. J.C. Manifacier, J. Gasiot and J.P. Fillard,
   J. Phys. E, 9 (1976) 1002.

CHAPTER   IV

PbS FILMS PREPARED BY REACTIVE EVAPORATION

4.1. INTRODUCTION

Lead sulphide (galena) is one of the oldest semiconducting materials. Historically, lead sulphide crystals were used as crystal diodes in the early days of radio. This material has been studied for a long period because of its applications in the field of infrared detectors.

A variety of physical and chemical deposition techniques have been developed for the deposition of polycrystalline and epitaxial thin films of lead sulphide /1-10/. They can be generally classified into two, vacuum evaporation and chemical deposition. The exact procedure for depositing and sensitizing these films varies between different laboratories. These techniques are usually worked out empirically and are more of an art rather than a science. For commercial applications the preferred method of preparation is chemical deposition. The yield and uniformity of response using chemical deposition are much better than that are generally obtained by evaporation.

Nobody has yet reported the reactive evaporation of lead in an atmosphere of sulphur vapour. This mode of physical deposition has been mainly developed for the preparation of high melting point oxides, nitrides, etc. which cannot be evaporated directly. Sulphides which are difficult to prepare by direct evaporation of the compounds are usually prepared by evaporating the respective metals in an atmosphere of H_2S. Obtaining high purity H_2S and handling the poisonous gas are rather difficult. Recently a technique has been developed for the preparation of sulphide films by evaporating pure sulphur and respective metal simultaneously /11-13/. This has been made possible because sulphur vapour will not stick to a clean substrate or bell jar even at room temperature at the ordinary sulphur vapour pressure ($\sim 10^{-4}$ torr) used in reactive evaporation, i.e., sulphur vapour behaves almost like a gas. Here, because of the presence of excess sulphur molecules, usually the most sulphur rich phase in any metal-sulphur system is formed, whereas in the reactive evaporation using H_2S, a sulphur deficient phase is formed. For example in the reactive evaporation of copper in an atmosphere of H_2S and sulphur, Cu_2S and CuS are formed respectively /13, 14/.

Inspite of the enormous number of theoretical and experimental investigations of the physical processes

responsible for the photoelectric, electrophysical and galvanomagnetic effects occuring in polycrystalline lead sulphide films, these processes are not yet fully understood. This is primarily due to the considerable differences between the experimental results obtained by different authors. The activation energies obtained by different authors, from the temperature dependence of the carrier concentrations, dark conductivity and photoconductivity, of polycrystalline PbS films are much different /15, 16/. Such large differences in these values are clearly due to two main factors. The first is the great variety of technologies used to prepare lead sulphide films and the second is the considerable disorder of the internal structure of each specific films. A consequence of the contradictions between the available experimental data, is the large number of theoretical models which have been proposed and which can be divided arbitarily into two classes: (1) barrier model, (2) carrier density model. These two models will be discussed in detail in chapter 5.

4.2. PREPARATION OF THE FILMS

Using reactive evaporation method thin films of lead sulphide were prepared by evaporating lead in an atmosphere of sulphur. For many materials a

stoichiometric interval exists with a limited freedom
in selecting the individual flux rates and the sub-
strate temperature /11-13, 19/. It has been found
that following parameters give good stoichiometric
films of PbS:

Pb atom flux = 1.3×10^{15} - 2.6×10^{15} atoms $cm^{-2}s^{-1}$.

S_2 molecule flux = 2.2×10^{16} - 1.1×10^{17} molecules $cm^{-2}s^{-1}$

Substrate temperature = 300 - 650K.

Evaporation was carried out in a conventional
vacuum system with an oil diffusion pump (chapter 3).
Optically flat glass slides (3x1 cm), cleaned ultra-
sonically followed by ion bombardment,were used as sub-
strates for the deposition of the films. 5N purity lead
and 4N purity sulphur were used as the evaporants. The
substrates were fixed onto a specially constructed heater
whose temperature could be controlled. The system was
then pumped to a vacuum of $\sim 10^{-5}$ torr. The temperature
of the substrate was measured by a chromel-alumel thermo-
couple placed in contact with it. Lead was evaporated
from a helical filament made of molybdenum wire and
sulphur, from a conical glass crucible with molybdenum
wire windings. The temperatures of each sources and hence
the flux could easily be controlled by adjusting the
current through the molybdenum wire. During deposition,

due to radiant heating from the lead source, the substrate temperature increased by about 15K. To minimise this the helical filament was covered with stainless steel heat shields and the temperature could then be controlled to within 2K.

When the substrate temperature had attained and stabilized at the required value with the shutter placed over the sulphur and lead sources, the current through sulphur source was switched on. The sulphur melted and the current through the source was so adjusted that a sulphur partial pressure of $\sim 10^{-4}$ was maintained in the chamber. The current through lead source was then switched on and increased to a value which could give the required lead flux. The shutter was then removed and the deposition of the compound film allowed to take place.

The sulphur vapour would not stick to the clean substrates even at room temperature at the partial pressure maintained ($\sim 10^{-4}$ torr). Only the compound film would be deposited on the substrates. When the shutter was withdrawn, the lead atoms reaching the substrate reacted with those sulphur atoms/molecules present on the substrate and the compound film was deposited. Films with thickness around 1μm were used for x-ray diffraction studies.

4.3. STRUCTURAL STUDIES

Structural characterisation of reactively evaporated thin films is very much important. It is necessary to identify the compound formed, and also to determine whether it is crystalline or amorphous in nature. For this, x-ray diffraction method was used. X-ray unit used for diffraction studies was a Philips PW 1140/90 X-ray unit fitted with a Philips PW 1050/70 goniometer.

X-ray diffraction patterns of the film substrate systems prepared at various substrate temperatures were taken. Fig.4.1(a-c) shows the x-ray diffractograms of films prepared on substrates kept at room temperature (300K), 317K and 323K. Films prepared at room temperature showed no sharp x-ray diffraction lines and as such it should be inferred that these films were amorphous in nature. These films had a uniform dark red colour in transmission. As the substrate temperature was increased sharp diffraction peaks were started to appear (fig.4.1b,c) and the dark red colour in transmission decreased. Further increase in substrate temperature resulted in films having a metallic lusture and these films were opaque to light. X-ray diffractogram of such a film is shown in fig.4.2a. This film, prepared at 400K, shows all the diffraction lines corresponding to PbS.
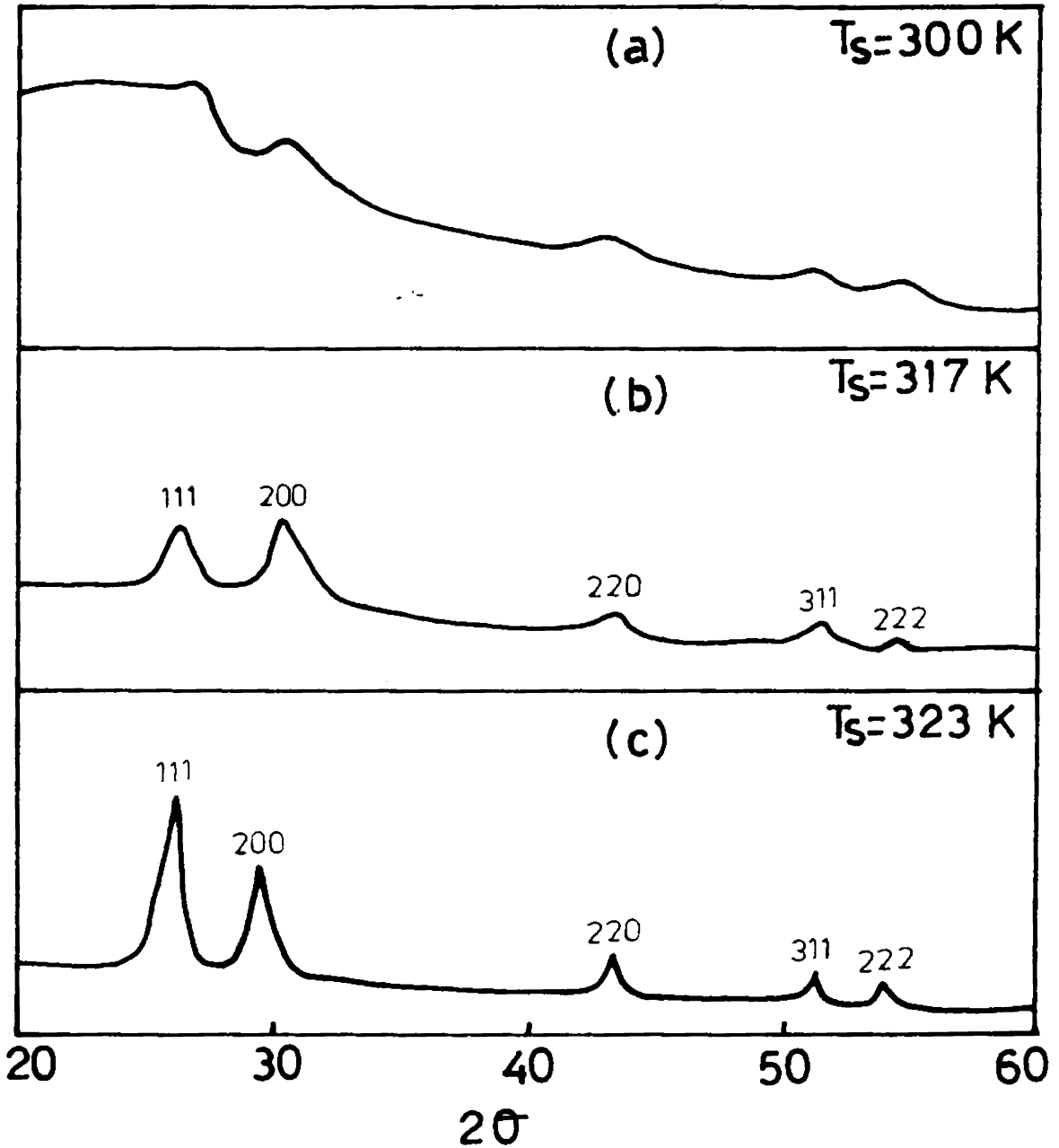
Fig.4.1 : X-ray diffractograms of films prepared at substrate
temperatures (T_s), (a) 300K, (b) 317K, (c) 323K.
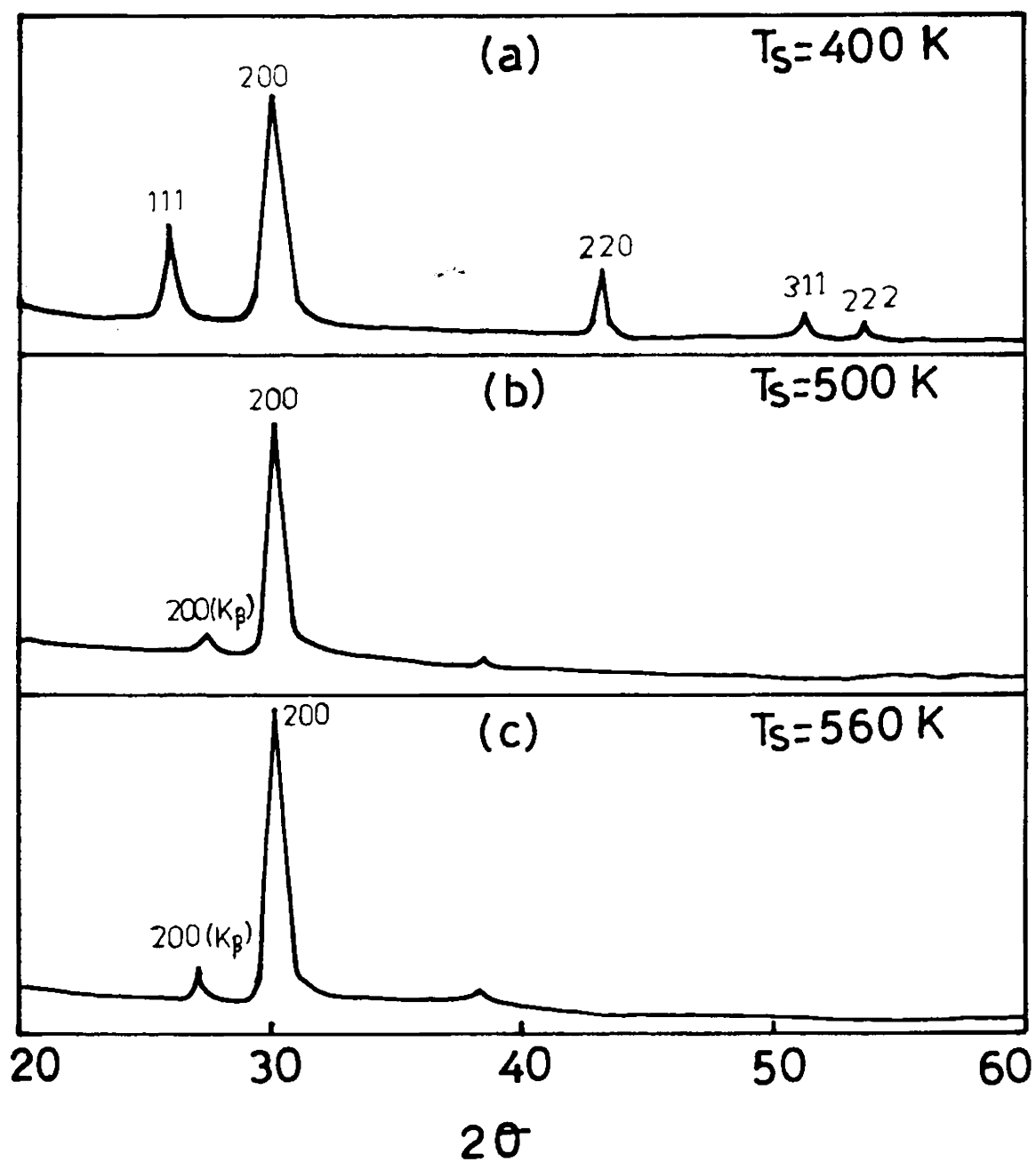
Fig.4.2 : X-ray diffractograms of films prepared at substrate temperatures (a) 400K, (b) 500K, (c) 560K.

Fig.4.2(b,c) shows the x-ray diffraction lines of films prepared at 500K and 560K. These films had grains with (100) planes parallel to the substrate surfaces.

When films were deposited onto substrates kept at room temperature, effectively the film forming atoms/ molecules were being quenched from the high source temperature to the low substrate temperature. Though chemical reaction can take place to form PbS, there was not sufficient energy for the arrangement of PbS molecules in a regular crystalline array and hence the formation of the amorphous phase. Chemical analysis of the amorphous phase films were not carried out to determine whether they really have the composition of PbS. Films prepared at substrate temperatures little above room temperature showed all the lines of polycrystalline PbS; since in both these experiments, substrate temperature was the only variable, sulphur and lead flux being held constant, it is quite possible that the amorphous phase had the composition of PbS.

As the substrate temperature was increased, the film forming particles acquire enough energy to form regular crystalline structures, and hence the formation of polycrystalline films. Further increase in substrate temperature gave a preferred orientation to the grains.

This temperature region was the same as the one which gave epitaxial films of PbS when deposited onto single crystal substrates /5/.

When the substrate temperature was increased to more than 650K, the re-evaporation rate from the substrate exceeded the deposition rate and practically no deposit was obtained.

4.4. CONCLUSIONS

PbS films have been prepared by reactively evaporated lead in an atmosphere of sulphur vapour. Films prepared onto room temperature substrates are amorphous in nature. As the temperature is increased polycrystalline films have been obtained. Further increase in substrate temperature gives films with grains oriented with (100) planes parallel to the substrate surface.

REFERENCES

1. T.S. Moss, Proc. IRE 43.(1955) 1869.

2. J. Bloem, Appl. Sci. Res. Sect. B6 (1956) 92.

3. R.J. Cashman, Proc. IRE 47 (1959) 1471.

4. D.E. Bode, Physics of Thin Films, (Ed. by G. Hass
    and R.E. Thun), Academic Press, New York and
    London, 3 (1966) 275.

5. J.N. Zemel, Solid State Surface Science, (Ed. by
    M. Green), Dekker, New York, 1 (1969) 291.

6. H.N. Acharya and H.N. Bose, Physics Status Solidi
    A6 (1971) K3.

7. B.K. Guptha, P. Thankaraj and O.P. Agnihotri,
    Solar Energy Mater, 1 (1979) 481.

8. A.J. Sievers, Top. Appl. Phys., (Ed. by B.O.Seraphin),
    31 (1979) 107.

9. A.S. Baranski and W.R. Fawcett, J. Electrochem.
    Soc., 127 (1980) 766.

10. T.K. Chaudhuri, H.N. Acharya and B.B. Nayak, Thin
    Solid Films, 83 (1981) L 169.

11. J. George and M.K. Radhakrishnan, Solid State
    Commun., 33 (1980) 987.

12. J. George and K.S. Joseph, J. Phys. D.15 (1982) 1109.

13. J. George and K.S. Joseph, J. Phys. Chem. Solids, 45 (1984) 341.

14. R.F. Bunshah, Solid Energy, Mater. 6 (1982) 445.

15. G. Giroux, Can. J. Phys. 41 (1963) 1840.

· 16. S. Espevik, Chem-Ho Wu, and R.H. Bube, J. Appl. Phys. 42 (1971) 3513.

17. J. de Klerk and E.F. Kelly, Rev. Sci. Instrum., 36 (1965) 506.

CHAPTER   V

ELECTRICAL PROPERTIES OF REACTIVELY EVAPORATED

POLYCRYSTALLINE PbS FILMS

5.1. INTRODUCTION

As stated in chapter 4, a large number of
theoretical models have been proposed to explain the
photoelectric, electrophysical and galvanomagnetic
effects occurring in polycrystalline lead sulphide
films /1-21/. These models can be divided arbitrarily
into two classes; (1) barrier model and (2) carrier
density model.

Barrier models are based on the assumptions
of the existence of potential barriers at the grain
boundaries in a polycrystalline film. According to these
models, in the interior of the grains PbS is n-type and
on the surface it is p-type, thus forming a p-n junction
/11,12,13/. This is possible because, when PbS is eva-
porated 10% of the charge decomposes /22,23/ and proceeds
to the substrate as individual lead and sulphur atoms.
Each of these sulphur atoms acts as an acceptor and each
excess lead atom acts as a donor. It is not necessary
that all these decomposed molecules recombine at the
surface. Some atoms, especially the sulphur atoms,

will evaporate from the heated substrate surface. This will lead to excess lead in the grain, thereby making them n-type. But the surface can become oxidised after deposition, due to the presence of any oxygen inside the vacuum chamber, and also while outside the chamber, to form p-n junctions. According to this theory the high resistance of the films arises from the n-p-n barriers at the surfaces between the crystallites forming the films. Under the action of light, electron-hole pairs are formed and these carriers are trapped in the n-type and p-type regions respectively; the resulting charge density lowers the barriers and hence the conductivity is increased.

On the other hand in the carrier density models, it is assumed that lead sulphide films have a p-type con-ductivity which is homogeneous throughout the grains and the high photosensitivity is attributed to various combi-nations of trapping and recombination levels, which are associated with oxygen,penetrating uniformly the interior of grains /6,10,17/.

The barrier models seems to be physically more realistic than the carrier density models because the former allow for the inhomogenity of the potential relief,

but they are very complex from the calculation point
of view /11/. This is the reason why the analytic
expressions obtained so far within the barrier model
framework can at best only account qualitatively for
the behaviour of the individual measured parameters.

Using the reactive evaporation method for the
preparation of PbS films (described in chapter 4) the
growing surface is always bombarded by sulphur atoms/
molecules at more than twenty times the required rate
for the formation of PbS. There is a good possibility
that every lead atom falling on the substrate surface
will react with sulphur atoms/ molecules. As such, un-
reacted lead remaining inside the grains, thus making
them n-type is a remote possibility and hence the present
film will not be having any such built-in p-n junctions
on the surface of the grains. But intercrystalline
potential barriers may arise due to other reasons /14,21/.
If charge carriers become localized at the grain boundar-
ies, the charged boundaries that arise could then act as
potential barriers preventing the flow of free carriers.
The charge density at the boundaries and consequently the
barrier height should be a function of temperature and
carrier density inside the blocks. For barrier heights
close to the Fermi-energy the boundaries should scatter
strongly the carriers with energies lower than the Fermi

value and much less strongly those with energies above the Fermi level. This should reduce the energy in a carrier flux and increase the thermoelectric power for the same parameters of the energy band structure.

Preparation of PbS thin films by reactive evaporation and their structural studies are described in chapter 4. Reported below is the electrical properties of these PbS films. In section 5.2 the electrical measurements on a typical PbS film prepared at a substrate temperature of 400K are reported. The variation of electrical properties with substrate temperature are reported in section 5.3.

5.2. ELECTRICAL MEASUREMENTS ON A TYPICAL POLYCRYSTALLINE FILM

Films with thickness around $0.5\,\mu m$ were used for electrical measurements. Thicknesses of the samples were found out using multiple beam interferometry. The electrical properties such as conductivity, carrier concentration, Hall mobility and thermoelectric power were measured using standard techniques (chapter 3). Satisfactory contacts to bridge shaped samples were made using pressed indium pellets. This was found to give good, noise free ohmic contacts to the films. The length to width ratio of the samples was greater than four so that

the influence of film geometry was negligible. Each measurements were repeated many times and found to be reproducible.

Hall coefficient, R_H of the samples was calculated using the relation,

$$R_H = \frac{V_H \cdot d}{I \cdot H} \times 10^8 \ cm^3/coulomb \qquad (5.2.1)$$

where V_H is the Hall voltage measured (volts), d the thickness of the film (centimeters), I the sample current (ampheres) and H the applied magnetic field (gauss).

Carrier concentration, p of the samples is given by,

$$P = \frac{1}{R_H \ e} \ / \ cm^3 \qquad (5.2.2)$$

where e is the electronic charge.

Conductivity σ was calculated using the relation,

$$\sigma = \frac{\ell}{R \cdot b \cdot d} \ (ohm. \ cm)^{-1} \qquad (5.2.3)$$

where ℓ is the length of the sample, R the resistance, b the width and d the thickness of the sample.

Product of the Hall coefficient R_H and conductivity give the Hall mobility μ_H of the film.

i.e. $\mu_H = \sigma \ R_H \ cm^2/Volt. \ Sec.$ \qquad (5.2.4)

Hall measurements showed that the films obtained were p-type. This obviously is due to the presence of excess sulphur vapour, which will not leave any unreacted lead inside the grains, during the deposition of the films.

Fig.5.1 shows the variation of conductivity on temperature for the typical PbS film prepared at 400K. It can be seen that conductivity increases with increasing temperature. The increase in conductivity with temperature is obviously due to the increase in mobility.

Fig.5.2 shows the dependence of carrier concentration on temperature. It may be seen that carrier concentration remains around 6×10^{17} cm^{-3} from room temperature to 125K. The essentially constant carrier density may arise from shallow acceptor levels associated with deviation from stoichiometry. As the film temperature is increased from room temperature, carrier concentration increases. It is not sure at present whether this change is due to some other impurity level or due to the onset of band to band transitions. The measurement range will have to be extended to high temperature to verify this. The indium contact used in the present case is not suitable for this.

Fig.5.3 shows the variation of mobility with temperature. Mobility increases sharply with temperature. This is typical of many polycrystalline films and is due
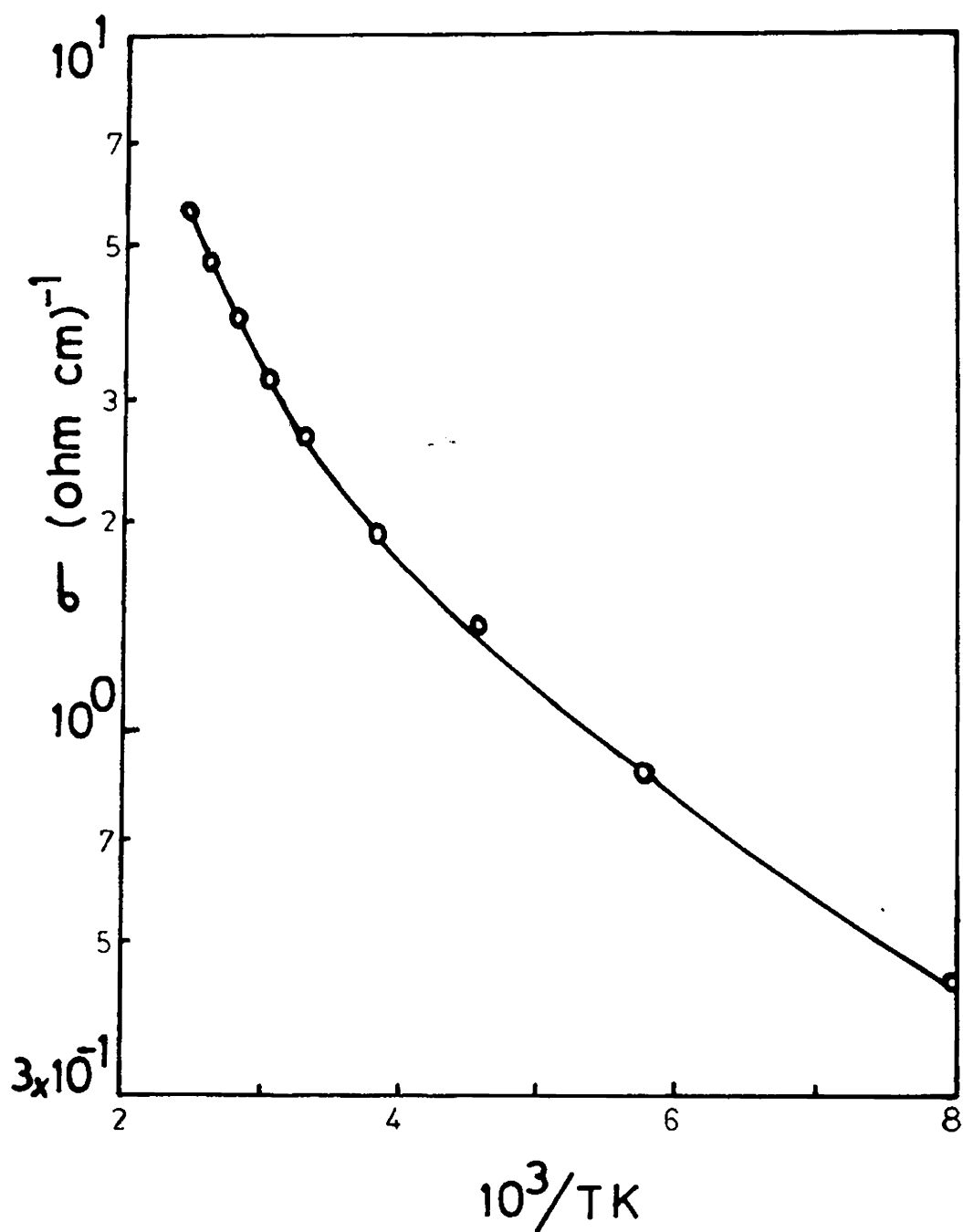
Fig.5.1 : Dependence of conductivity on inverse temperature.
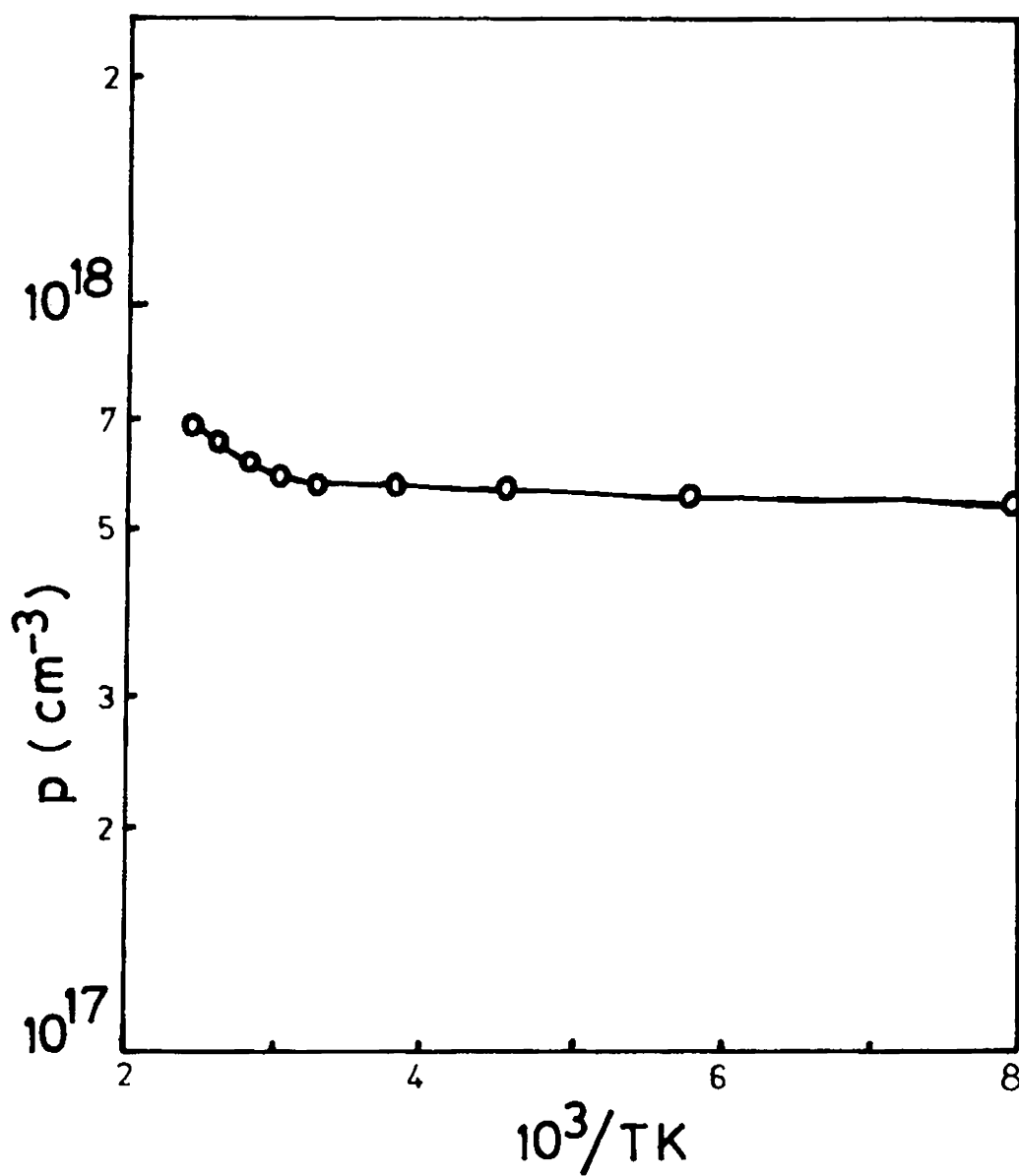
Fig.5.2 : Dependence of carrier concentration on
inverse temperature.
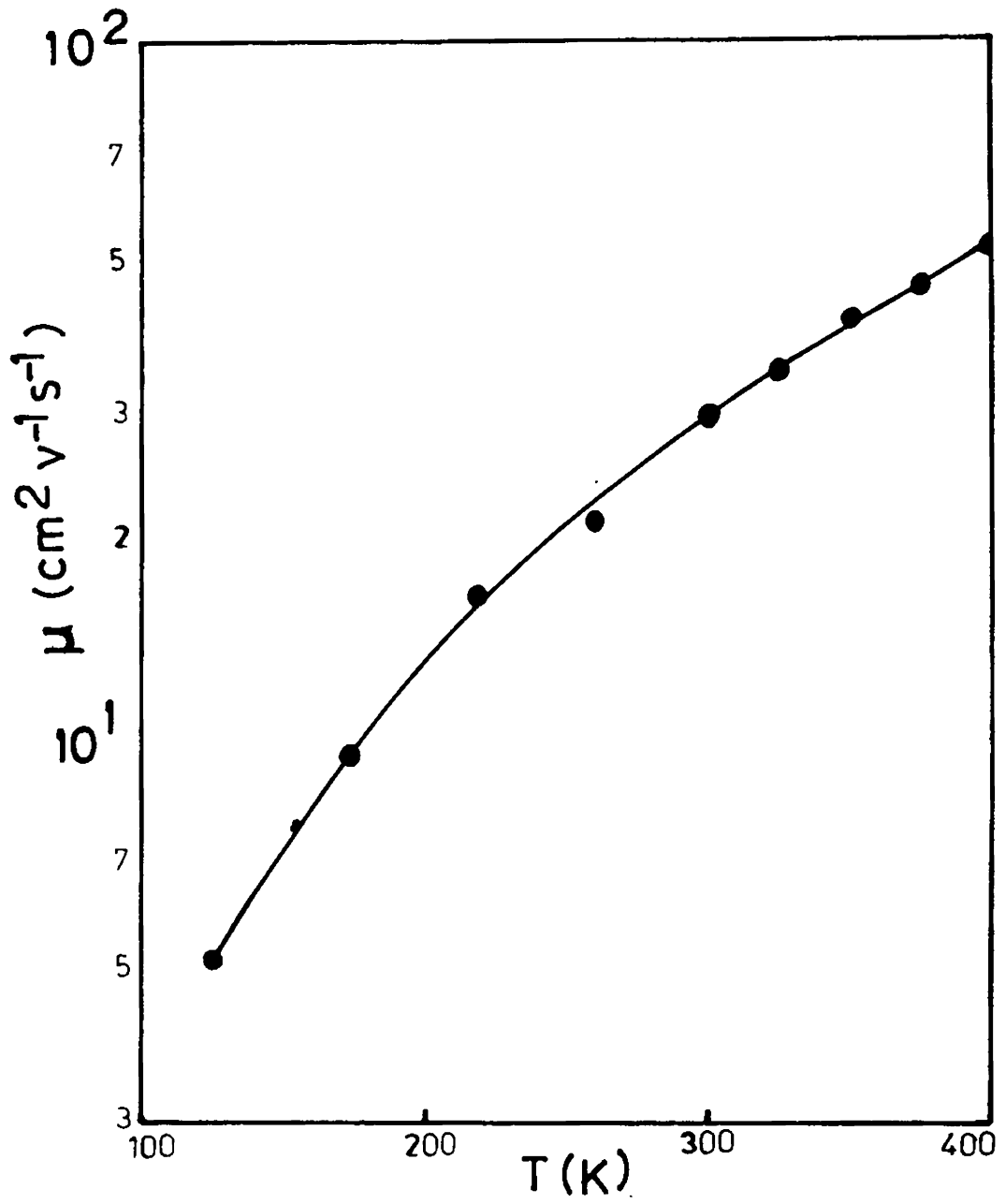
Fig.5.3 : Temperature dependence of mobility.

to the existence of potential barriers in the grain boundaries. Petritz /24/ has shown that mobility in such cases is temperature activated, and obeys a law of the form,

$$\mu = \mu_o \, T^{-1/2} \, \exp \frac{-E_a}{KT}$$

where E_a is the height of the potential barrier. The polt of $\mu \, T^{1/2}$ versus I/T is given in fig.5.4. This gives a barrier height of 0.07 $\pm$ 0.002 eV. This barrier height is approximately the same as that obtained by several other authors in chemically deposited PbS films /10, 11/.

Fig.5.5. shows the variation of thermoelectric power with temperature from 150 to 400K. It is seen that thermoelectric power increases with temperature. Bloem /25/ has reported that the room temperature value of the thermoelectric power in PbS crystals obeys the following empirical formula over a range of carrier concentration extending from 10^{17} to 10^{19} cm^{-3}

$$\alpha = \pm 200 \, (19.4 - \log n) \, \mu V/K$$

where α is the thermoelectric power and n is the carrier concentration. If we use this formula to calculate the thermoelectric power corresponding to a carrier concentration of 5.6 x 10^{17} cm^{-3}, we get a thermoelectric power
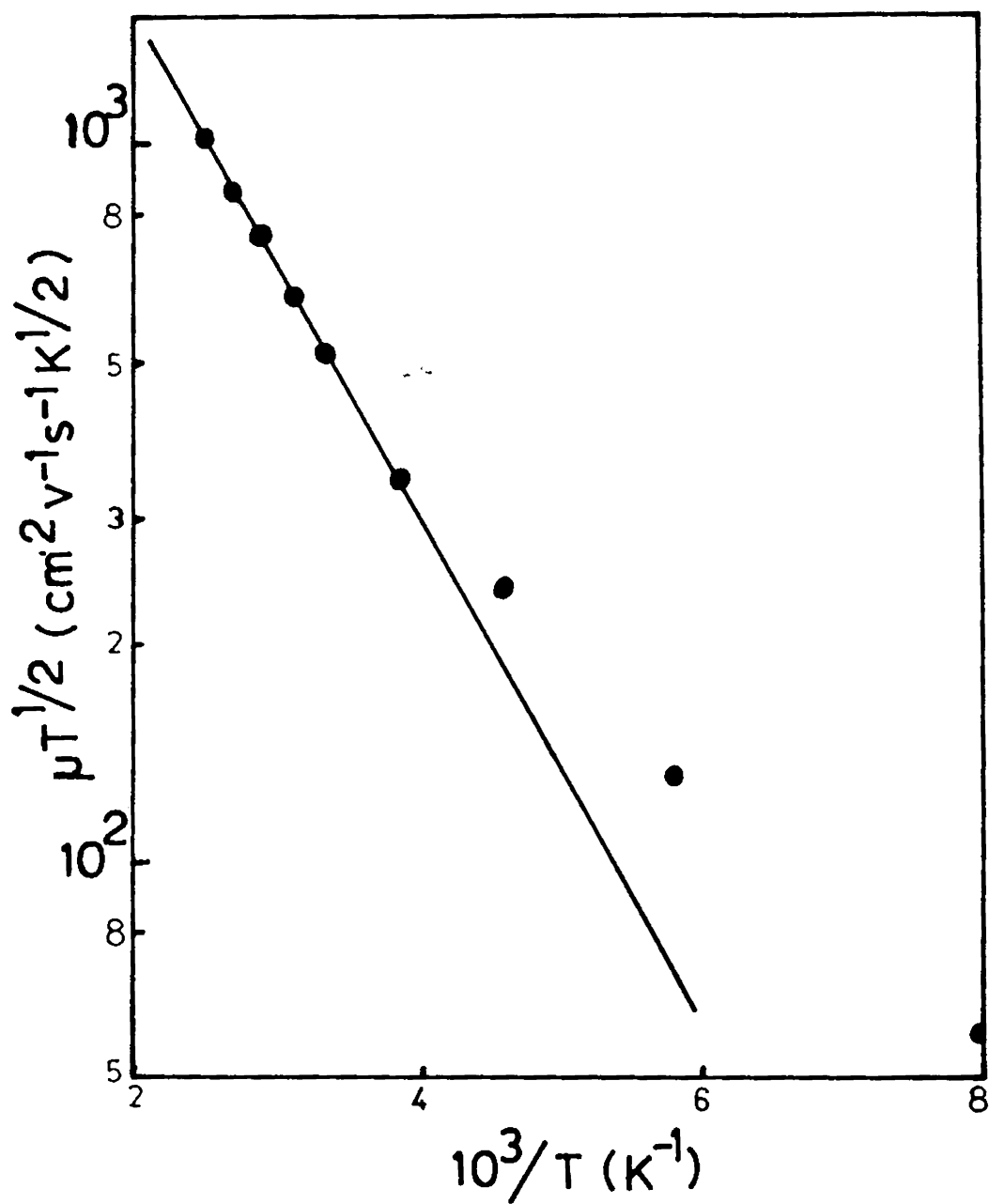
Fig.5.4 : log ($\mu T^{1/2}$) versus 1/T. Activation energy, E_a = 0.07 $\pm$ 0.002 eV.
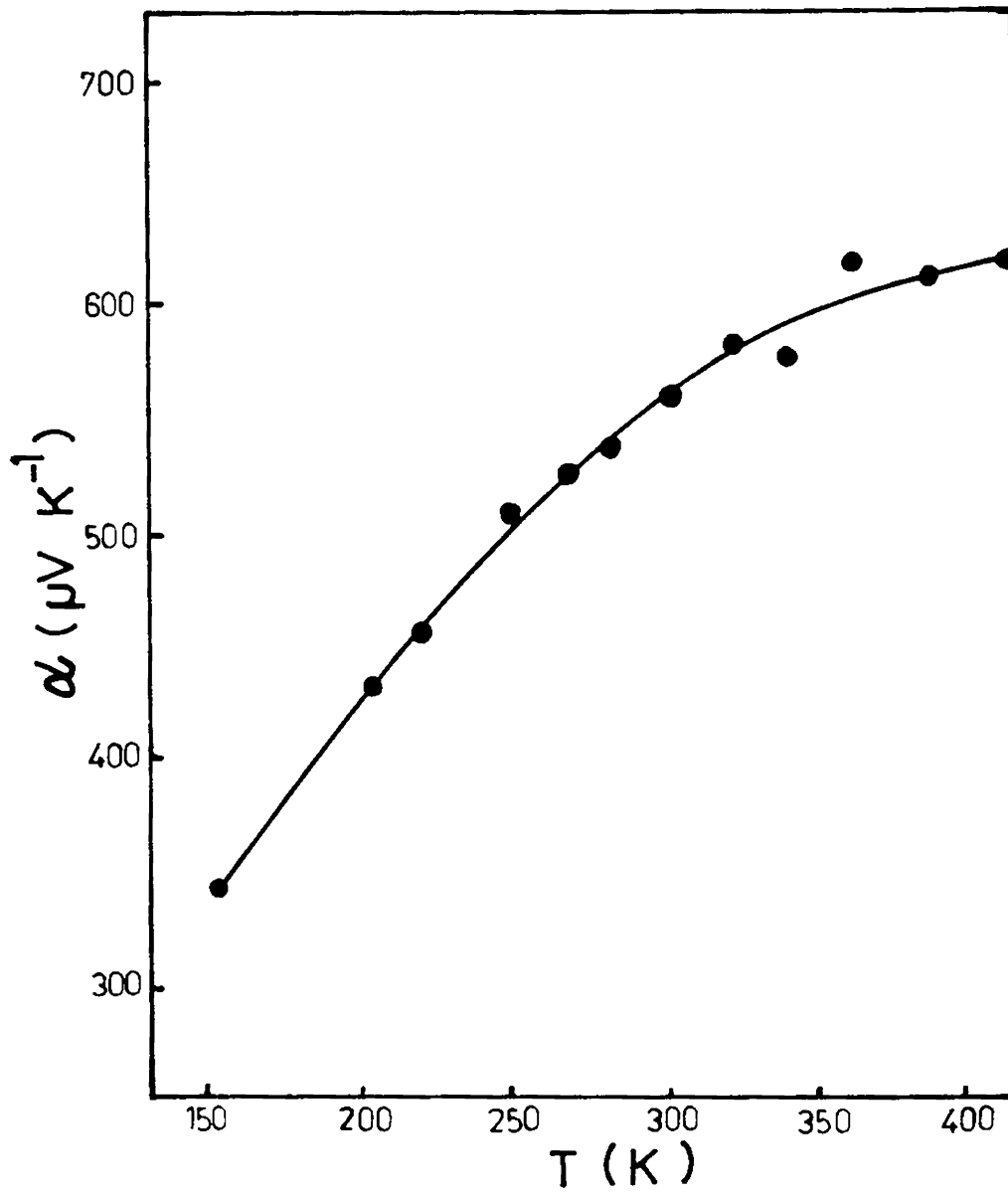
Fig.5.5 : Temperature dependence of thermoelectric power.

of 329 μV/K. But room temperature thermoelectric power
obtained in the present case if 550μV/K; which is
around 1.7 times the single crystal value. When the
heights of the potential barriers between the crystall-
ites are close to the Fermi energy, the boundaries should
scatter strongly the carriers with energies lower than
the Fermi level while the boundaries scatter much less
strongly the carriers with energies above the Fermi level.
This should reduce the energy in a carrier flux and increa-
se the thermoelectric power for the same parameters of the
energy band structure; that is, it should increase the
scattering parameter. Thermoelectric power as high as
2.3 times the single crystal value has been reported in
evaporated PbSe polycrystalline films /21, 26/ which is
very similar to PbS films. This also has been explained
as due to energy selective carrier scattering by potential
barriers associated with grain boundaries.

5.3. VARIATION OF ELECTRICAL PROPERTIES WITH SUBSTRATE TEMPERATURE

Fig.5.6 shows the variation of carrier concent-
ration (p) on inverse temperature (log p versus 1/T) for
films prepared at different substrate temperatures. It
can be seen from this graph that the carrier concentration
is less for films prepared at higher substrate temperatures
and the nature of variation of p with temperature of the
films is the same, the carrier concentration remaining
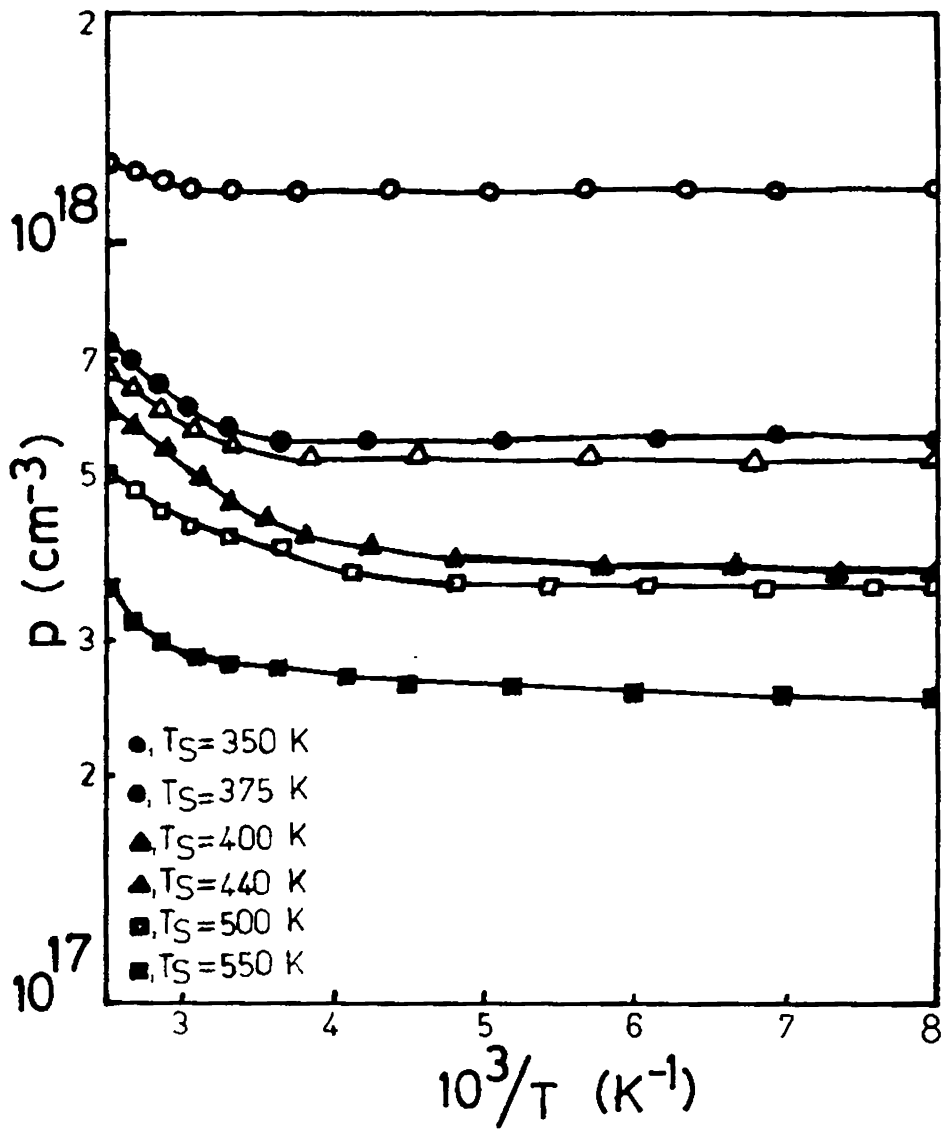
Fig.5.6 : Variation of carrier concentration on inverse
temperature (log p vs. 1/T) for films prepared
at different substrate temperatures.

constant irrespective of the substrate temperatures.
As stated earlier the growing surface of PbS is always
bombarded by sulphur atoms/molecules more than twenty
times the required rate for the formation of PbS.
P-type nature of these films is obviously due to the
presence of excess sulphur vapour, which will not leave
any unreacted lead inside the grains, during the deposit-
ion of the films. As the substrate temperature increases
the concentration of these excess sulphur will decrease
thereby decreasing p as shown in fig.5.6.

Fig.5.7 shows the variation of mobility with
temperature of the films. The substrate temperatures are
indicated in the figure. In samples prepared at high
substrate temperatures, due to the decrease in excess
sulphur atoms, the carrier concentration will be less with
consequent decrease in carrier scattering. The higher
mobility observed in samples prepared at higher substrate
temperatures can be accounted for, by this decrease in
carrier scattering. Another factor contributing to the
increase in mobility is the increase in mean free path
of the charge carriers due to the possible larger grain
size of the films prepared at higher substrate temperatures.

From fig.5.7 it can be seen that the rate of
increase in mobility with temperature remains the same
upto about 200k irrespective of the substrate temperatures
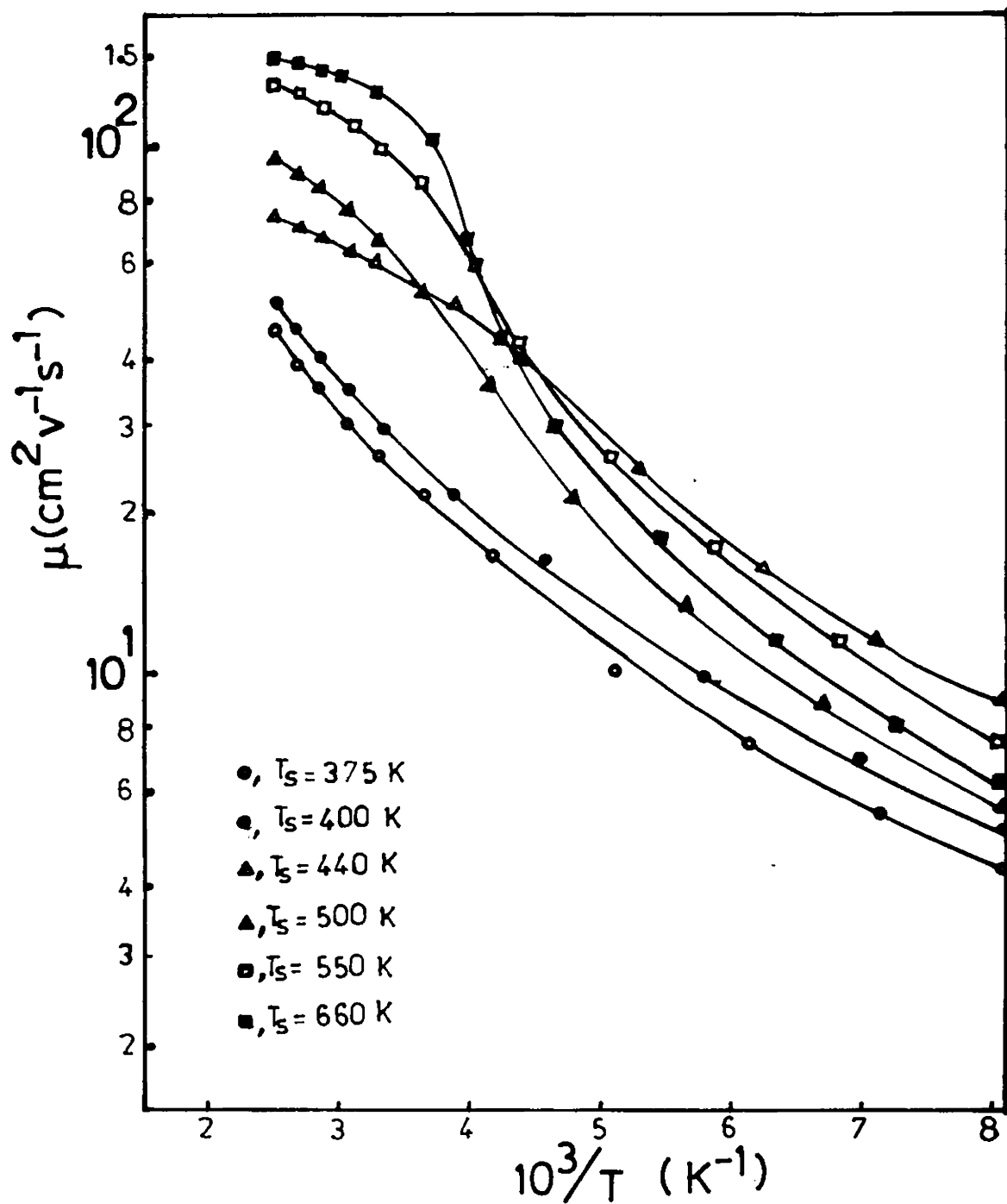
Fig.5.7 : Temperature dependence of mobility of
samples prepared at different temperatures.

of the samples. For samples prepared at higher substrate temperatures, for further increase in temperature of the films, rate of increase in mobility is observed upto about 260K and then the rate decreases. In the present mode of preparation of PbS films, it can be stated that these films consist of p-type crystallites with relatively lower resistivity separated by intercrystalline barriers. These barriers are made up of oxides of lead or lead salts /10,24/ formed by the adsorption of oxygen from the residual gas in the system, sulphur molecules and sulphur compounds formed because of the high sulphur vapour pressure used. The presence of this adsorbed oxygen and excess sulphur molecules and compounds will be less in samples prepared at higher substrate temperatures. So, it can be stated that, the barrier height decreases with increase in substrate temperature during the film preparation and the mobility in this case is thermally activated. At film temperatures below 200K, carrier transport past the potential barrier occur primarily by hole tunneling through intergrain potential barriers rather than by thermal excitation over the barriers /10,24/, for all the samples prepared at different substrate temperatures. Since the potential barrier height is less in high substrate temperature samples, the thermal excitation over potential barriers take place in these samples and is responsible for the

observed increase in the rate of change in mobility
above 200K. As the film temperature increases above
$\sim$260K, the mobility does not change appreciably in the
films prepared at high substrate temperatures. This is
because, above this temperature, the carrier transport
is fully by thermal excitation over the potential barrier,
the barrier height being less, compared to the films pre-
pared at lower substrate temperatures. From the fig.5.8
(log $\mu T^{1/2}$ versus 1/T) it is evident that activation
energy in samples prepared at high substrate temperatures
are lower compared to that prepared at low substrate tem-
peratures. Activation energy E_a obtained in case of films
prepared at 400K is 0.07 $\pm$ 0.002 eV, whereas in case of
films prepared at 600K is 0.023 $\pm$ 0.002 eV.

Fig.5.9 shows the variation of conductivity with
temperature of the films prepared at different substrate
temperatures. It can be seen that conductivity increases
with temperature in all the samples. Films prepared at
low substrate temperatures have a higher carrier concent-
ration and as such these films show a higher conductivity
at low film temperatures. It is already shown that in
samples prepared at high substrate temperatures, the mobi-
lity is higher and so in these samples the conductivity
will be mobility dominated and show higher conductivity.
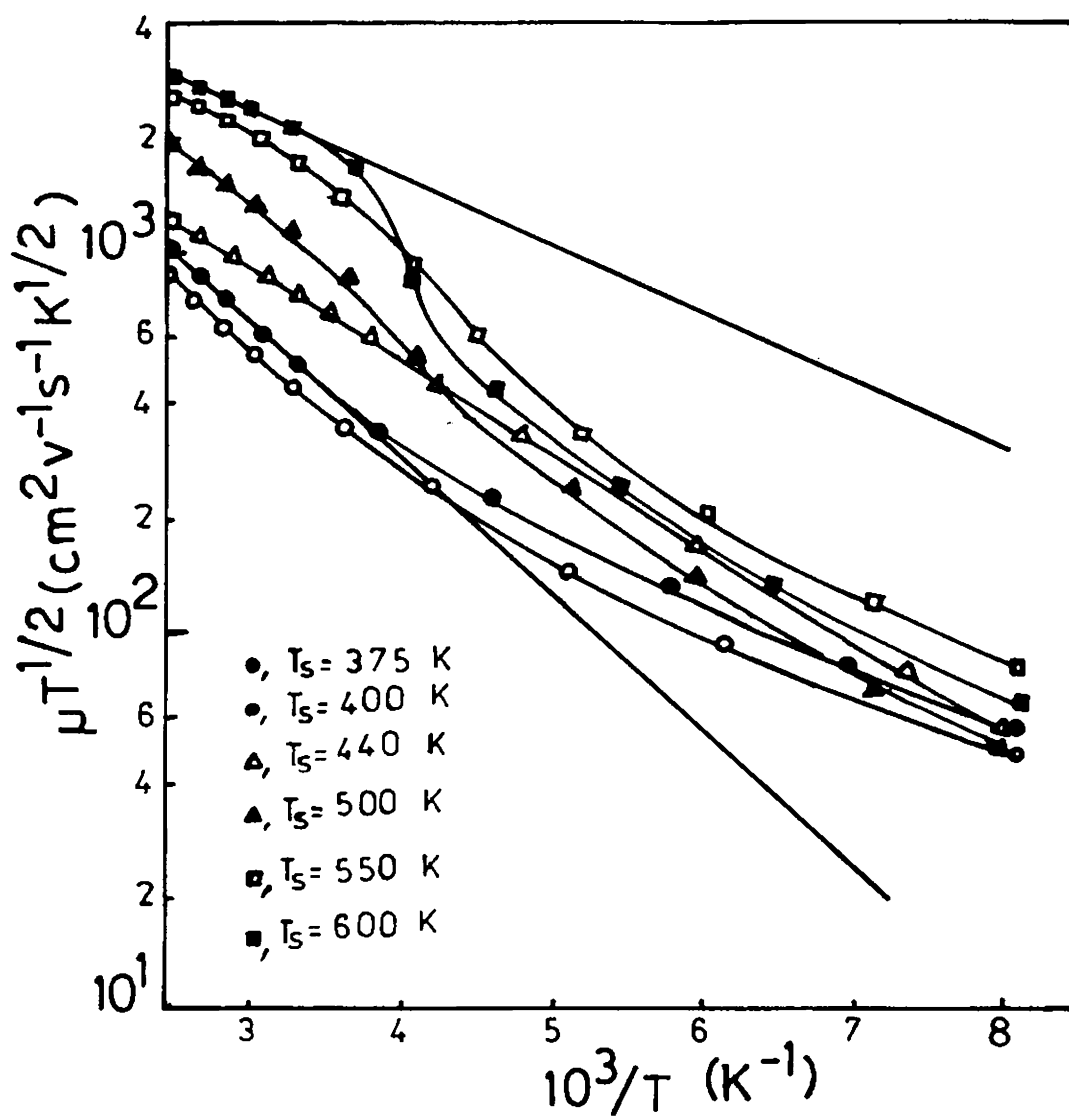
Fig.5.8 : $\mu T^{1/2}$ versus 1/T for samples prepared at different substrate temperatures.
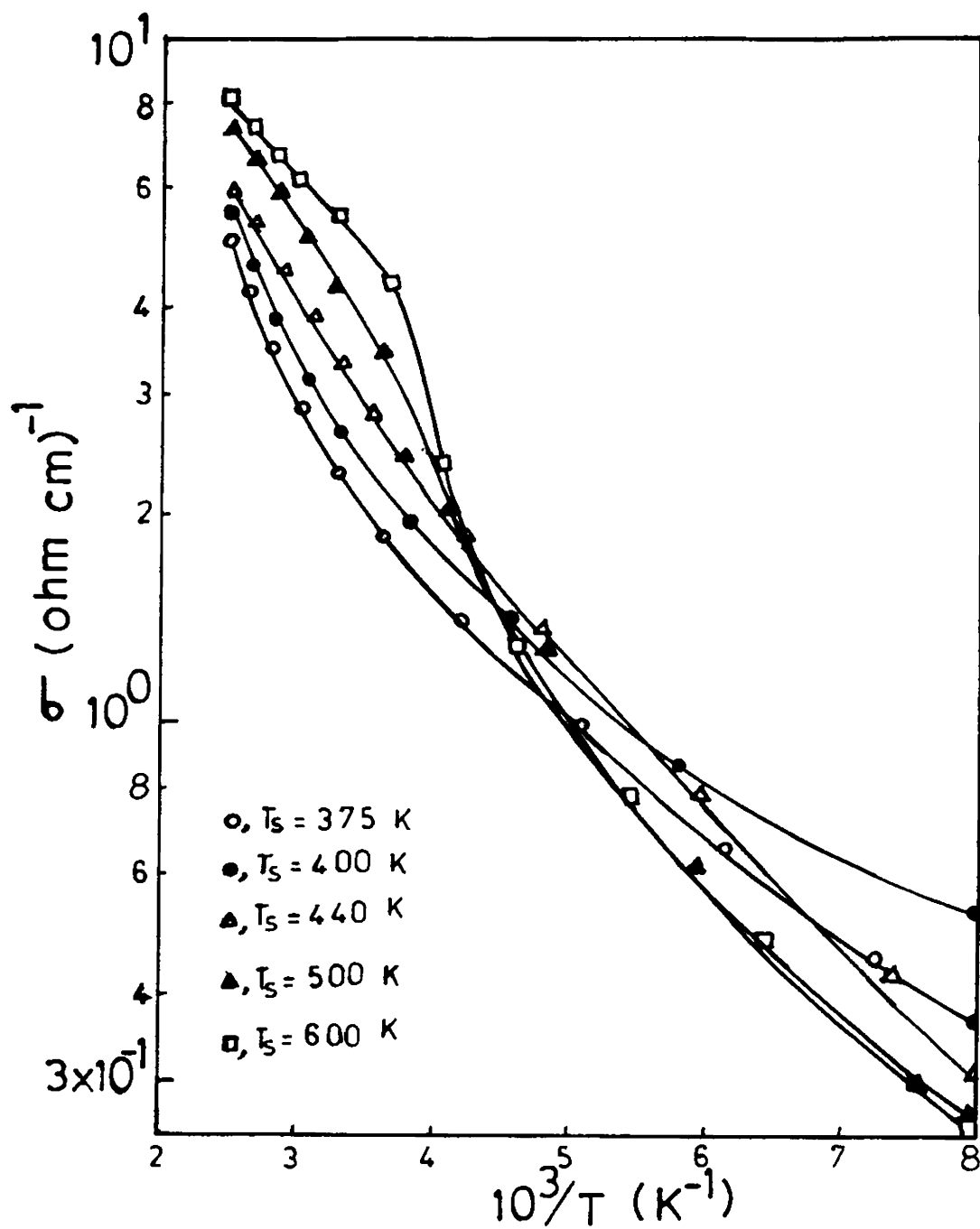
Fig.5.9 : Variation of conductivity with temperature
of the films prepared at different substrate
temperatures.

In thermal equilibrium, the thermoelectric power of a semiconductor is given by /27,28/

$$\alpha = \alpha_e + \alpha_p = \frac{\Delta V}{\Delta T} \qquad (5.3.1)$$

where α is the measured thermoelectric power, α_e is the electronic contribution, α_p is the phonon drag contribution, ΔT is the temperature difference and ΔV is the thermoelectric voltage associated with the existence of ΔT.

The value of α_e for an extrinsic semiconductor dominated by carriers of one type is given by /27,29/.

$$\alpha_e = \pm \frac{K}{e} \left(A + \ln \frac{N_i}{n_i} \right) \qquad (5.3.2)$$

where the positive sign is for holes and the negative sign is for electrons, A is the scattering parameter, N_i is the effective density of states in the band, and n_i is the density of free carriers.

From equation (5.3.2), it can be seen that an increase in carrier density results in a decrease in α_e whereas increase in scattering parameter results in an increase in α_e.

Fig.5.10 shows the variation of thermoelectric power with temperature of films prepared at different substrate temperatures. It is already seen that, as the
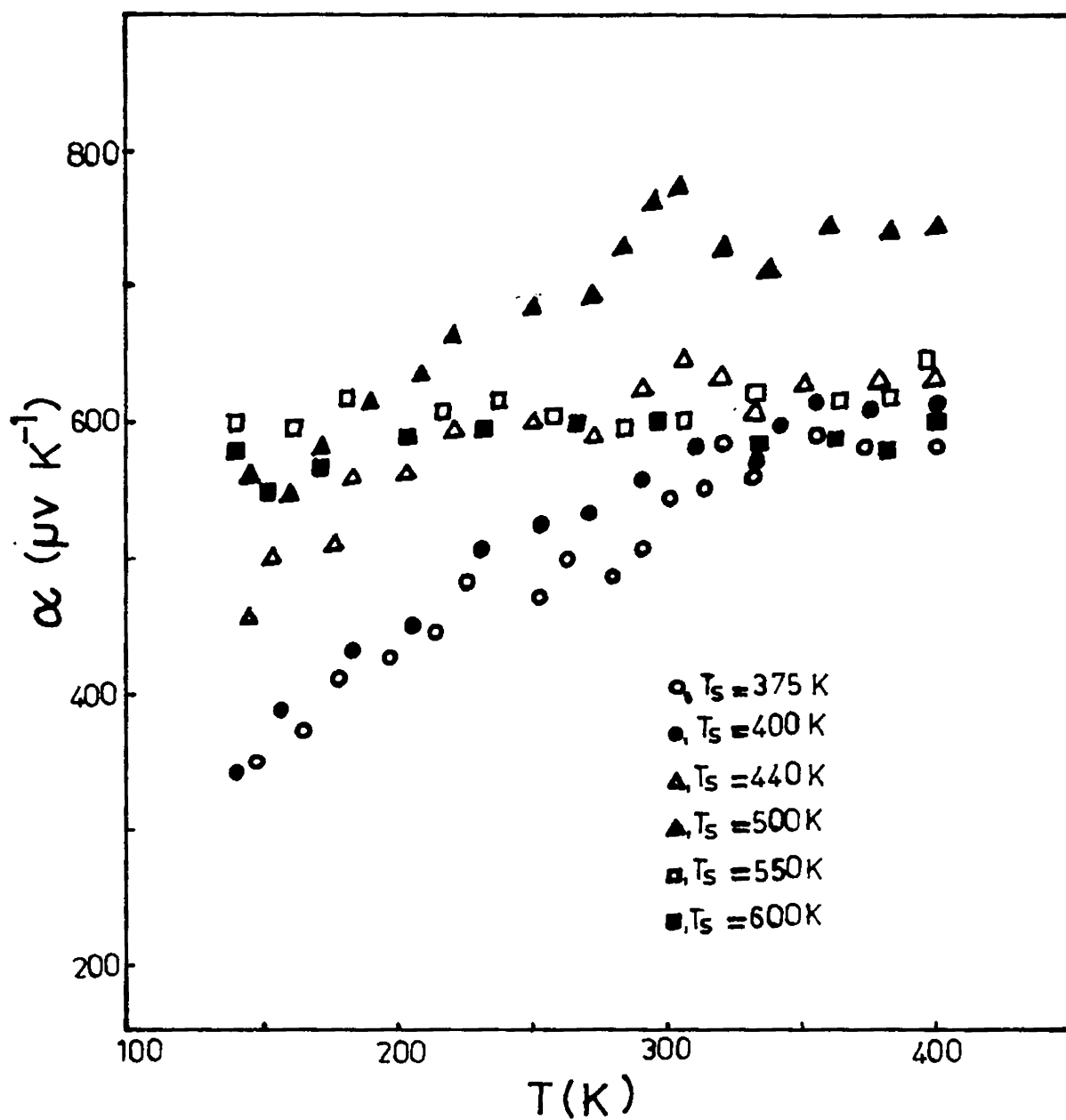
Fig.5.10 : Variation of thermoelectric power with temperature of films prepared at different substrate temperatures.

preparation temperature increases carrier concentration decreases and so it can be observed from fig.5.10 that the thermoelectric power increases with substrate temperature satisfying the relation (5.3.2) for electronic contribution for thermoelectric power. But for films prepared at substrate temperatures above 500K the thermoelectric power is found to be lower. As already pointed out, the potential barriers between **crystallites** will scatter strongly the carriers with lower energies and this should reduce the energy in a carrier flux and increase the thermoelectric power. That is, it should increase the scattering parameter /21/, It may be noted that the barrier height in samples prepared at higher substrate temperatures are lower, as evidenced from the variation of mobility with temperature for films prepared at different substrate temperatures, and so the scattering parameter A will be less in these samples. This should account for the decrease in thermoelectric power (from equation 5.3.2) in films prepared at high substrate temperatures.

5.4. CONCLUSIONS

Hall effect measurements show that the reactively evaporated PbS films are p-type and a typical PbS film prepared at 400K has a carrier concentration of $\approx 6 \times 10^{17}$ cm^{-3}. Carrier concentration decreases with

increase in substrate temperature and it is due to the
decrease in excess sulphur vapour inside the films.
The dependence of mobility with temperature is explained
in terms of intergrain potential barriers. The mobility
is thermally activated and the intergrain potential barr-
ier in a sample prepared at 400K has a height of 0.07 eV,
whereas for a sample prepared at 600K has a height of
0.023 eV. The films show a high thermoelectric power
compared to the simple crystal value and is due to the
energy selective carrier scattering by potential barriers
associated with grain boundaries. The variation in thermo-
electric power in samples prepared at different substrate
temperatures are explained on the basis of a well known
equation for electronic contribution of thermoelectric
power.

REFERENCES:

1. J.F. Woods, Phys. Rev. 106 (1957) 235.

2. D.E. Bode, Proc. Nat. Electron. Conf. 19 (1963) 630.

3. J. Volger, Phys. Rev. 79 (1950) 1023.

4. J.L. Davis and R.F. Greene, Appl. Phys. Letters
   11 (1967) 227.

5. D.P. Snowden and A.M. Portis, Phys. Rev. 120 (1960)
   1983.

6. R.L. Petritz, P.L. Lummis, H.E. Sorrows and J.F. Wood,
   Semiconductor surface physics (University of
   Pennsylvania Press, Philadelphia, 1957), p.229.

7. R.H. Bube, Appl. Phys. Lett. 13 (1968) 136.

8. R.H. Bube, ibid 14 (1969) 84.

9. G.H. Blount, R.H. Bube, and A.L. Robinson, J. Appl.
   Phys., 41 (1970) 2190.

10. S. Espevik, C. Wu and R.H. Bube, J. Appl. Phys.
    42 (1971) 3513.

11. L.N. Neustroev and V.V. Osipov, Sov. Phys. Semicond.
    18 (1984) 224.

12. E.S. Rittner, Science, 111 (1950) 685.

13. J.C. Slater, Phys. Rev. 103 (1956) 1631.

14. A.F. Gibson, Proc. Phys. Soc. B64 (1951) 603.

15. H.T. Minden, J. Chem. Phys. 25 (1956) 241.

16. V.N. Agarev and V.I. Stafeev, Sov. Phys. Semicond. 11 (1977) 990.

17. G. Giroux, Can. J. Phys. 41 (1963) 1856.

18. G. Giroux, Can. J. Phys. 41 (1963) 1840.

19. H.T. Minden, J. Chem. Phys. 23 (1955) 1948.

20. R.H. Harada and H.T. Minden, Phys. Rev. 102 (1956) 1258.

21. L.I. Bytenskii, T.S. Gudkin, E.K. Iordanishvili, S.A. Kaz'min, V.I. Kuidanov, S.A. Nemov and Yu. I. Ravich, Sov. Phys. Semicond. 11 (1977) 894.

22. R.F. Brebrick and A.J. Strauss, J. Chem. Phys. 40 (1964) 3230.

23. R.S. Allgaier and W.W. Scanlon, Phys. Rev. 111 (1958) 1029.

24. R.L. Petritz, Phys. Rev. 104 (1956) 1508.

25. J. Bloem, Philips Research Repts. 11 (1956) 273.

26. T.S. Gudkin, I.A. Drabkin, V.I. Kaidanov and O.G. Sterlyadkina, Sov. Phys. Semicond., 8 (1975) 453.

27. J.G. Harper, H.E. Mathews, and R.H. Bube, J. Appl. Phys. 41 (1970) 765.

28. C. Herring, Phys. Rev. 96 (1954) 1163.

29. R.A. Smith, Semiconductors (Cambridge University Press, Cambridge, England, 1961)

CHAPTER VI

AMORPHOUS FILMS OF PbS

6.1. INTRODUCTION

Lead sulphide, because of its applications in infrared detector technology, has been studied for a long time. Thin films of PbS obtained by direct evaporation on to amorphous substrates are polycrystalline in nature. Epitaxial films can be obtained by depositing PbS on to heated alkali halide single crystal substrates. No work has yet been reported in the literature on amorphous PbS films. In chapter 4 the preparation of PbS films using the reactive evaporation technique has been described, where lead is evaporated in an atmosphere of sulphur. It is found that when the substrates are kept below 325K, during the deposition, the films obtained are amorphous in nature. As the substrate temperature is increased polycrystalline films are obtained. In this chapter, the optical and electrical properties of these amorphous films and their crystallisation are reported.

6.2. EXPERIMENTAL DETAILS

Thin films of PbS are prepared by the reactive evaporation technique. The deposition procedure is fully

described in chapter 4. Glass/ quartz substrates of
dimensions $3 \times 1 \times 0.12$ cm^3 are used for the deposition
of the films. Amorphous PbS films deposited on to sub-
strates kept at 300K are studied and reported in this
chapter.

Two types of amorphous PbS films can be prepared
using the reactive evaporation technique. In the first
type, referred as stoichiometric films, the sulphur source
is baffled and the sulphur vapour beam does not strike the
substrate directly as such. The number of sulphur mole-
cules striking the substrate surface per unit area in unit
time in this case will be that due to the partial pressure
of sulphur vapour inside the chamber. In the second type,
referred as sulphur rich films, the sulphur source is not
baffled and evidently the number of sulphur molecules
striking the substrate surface will be more for a given
sulphur partial pressure inside the chamber. Unless other-
wise stated a-PbS films refer hereafter to stoichiometric
amorphous lead sulphide films.

Optical measurements were made in the visible and
NIR region using a Hitachi model No.330 UV-Vis-NIR spectr-
photometer. The optical constants and the thickness of
the films were calculated by the method of Manifacier et al
/1/ as explained in chapter 3. Electrical measurements

were carried out on films with thicknesses approximately
equal to 200 nm. Thicker films (>400 nm) have a tend-
ency to crack when heated. Evaporated silver and gold
electrodes have been found to give good noise free ohmic
contacts to the films. All the electrical measurements
were carried out in an evacuated all metal cell with
teflon insulated connectors. The cell has provisions
for heating and temperature measurements.

6.3. RESULTS AND DISCUSSIONS

a. Optical

    Fig.6.1 and 6.2 show the optical transmission
spectra of selected a-PbS and sulphur rich a-PbS films
respectively. Film thicknesses are indicated in the
figures. It can be seen that the films are transparent
in the NIR and red regions. Crystalline PbS film of com-
parable thickness will not be transmitting any NIR or red
light. The refractive index calculated from the trans-
mission spectra is shown in fig.6.3. Fig.6.4 shows the
absorption coefficient as a function of photon energy of
a-PbS together with sulphur rich a-PbS films. The data
for crystalline PbS films /2-4/ are also shown in the
same figure.

    It may be seen that absorption coefficient before
the onset of band to band transitions in these amorphous
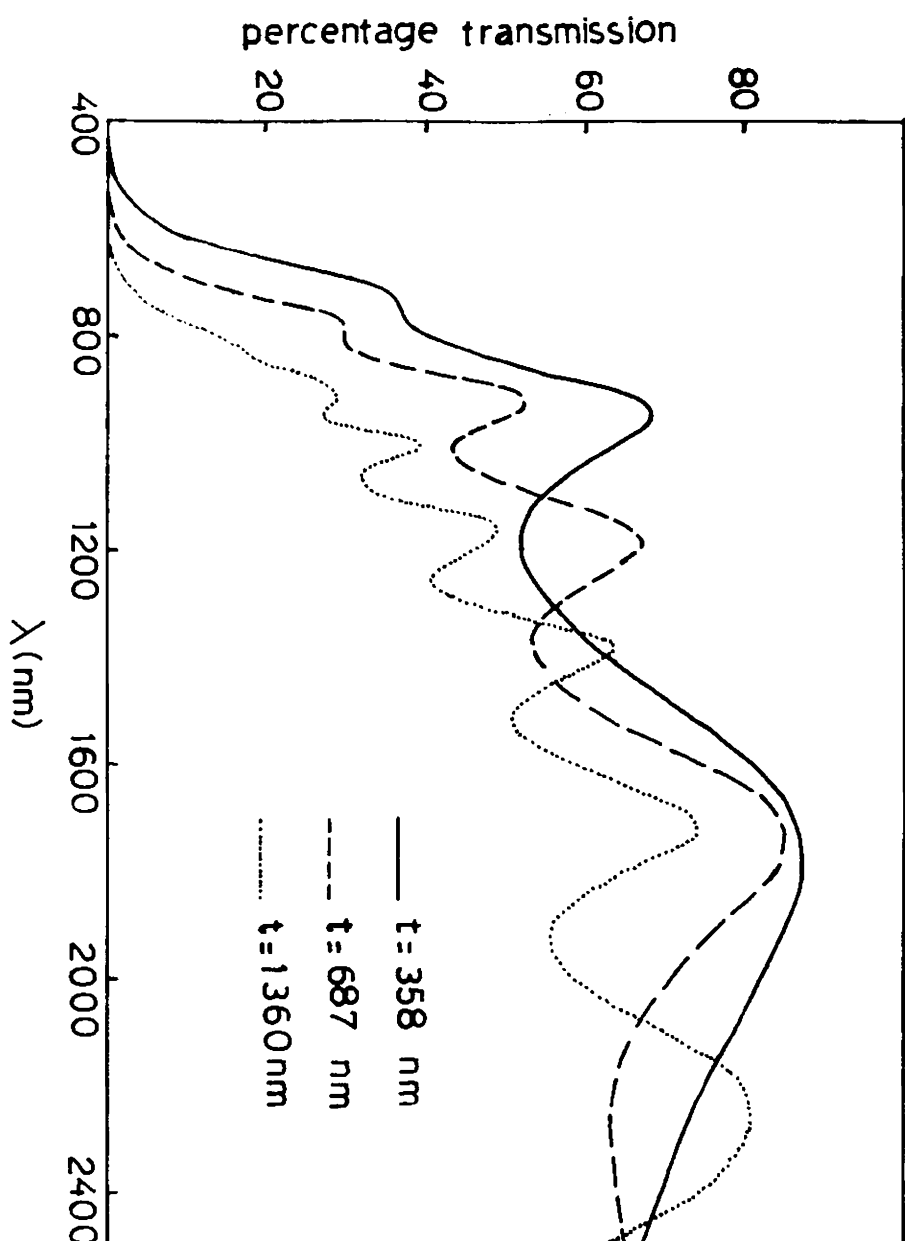
Fig.6.1 : Transmission spectra of a-PbO films for different thicknesses (t).
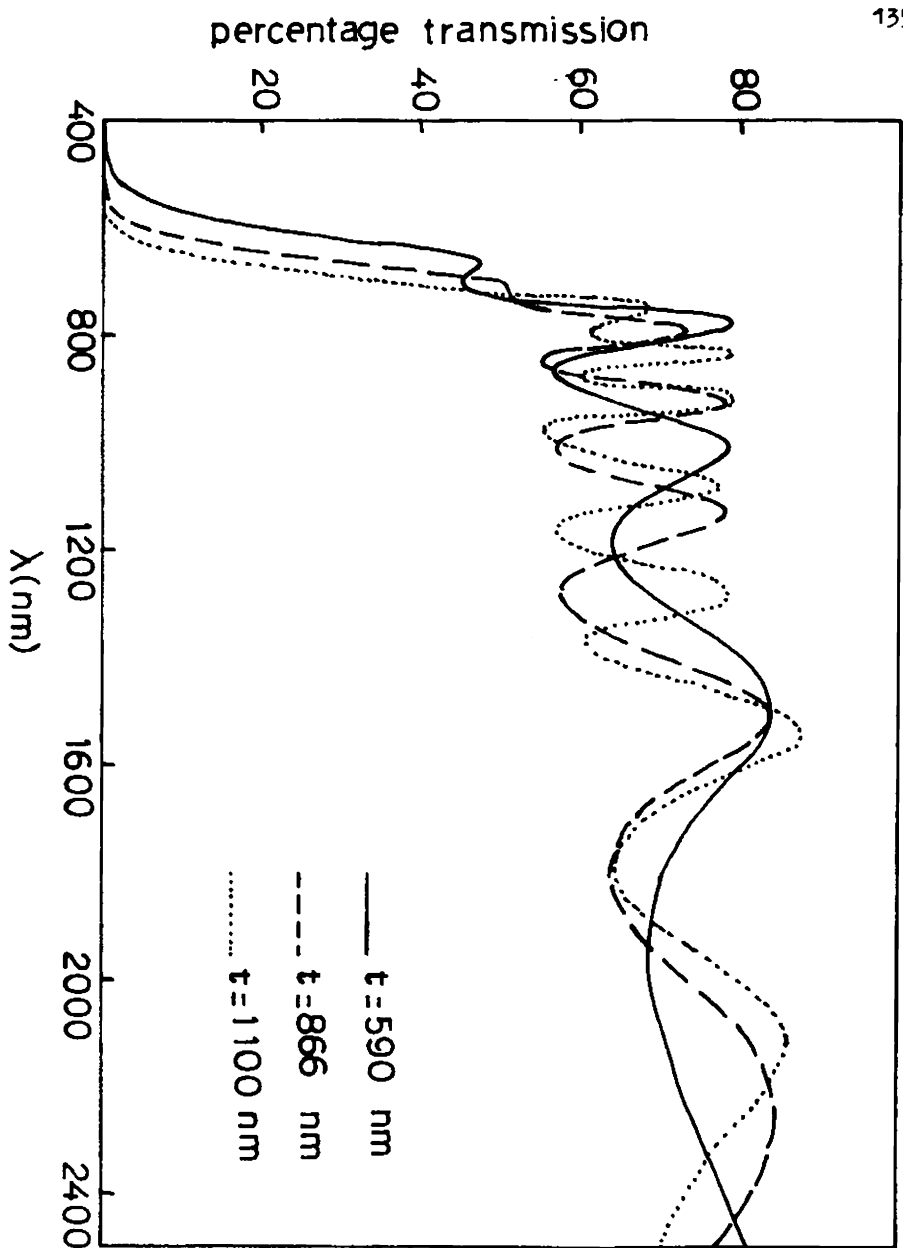
Fig.6.2 : Transmission spectra of sulphur rich a-PbS films for
different thicknesses(t).
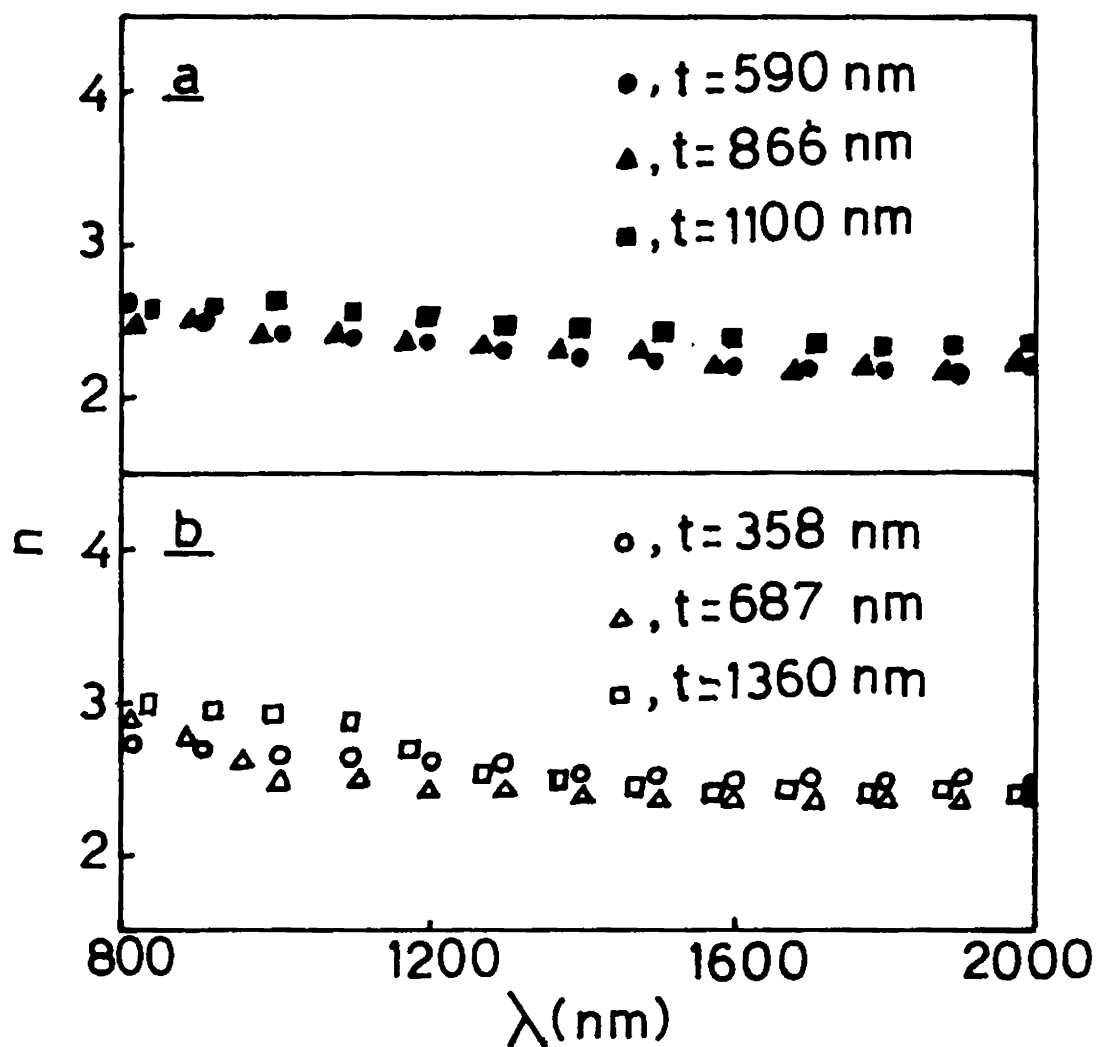
Fig.6.3 : Refractive index (n) calculated from the
transmission spectra of (a) sulphur rich
a-PbS film and (b) a-PbS films.
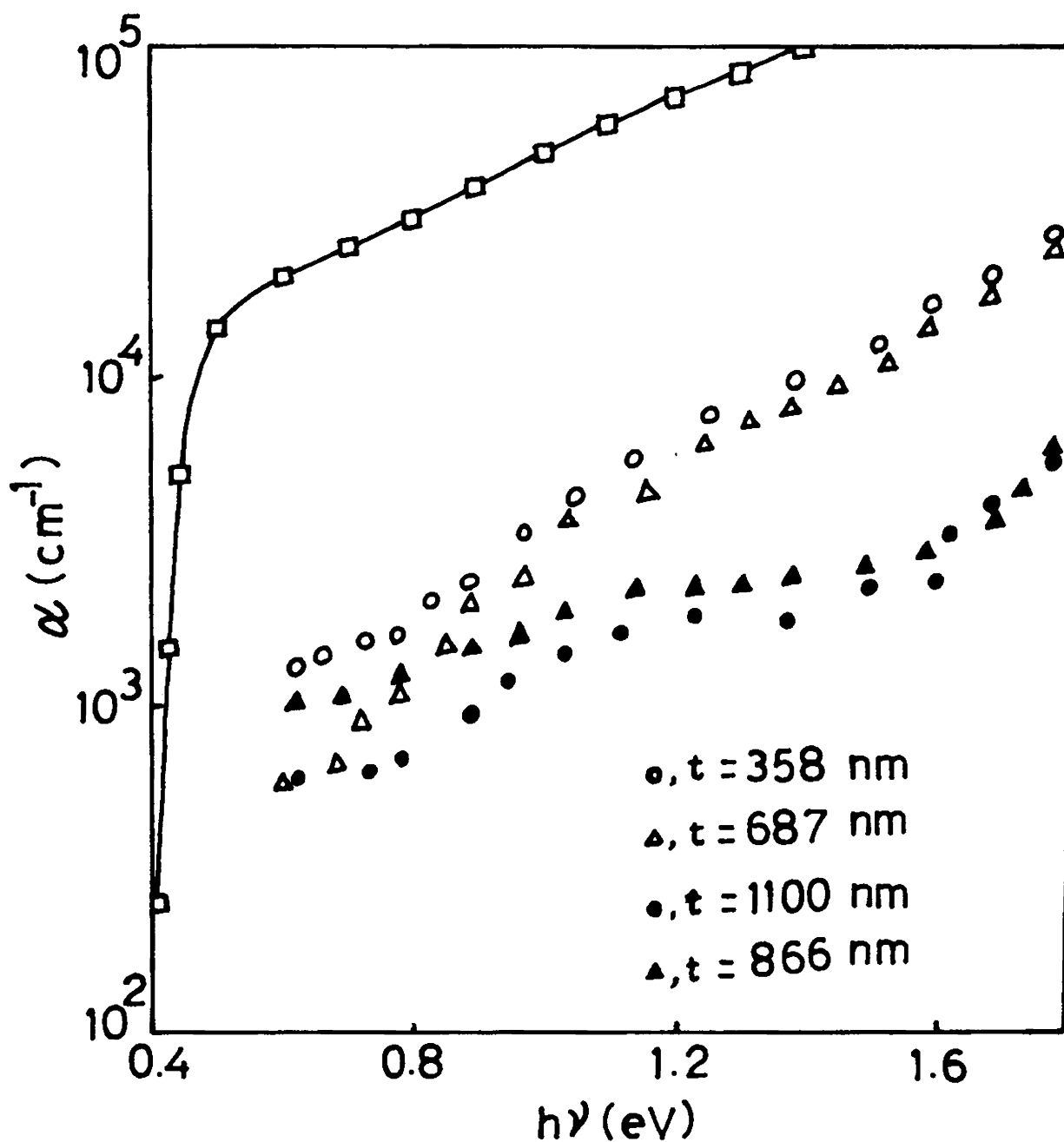
Fig.6.4 : Absorption coefficient (α) vs. photon energy (hγ) for (a) a-PbS films, O,$\triangle$; (b) sulphur rich a-PbS films, $\bullet$, $\blacktriangle$; and crystalline PbS films, $\square$.

films is about an order of magnitude less than that for crystalline PbS films. Assuming a law of the form

$$\alpha h\nu \propto (h\nu - Eg)$$

where α is the absorption coefficient and Eg is the optical band gap (obeyed by some amorphous materials /5,6/ for absorption coefficient in the range 10^4 to 10^5 cm^{-1}), the optical band gap obtained in the case of a-PbS films is 1.66 ± 0.03 eV (fig.6.5, $\alpha h\nu$ versus $h\nu$). Obviously this value is considerably higher than the band gap of crystalline PbS, which is 0.39 eV at room temperature.

Lead sulphide always crystallises in the NaCl structure with a coordination number six. The band gap corresponding to this structure is 0.39 eV. Amorphous phases of any material with the same coordination as that of crystalline phase will be having approximately the same band gap; that is, the band gap does not depend on whether it is crystalline or not, but only on the coordination. The band gap value of 1.66 eV obtained in the present case is very much larger than the crystalline value. It must then be concluded that the amorphous phase is having a different coordination than the crystalline phase and hence a different band gap. Ordinarily in amorphous phases the average coordination will be low /7,8/.
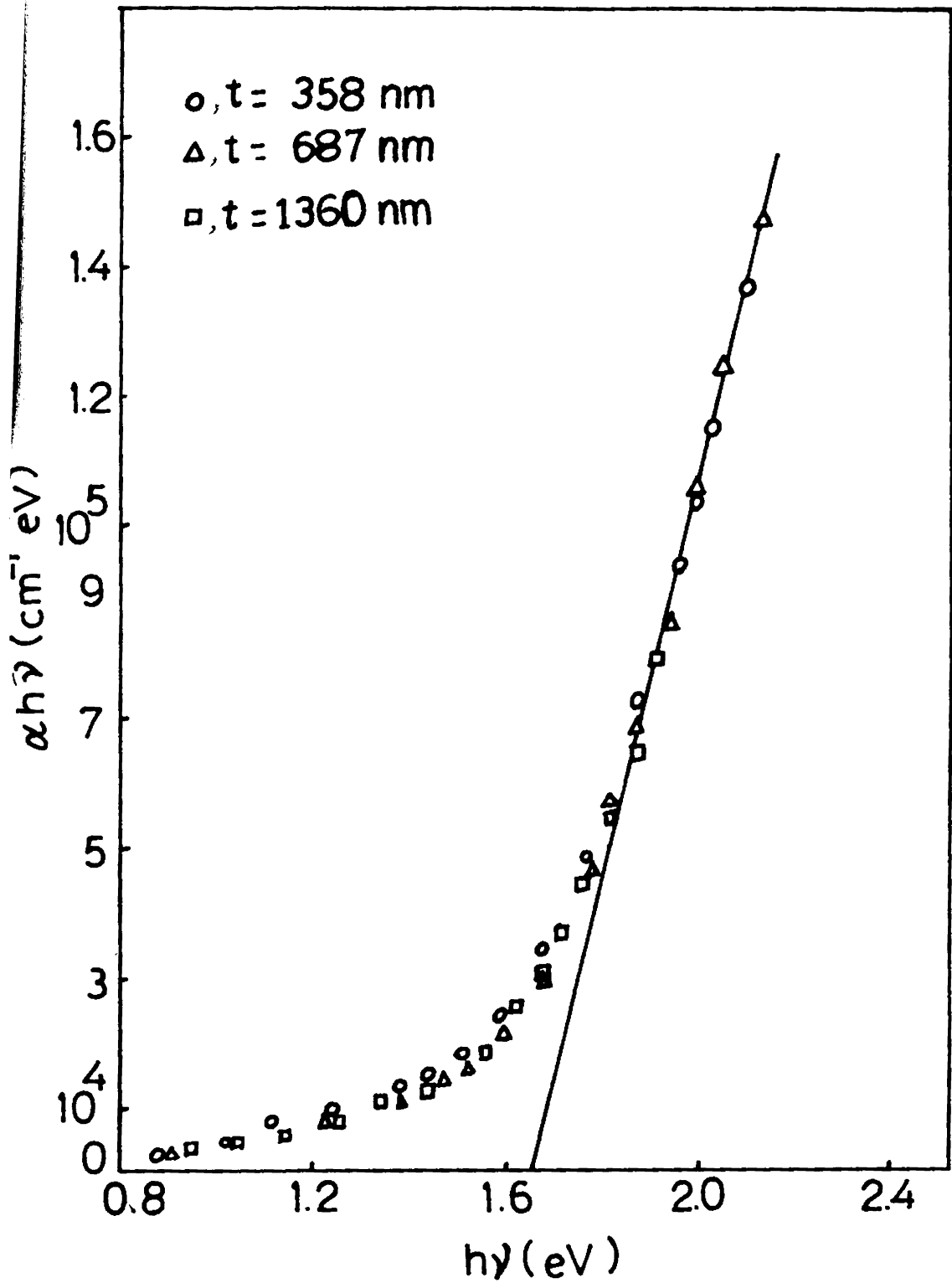
Fig.6.5 : $\alpha h\gamma$ vs. $h\gamma$ calculated from transmission
spectra of a-PbS films.

And as such the coordination number six which PbS is having in its crystalline form is difficult to be realised in the amorphous state and hence the present material may be having a coordination number which is less than six. The dielectric constant measurements support this view.

It is reported that the bonding in crystalline PbS has a high ionic contribution and consequently the low frequency dielectric constant (ϵ_o = 174.4) is very much greater than the high frequency dielectric constant (ϵ_∞ = 17.3) /9,10/. Low frequency dielectric constant of a-PbS films was measured by using MIM (gold - a-PbS - indium) structure. Fig.6.6 shows the dependence of dielectric constants of a-PbS films on frequency in the frequency range 20 Hz to 20 KHz for a few typical samples. From this graph it can be seen that the low frequency dielectric constant of a-PbS films is $\approx$ 10. The high frequency dielectric constant in this case is $\approx$ 5 (from fig.6.3). This closeness of the values of the high frequency and low frequency dielectric constants indicates that the bonding in a-PbS does not have an ionic character and is covalent in nature. It is well known that the difference in electronegativity of the constituent elements determines the character of the bond. The difference in electronegativity of Pb and S is 0.7 and is not very
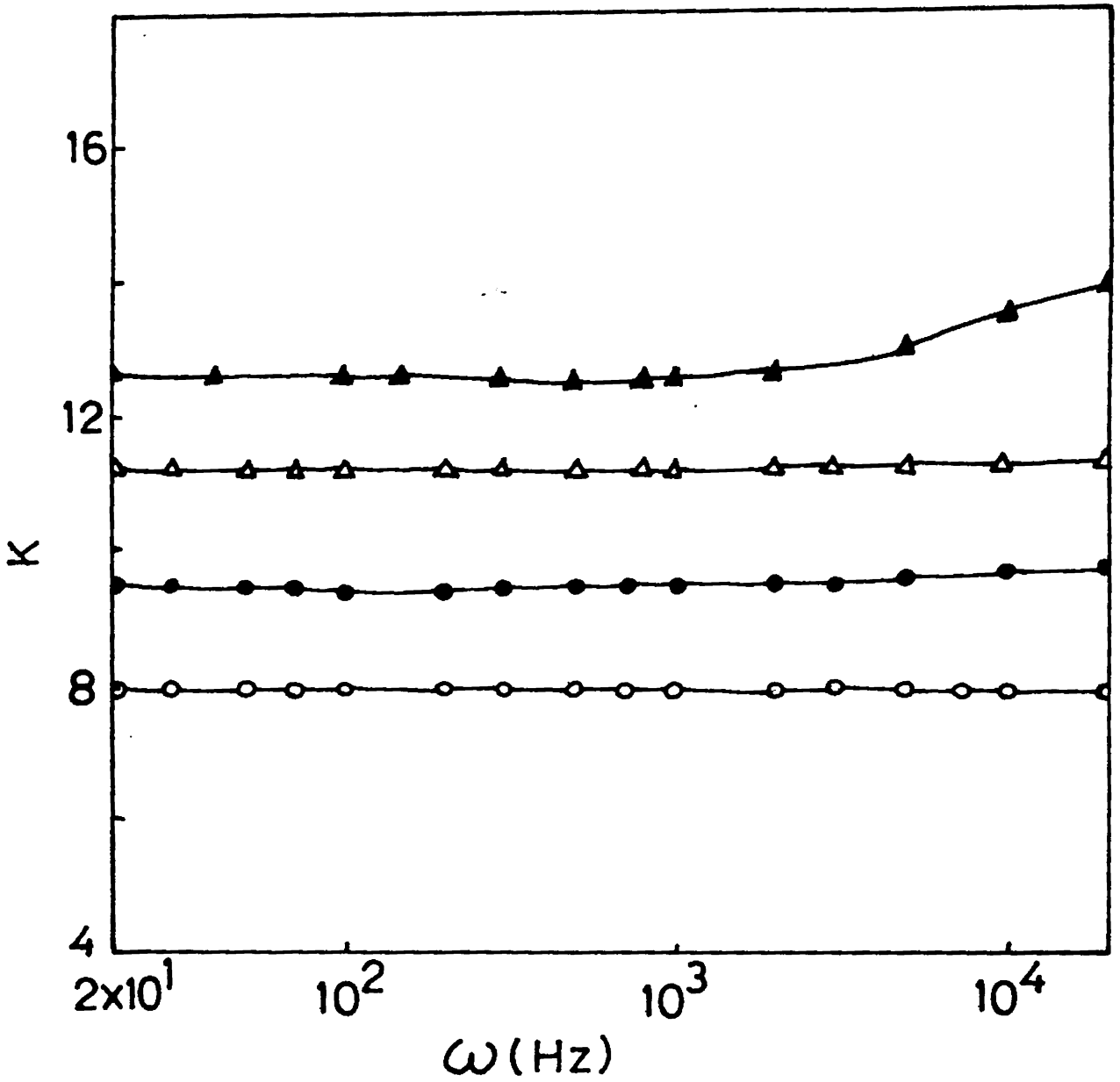
Fig.6.6 : Dielectric constant (K) versus frequency of
a-PbS films.

large. In these circumstances a covalent network satisfying the local valence requirements of Pb and S is highly probable. Fig.6.7 shows a classification of non-crystalline solids /11/ based on average covalent coordination number. The average coordination number m is shown decreasing from left to right. It is shown that, the internal strain increases with coordination number, whereas the entropy increases with decreasing coordination number (i.e. the materials becomes insufficiently cross linked). The mean covalent coordination number m = 4 separates non-crystalline metals from semiconductors or insulators. This also substantiates our earlier conclusion. Another IV-VI material GeTe, which is also six fold coordinated in the crystalline state is having a lower coordination in the amorphous state with Ge and Te four and two fold respectively /12-15/.

In the case of sulphur rich a-PbS films (fig.6.2)it can be seen that the transmission decreases abruptly with the beginning of band to band transitions. But in a-PbS films this decrease is not abrupt and this is definitely due to the tailing of states into the forbidden band. Excess sulphur in sulphur rich a-PbS films somehow remove these tail states and hence does not show any absorption before the onset of band to band transitions. In the case of sulphur rich a-PbS films the band
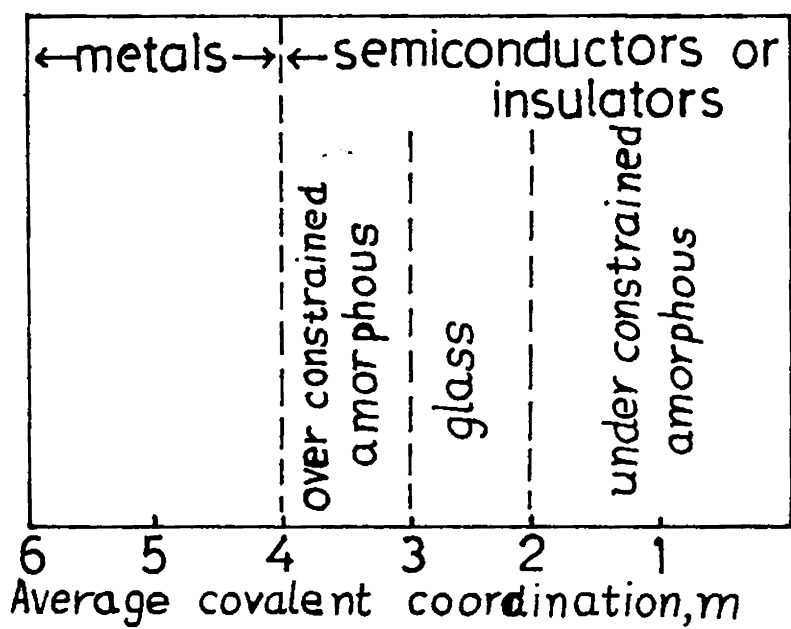
Fig.6.7 : Classification of non-crystalline solids.

gap obtained from fig.6.8 (αh$^\gamma$ versus h$^\gamma$) is
1.83 $\pm$ 0.03 eV.

b. **Electrical**

Electrical resistivity of amorphous PbS films
were measured using d.c. techniques. Fig.6.9 shows the
variation of electrical resistivity with inverse temper-
ature of a-PbS and sulphur rich a-PbS films. It can be
seen that the resistivity decreases slowly with temper-
ature to about 330K and then there is a sharp fall in
resistivity. This obviously is due to the crystallisat-
ion of amorphous film. Further increase in temperature
does not appreciably change the resistivity of the film.
When these crystallised films are cooled the resistivity
slowly increases as shown in the figure. The variation
in resistivity with temperature of the amorphous and
crystallised films may be represented by the well known
formula

$$\rho = \rho_0 \exp \frac{E_a}{KT}$$

where ρ is the resistivity and E_a is the activation
energy for conduction. Activation energy E_a obtained
from the fig.6.9 for a-PbS film is 0.056 $\pm$ 0.002 eV and
for sulphur rich a-PbS film is 0.086 $\pm$ 0.002 eV. The
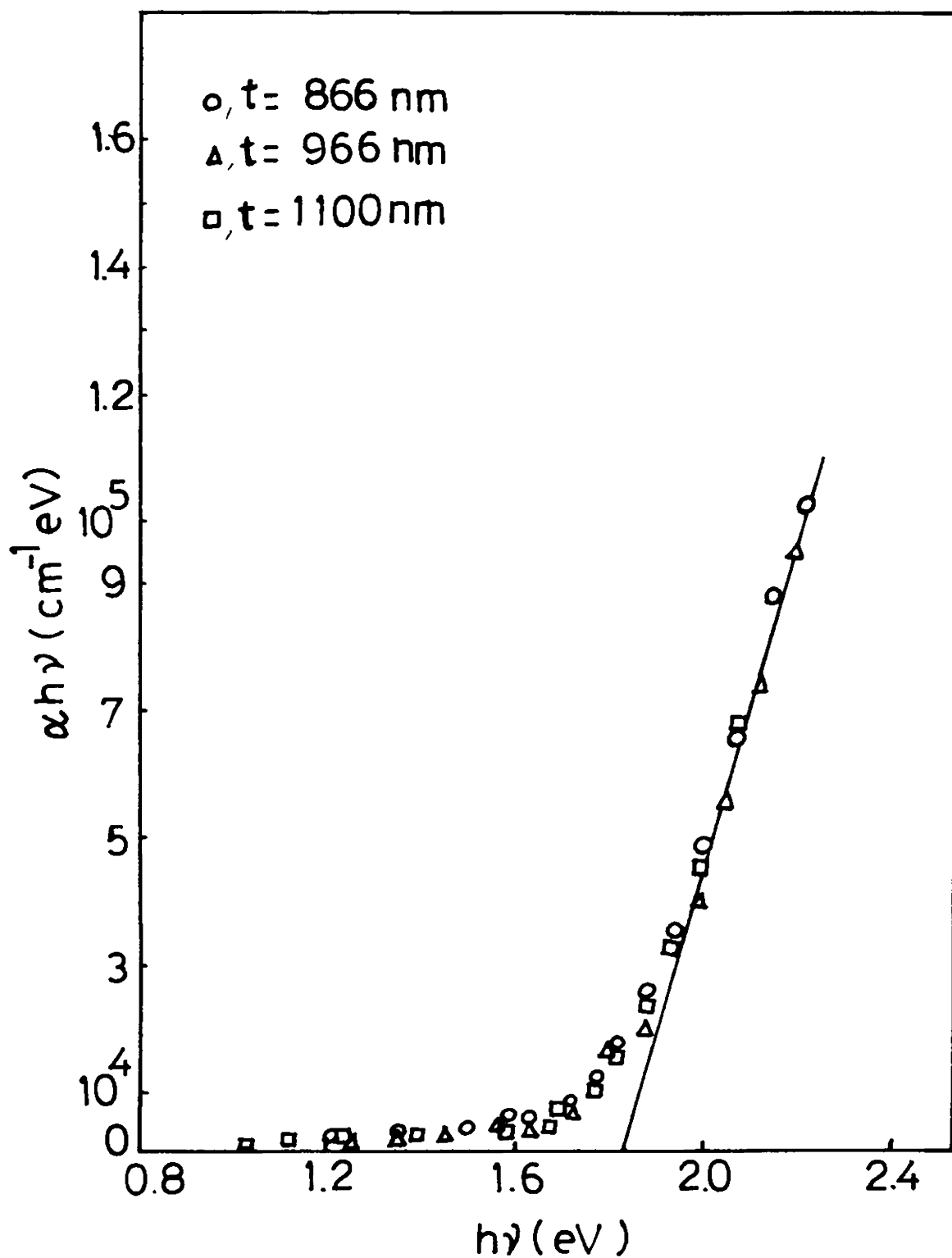
Fig.6.8 : $\alpha h\nu$ versus $h\nu$ calculated from transmission spectra of sulphur rich a-PbS films.
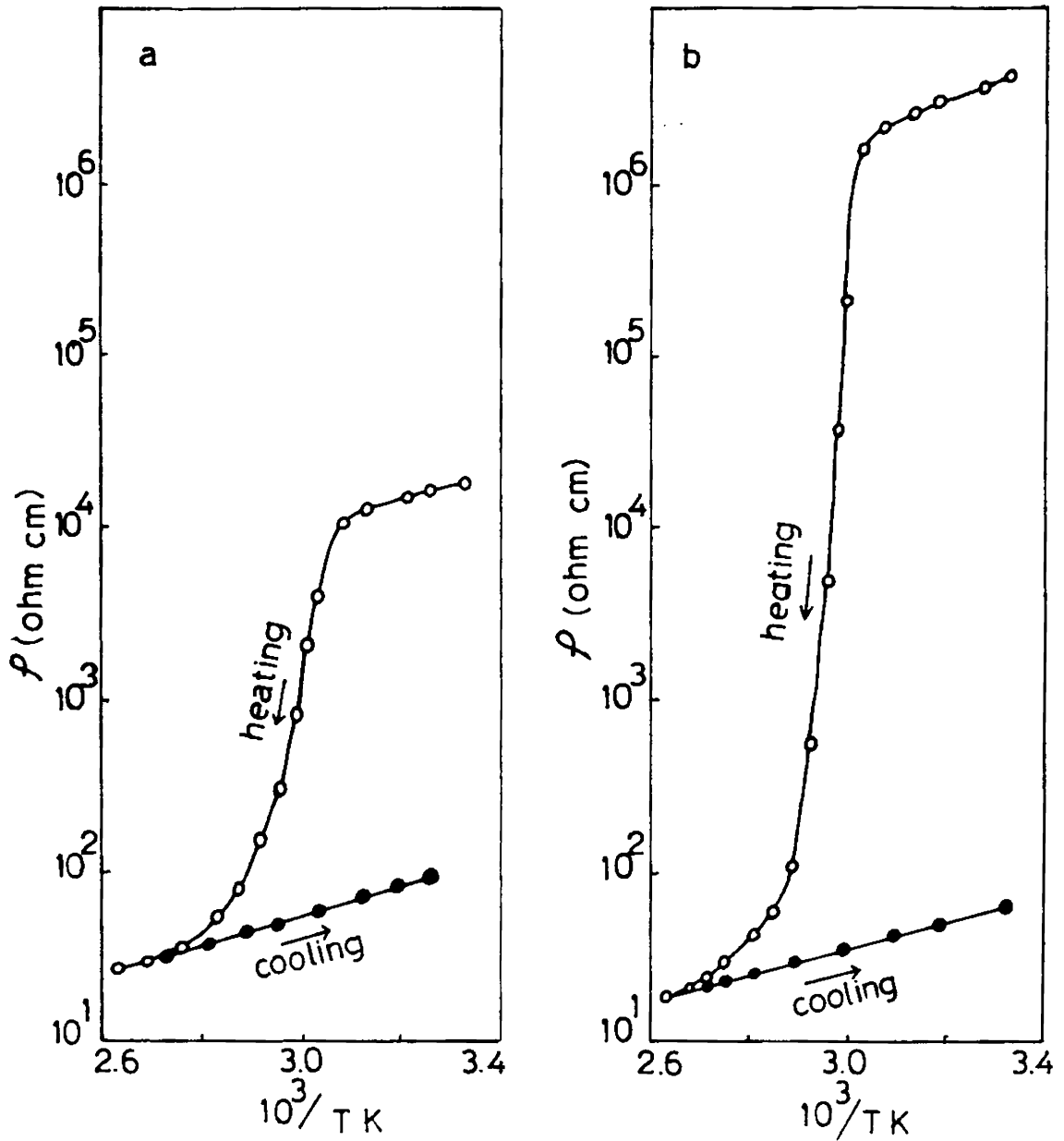
Fig.6.9 : Dependence of resistivity (ρ) on inverse temperature for

(a) a-PbS and (b) sulphur rich a-PbS films.

value of E_a obtained in case of crystallised a-PbS is 0.072 $\pm$ 0.002 eV and is the same as that obtained in the case of polycrystalline PbS films (chapter 5).

It can also be seen from fig.6.9 that in the case of sulphur rich a-PbS films the initial resistivity is approximately two orders of magnitude higher than that of a-PbS. Even then after crystallisation both stoichiometric and sulphur rich a-PbS films have approximately the same resistivity and activation energy.

6.4. CONCLUSIONS

Optical studies of amorphous PbS films give a band gap of 1.66 eV at room temperature. Optical studies and dielectric measurements lead to the conclusion that a covalent network is highly probable for amorphous PbS with a low coordination number, instead of the rock-salt structure of crystalline PbS. Electrical resistivity measurements give an activation energy 0.056 eV for a-PbS films, 0.086 eV for sulphur rich a-PbS films and 0.072 eV for crystallised films. The value obtained in case of crystallised PbS films is the same as that of polycrystalline films.

REFERENCES

1. J.C. Manifacier, J. Gasiot and J.P. Pillard,
    J. Phys. E, 9 (1976) 1002.

2. W.W. Scanlon, J. Phys. Chem. Solids 8 (1959) 423.

3. R.B. Schoolar and J.R. Dixon, Phys. Rev. 137 (1965)
    A 667.

4. R. Dalven, Infrared Physics, 9 (1969) 141.

5. E.A. Davis, J. Non-Cryst. Solids, 4 (1970) 107.

6. E.A. Davis and N.F. Mott, Phil. Mag. 22 (1970) 903.

7. S.R. Ovshinsky, Physical Properties of Amorphous
    materials, (1985), Ed. by D. Adler, B.B. Schwartz
    and M.C. Steels (Plenum Press, New York) p.105.

8. J. Robertson, Phil. Mag. B, 44 (1981) 239.

9. R. Dalven, Solid State Physics - Advances in Research
    and Applications, Vol.28, Ed. by H. Ehrenreich, F.
    Seitz and D. Turnbull (Academic Press: New York,
    1973) p.179.

10. J.M. Zemel, Solid State Surface Sciences, Vol.1,
    Ed. by M. Green (Dekker: New York, 1969) p.291.

11. H. Fritzsche, Fundamental Physics of Amorphous
    Semiconductors - Series in Solid State Sciences,
    Vol.25, Ed. by F. Yonezawa (Spring-Verlag: Berlin,
    19) p.1.

12. A Biemenstock, E. Betts and S.R. Ovshinsky, J. Non-Cryst. Solids, 2 (1970) 347.

13. D.B. Dove, M.B. Heritage, K.L. Chopra and S.K. Bahl, Appl. Phys. Letters (USA), 16 (1970) 138.

14. I.D. Nabitorich, Ya I. Stetsir, A.M. Andreiko, and R. Ya Yurechko, Sov. Phys. Crystallogr. (USA), 20 (1975) 758.

15. A.S. Avilov and S.A. Semiletov, Inorg. Mater. (USA), 15 (1979) 1483.

CHAPTER VII

SnTe THIN FILMS PREPARED BY REACTIVE EVAPORATION

7.1. INTRODUCTION

The electrical and optical properties of SnTe have received considerable attention in recent years owing to the narrow band gap (0.33 eV) of this material and its potential use as an IR detector material /1-3/. Crystalline and non-crystalline SnTe films have been grown and their electrical, optical and structural properties have been reported. Several authors have reported the influence of subsidiary bands on the transport properties of SnTe single crystals and epitaxial films /4-13/. The preparation of epitaxial films of SnTe on NaCl, KBr and KCl by different methods and studies of their structural, galvanomagnetic and optical properties have been reported by many workers /14-19/. Ota and Zemel /15/ and Samantary and Chaudhuri /20/ have reported the effect of film thickness, the substrate material and temperature and the evaporation time on the electrical transport properties of SnTe thin films. Goswami and Jog /17/ prepared the epitaxial films on NaCl and mica substrates by resistive heating and have studied the

structural properties by electron diffraction. Zheleva /19/ prepared the epitaxial films on NaCl, PbS and mica substrates by closed-hot-wall technique and has studied their structural properties. The effect of non-stoichiometric excess of tin on the electrical transport properties /21/ and of thermal treatment on the composition and crystal structure /22/ of SnTe films have also been investigated.

SnTe is a IV-VI compound, which has got the NaCl structure. In perfectly stoichiometric and chemically pure form it would be an intrinsic semiconductor. In practice, however, the bulk and thin film form is always deficient in tin. This is due to the low chemical diffusion constant of tin vacancy concentration /23/. As a result, the material is extrinsic with a carrier concentration of two holes per tin vacancy. Consequently, all samples of SnTe behave as heavily doped degenerate p-type semiconductors. Lorenz and Jepson /24/ have calculated that the energy necessary to create an ionized Sn-vacancy is only about 5K Cal/g-atom. In order to explain why this energy is so small, they proposed that the energy level of Sn-vacancy acceptor lies below the top of the valence band. The model is generalised to state that the metal vacancy acceptor level in a semiconductor will be below the top of the valence band whenever the more metallic component does not exhibit

its highest valence in the compound.

In all the earlier mentioned cases SnTe thin films were prepared from p-type SnTe ingots prepared by fusing stoichiometric proportions of tin and tellurium. Therefore it was thought interesting to investigate the electrical transport properties of SnTe films prepared using the three temperature method.

In the work reported here SnTe thin films were prepared by co-evaporation of the constituent elements to avoid incongruent evaporation from a single source and the consequent lack of stoichiometry. The temperature dependences of the electrical transport properties such as, conductivity σ, the Hall coefficient R_H, and Hall mobility μ_H of these films were studied in the temperature range 100-450K. The effect of annealing on these properties has also been investigated. These results are interpreted in terms of a model involving two valence bands.

7.2. EXPERIMENTAL DETAILS

As explained in chapter 3, in the three temperature method the components of the binary alloy are evaporated from separate sources with the substrate kept at a given temperature. It has been reported for many materials that a stoichiometric interval exists within a limited range of flux and substrate temperature /25,26/.

It has been found that good stoichiometric films
of SnTe are obtained with the following parameters:

tin flux $= 4.1 \times 10^{14}$ to 2.4×10^{15} atoms $cm^{-2}s^{-1}$

tellurium flux $= 7.4 \times 10^{15}$ to 2.2×10^{16} atoms $cm^{-2}s^{-1}$

substrate temperature $= 568 - 598K$.

Tin and tellurium (purity — 99.999%) were used
as evaporants. Tin was evaporated from a helical filament
made of molybdenum wire and tellurium from a conical glass
crucible with molybdenum wire windings. The coating was
performed in a Hind High Vacuum coating unit under a vacuum
of the order of 10^{-6} torr. The substrates used were opti-
cally flat glass slides of dimensions 3cm x 1.1cm x 0.2cm
which were cleaned ultrasonically and then subjected to
ion bombardment. The substrate temperature was measured
using a chromel-alumel thermocouple in contact with the
substrate. The flux rate from each source could easily be
adjusted by controlling the current through each filament.
The tin source was shielded to minimise heating of the
substrate by radiation.

When the substrate temperature had stabilized
at the required value, the current through the tellurium
source was switched on and the tellurium was allowed to
melt in the crucible with the shutter placed over the tin

and tellurium sources. The tin source current was then switched on. After adjusting the flux rate from the two sources by varying the source current, the shutter was removed. Tellurium atoms were unable to stick to the substrate independently at the elevated temperature. The tin atoms reaching the substrate reacted with those tellurium atoms present on the substrate and the compound film was deposited. The films obtained in this way were metallic grey in colour and opaque. Highly reproducible films were obtained under these conditions. Films deposited at substrate temperatures below 568K were found to contain tellurium rich regions, and those deposited at temperatures above 598K were found to have a non-uniform thickness.

X-ray diffraction patterns of the film - substrate system were obtained and it was found that the diffraction lines compared well with the literature data /27/. Fig.7.1 shows the diffraction patterns obtained, using Cu K_α radiation. The corresponding (hkl) planes are indicated. From the x-ray diffraction patterns it could also be found that these films had grains oriented such that (111) planes were parallel to the substrate surface.

X-ray powder patterns of the films were also obtained using a Debye-Scherrer powder camera. Fig.7.2 shows the patterns obtained using Cu K_α radiations.

Fig.7.1 : X-ray diffraction patterns of SnTe films using
Cu K_α radiation.
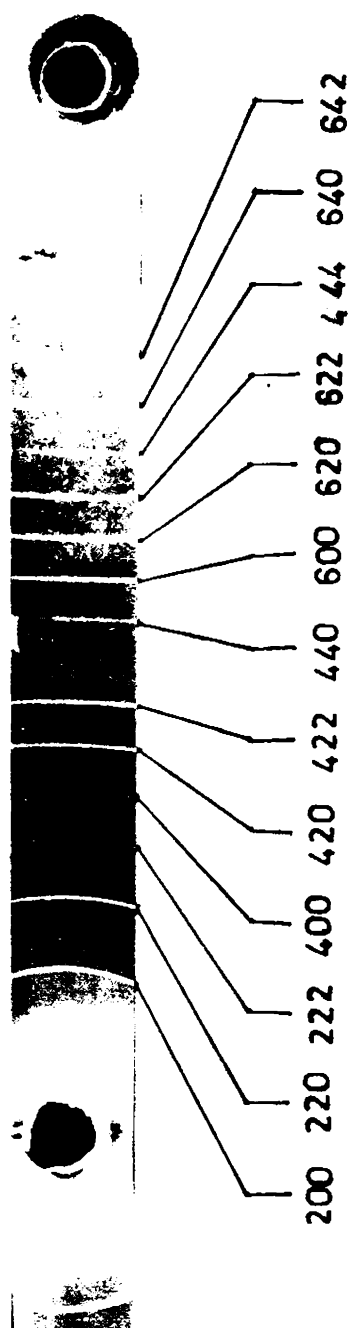
Fig.7.2 : X-ray powder patterns obtained using Cu K$_\alpha$
radiation and the corresponding (hkl) planes.

The corresponding (hkl) planes are also indicated.

The film thickness was measured using multiple-beam interferometry. The films prepared for electrical measurements were 4000 - 5000 Å thick. The systems described in chapter 3 were used to measure the conductivity σ, and the Hall coefficient R_H. Satisfactory contacts to bridge shaped samples were made using silver paste. The ohmic nature of the contacts was verified throughout the temperature range by the linearity of the current-voltage (I-V) characteristics. The sample was mounted on a copper block which was the cold finger of a vacuum cryostat containing liquid nitrogen. This had provisions for electrical connections, film heating and temperature measurements. The temperature was measured using a chromel-alumel thermocouple in contact with the substrate. The error in this measurement was only 3K. The conductivity of the film was measured by passing a known current through the film and measuring the voltage across the film. A stabilized magnetic field was applied across the sample and the Hall voltage developed was measured using a digital multimeter (Hewlett-Packard Model 3465A). The length to width of the samples used for the Hall measurements was greater than four so that the influence of film geometry was negligible. The conductivity

and Hall coefficient measurements were repeated many times and were found to be reproducible.

7.3. RESULTS AND DISCUSSIONS

The electrical measurements were carried out on freshly prepared films and on films which had been annealed for six hours after deposition without breaking the vacuum. The electrical characteristics such as Hall coefficient, Hall mobility and conductivity were calculated as in the case of PbS films, explained in chapter 5. The properties of the freshly prepared films agreed well with those reported by earlier workers /14, 21/.

The dependence of the Hall coefficient on temperature (log R_H versus $10^3/T$) for annealed and unannealed films is shown in fig.7.3. It can be seen that for any particular temperature R_H increases with annealing. This is because the tin vacancies, which are the predominant defects in SnTe, are annealed out and therefore the number of carriers resulting from the deviation from stoichiometry is reduced /23/. It should also be noted that R_H remains constant at low temperatures for both annealed and unannealed films. This is characteristic of an extrinsic degenerate semiconductor. It can also be seen that R_H increases with temperature at higher temperatures as has
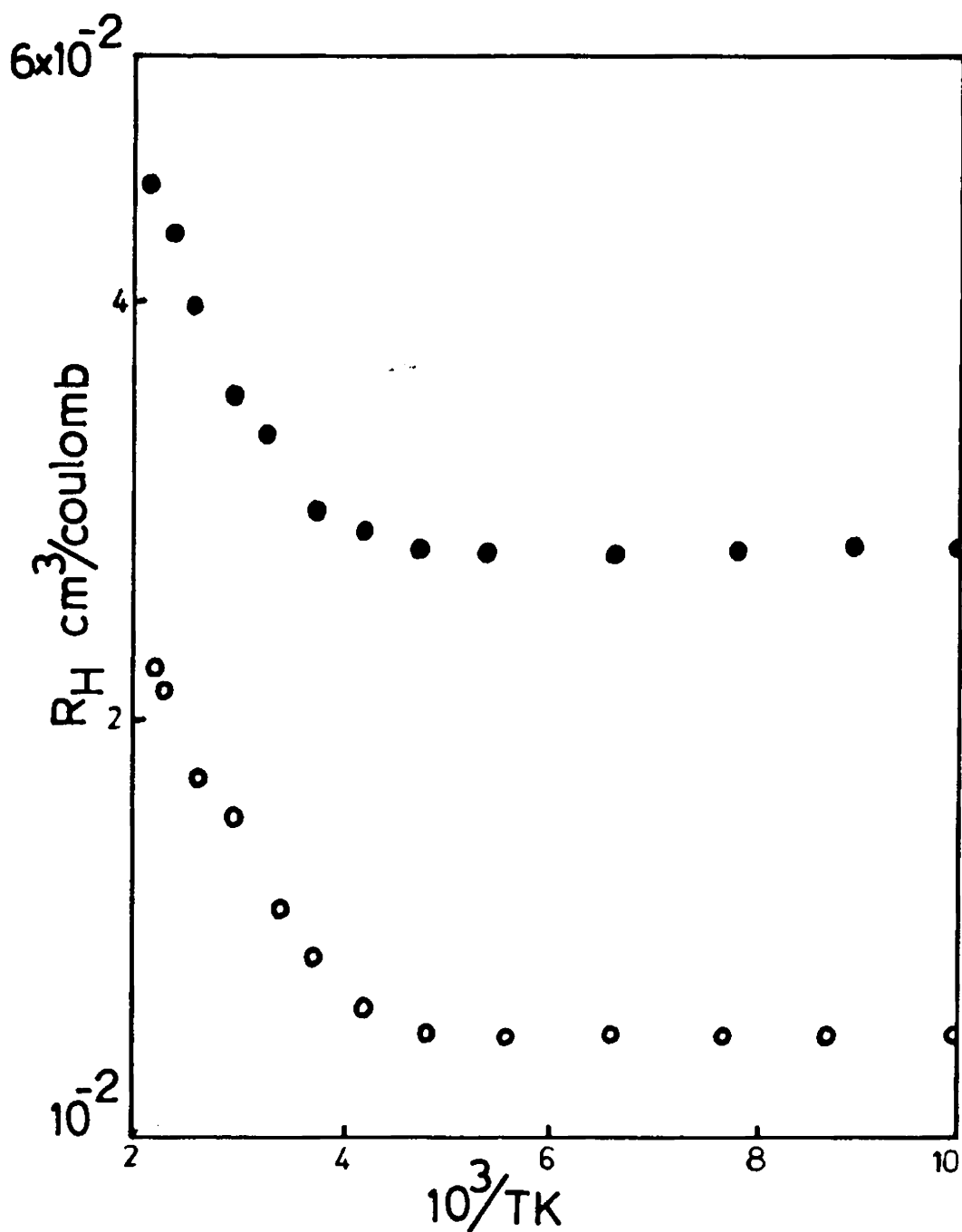
Fig.7.3 : Variation in the Hall coefficient R_H with the temperature (log R_H vs. $10^3/T$): O, unannealed; ●, annealed.

been reported for epitaxial films /14,21/. This could be explained as follows. A set of subsidiary maxima in the valence band plays an important role in the conduction process in SnTe samples /28/. The main and subsidiary maxima of the valence band are identified as light hole L valence band and heavy hole Σ valence band. It had become traditional to refer to the subsidiary maxima as a second valence band /29,30/, but the band calculations have made it quite clear that both sets of maxima belong to the same valence band. In SnTe samples above 150K significant numbers of holes begin to be thermally generated in the Σ valence band region /23,29,30,31/. At lower temperature, holes appear near Σ valence band only when the total density of holes exceeds 2×10^{20} cm^{-3} /30,32,6/. At higher temperatures Hall coefficient increased with temperatures due to the onset of hole transfer from light hole L valence band to the heavy hole Σ valence band.

The energy separation ΔEg between the light and heavy hole valence bands was found out by studying the variation of Hall coefficient in the high temperature region.

The change in Hall coefficient relative to its low temperature limit can be expressed as /33/

$$\frac{R_T - R_L}{R_L} = (1 - \frac{1}{b})^2 \frac{m_2^*}{m_1^*}^{3/2} \exp \frac{-\Delta E_g}{kT}$$

where R_T is the Hall coefficient at temperature T, R_L is the low temperature value of Hall coefficient which can be obtained by extrapolating the low temperature values from the regions were R_H remains constant (Fig.7.3), b is the ratio of the mobility of light holes to that of the heavy holes, m_1^* and m_2^* are the effective masses of light and heavy holes and k is the Boltzman's constant.

The dependence of $\frac{R_T - R_L}{R_L}$ on inverse temperature is shown in fig.7.4. The values of ΔE_g for unannealed and annealed films were calculated from the slopes of the corresponding plots. The calculated values from the graph are, $\Delta E_g = 0.147$ eV for unannealed film and $\Delta E_g = 0.133$ eV for annealed film and these are in good agreement with the reported values /10,11/. If we consider the temperature variations of $\frac{m_2^*}{m_1^*}$ and b, the values obtained for ΔE_g will be slightly different.

The dependence of the d.c. conductivity on temperature ($\log \sigma$ versus $10^{3/T}$) is shown in fig.7.5. As the temperature is increased and conductivity decreases because the defect scattering is higher in these films owing to the high carrier concentrations. At any particular temperature the conductivity is higher in the
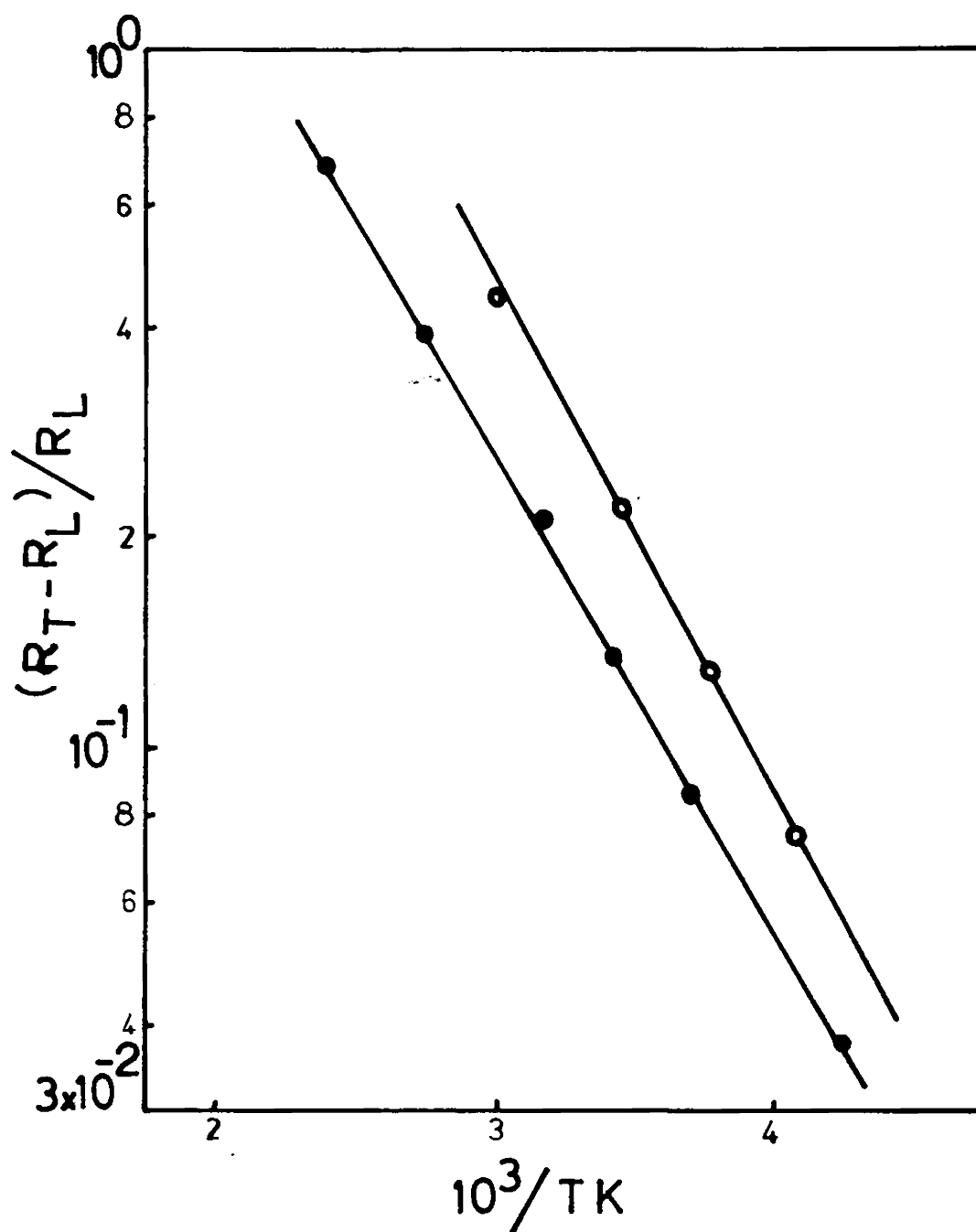
Fig.7.4 : Variation in $\dfrac{R_T - R_L}{R_L}$ with temperature

(log $\dfrac{R_T - R_L}{R_L}$ vs. $10^3/T$) : O, unannealed;
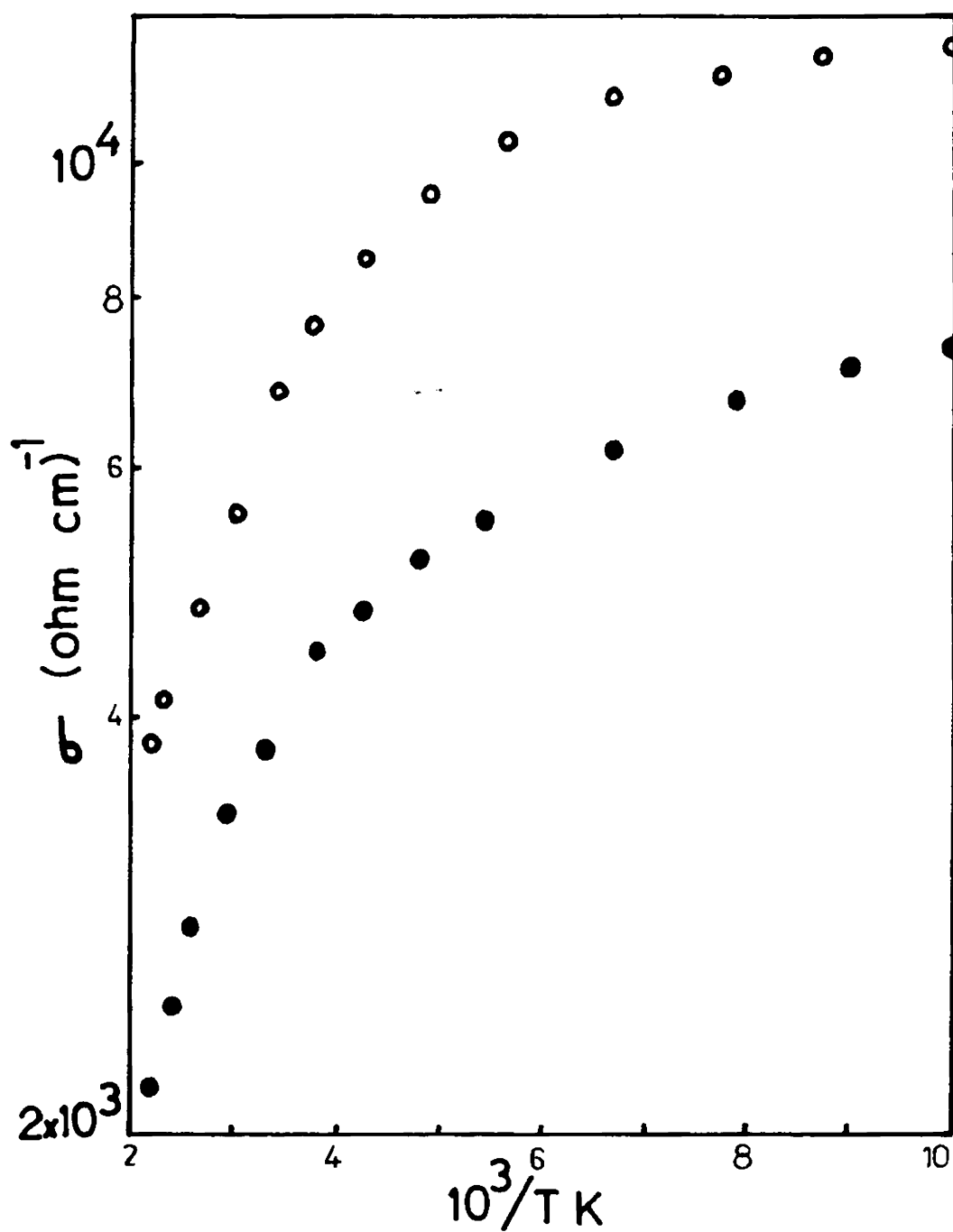
●, annealed.

Fig.7.5 : Variation in the d.c. conductivity σ with
temperature (log σ vs. $10^3/T$) : O, unannealed
●, annealed.

unannealed samples because of the comparatively high
carrier concentrations in the unannealed films. In the
low temperature regions the conductivity is found to be
a weak function of temperature in both samples. At higher
temperatures the concentration of light holes will be
decreased owing to light hole conduction to the heavy
hole. valence band, and the effect of these heavy holes,
which have lower mobility, will be increased. This is
the reason for the abrupt change in the variation in
conductivity at about 200K.

The variation in the mobility with temperature
(μ_H versus T) is shown in fig.7.6. In both cases
(unannealed and annealed) the mobility decreases with
increasing temperature, and at a given temperature μ_H is
greater in the annealed sample than in the unannealed
sample. The boundary regions between crystallites in
polycrystalline films should exert a pronounced effect
on the various properties of the thin films. The bound-
ary region should be effective in scattering the current
carriers and this should lead to a reduction in the carrier
mobility. Since the substrate temperature and the temper-
ature at which the films are annealed are the same in the
films studied, the effect of carrier scattering at the
grain boundaries and the consequent reduction in the
mobility will be the same. In other words the relative
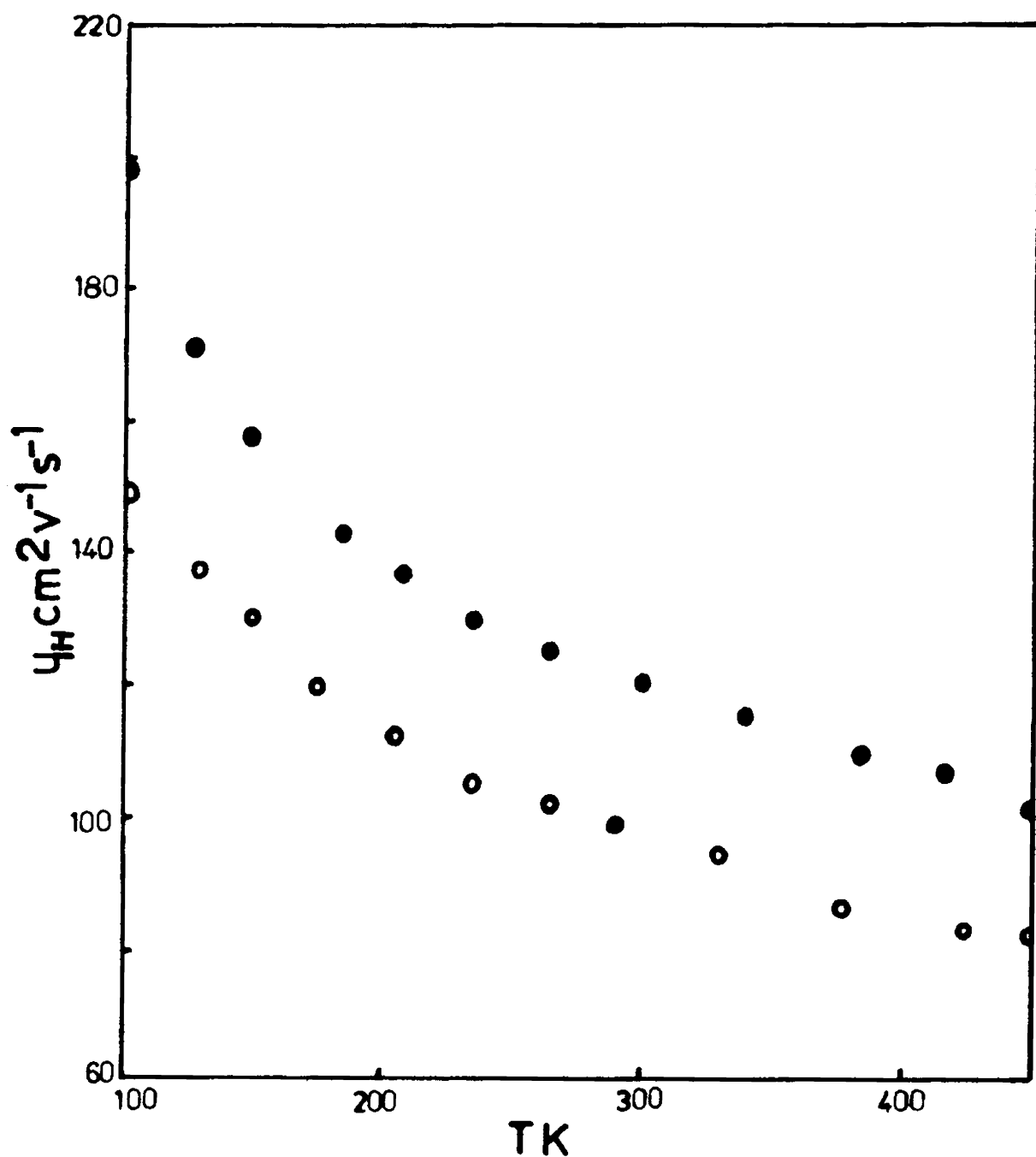
Fig.7.6 : Variation in the Hall mobility μ_H with
temperature (μ_H vs. T) : O, unannealed;
•, annealed.

effect of the boundary scattering on mobility is not affected by the annealing process. No change in the grain size of the specimens is observed after annealing. Fig.7.7 shows photomicrographs of the surface of the unannealed and annealed films. However, the contribution of defect scattering to the reduction in mobility is higher in unannealed films with high carrier concentrations. The slow rate of decrease in carrier mobility at high temperatures observed in both the annealed and the unannealed films is due to the onset of heavy hole conduction.

7.4. CONCLUSIONS

Using the co-evaporation technique, polycrystalline films of SnTe have been prepared for the first time. The electrical transport properties (Hall coefficient, d.c. conductivity and Hall mobility) of unannealed and annealed films are measured in the temperature range 100 - 450K and these agree well with the values reported by earlier authors. The carrier concentration and conductivity decreases after annealing whereas the Hall mobility increases. Energy separation ΔEg between light and heavy-hole valance bands have been found out in case of unannealed and annealed films and are in good agreement with the earlier reported data.

(a)
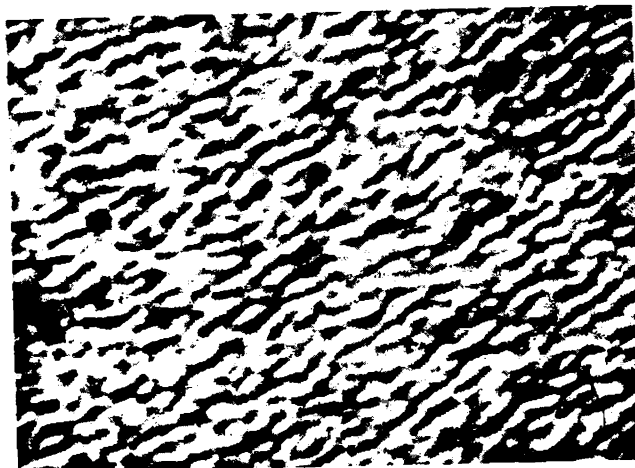
(b)

Fig.7.7 : Optical micrographs of SnTe thin films;
(a) unannealed; (b) annealed.
(Magnification, 3800X)

REFERENCES

1. H.R. Riedl, J.R. Dixon and R.B. Schoolar, Phys. Rev. 162 (1967) 692.

2. R.F. Bis and J.R. Dixon, Phys. Rev. B, 2 (1970) 1004.

3. E.G. Bylander, J.R. Dixon, H.R. Riedl and R.B. Schoolar, Phys. Rev., 138 (1965) 864.

4. R.F. Brebrick and A.J. Strauss, Phys. Rev., 131 (1963) 104.

5. J.A. Kafalas, R.F. Brebrick and A.J. Strauss, Appl. Phys. Lett. 4 (1964) 93.

6. B.B. Houston and R.S. Allgaier, Bull. Am. Phys. Soc. 9 (1964) 293.

7. B.A. Efimova, V.I. Kaidanov, B. Ya. Moizes and I.A. Chernik, Sov. Phys. - Solid State, 7 (1966)2032.

8. A.A. Andreev, Sov. Phys. - Solid State, 9(1967)1237.

9. R. Tsu, W.E. Howard and L. Esaki, Phys. Rev. 172 (1968) 3.

10. Y.W. Tung and M.L. Cohen, Phys. Rev. 180 (1969) 823.

11. S. Rabii, Phys. Rev. 182 (1969) 821.

12. Y. Ota and S. Rabii, Physics of IV-VI Compounds and Alloys, ed., S. Rabii (Gordon and Breach, New York, 1974) p.113.

13. S. Santhanam and A.K. Chaudhuri, Mat. Res. Bull. 16 (1981) 911.

14. J.N. Zemel, J.D. Jensen and R.B. Schoolar, Phys. Rev. 140 (1965) A 330.

15. Y. Ota and J.N. Zemel, J. Vac, Sci. Technology 6 (1969) 558.

16. J.N. Zemel, Solid State Surface Science, ed., M. Green Vol.1 (M. Dekker, New York, 1969) p.291.

17. A. Goswami and R.H. Jog. Indian J. Pure and Appl. Phys. 7 (1969) 273.

18. A.G. Mikolaichuk and D.M. Friek, Sov. Phys. - Solid State 11 (1970) 2033.

19. N.N. Zheleva, Thin Solid Films, 56 (1979) 369.

20. B.K. Samantary and A.K. Chaudhuri, J. Phys. D, 15 (1982) 2531.

21. A.L. Dawar, P.C. Mathur, A.O. Mohammed and O.P. Taneja, Thin Solid Films, 82 (1981) 273.

22. D. Freik, J. Baltraunas, Ya. Solonichny, A. Amulevicins and I Perkatyuk, Sov. Phys. Collect; 20 (1980) 65.

23. H.T. Savage, B. Houston and J.R. Burke, Jr., Phys. Rev. B, 6 (1972) 2292.

24. M.R. Lorenz and D.W. Jepson, J. Phys. Chem. Solids 26 (1965) 1177.

25. J. George and K.S. Joseph, J. Phys. D, 15 (1982)1109.

26. J. George and K.S. Joseph, J. Phys. Chem. Solids, 45 (1984) 341.

27. Powder Diffraction File, AsTM, Philadelphia, PA, Card 8-47.

28. R.S. Allgaier and B. Houston, Phys. Rev. B, 5 (1972) 2186.

29. R.S. Allgaier, J. Appl. Phys. 32 (1961) 2185.

30. R.S. Allgaier and P.O. Scheie, Bull. Am. Phys. Soc. 6 (1961) 436.

31. R.S. Allgaier and B.B. Houston, J. Appl. Phys., 37 (1966) 302.

32. I.A. Chernik, V.I. Kaidanov, M.N. Vinogradova and N.V. Kolomoets, Sov. Phys. Semicond. 2 (1968) 645.

33. L.W. Aukerman and R.K. Willardson, J. Appl. Phys. 31 (1960) 939.

CHAPTER VIII

HIGH MOBILITY POLYCRYSTALLINE SnTe:Ge FILMS

8.1. INTRODUCTION

The narrow band gap semiconductor SnTe has been studied for a long time owing to its similarities with lead chalcogenides which are extensively used as IR detector materials. Though its band gap value is favourable for its use as an IR detector in the NIR region, SnTe has not yet been used in pure form for this purpose. This is mainly due to the existence of a high concentration of tin vacancies in stoichiometric SnTe which reduces the carrier life time. Stoichiometric material is extrinsic with a carrier concentration of two holes per Sn vacancy /1/. The chemical diffusion coefficient of Sn in SnTe is small below 600K and equilibrium vacancy concentration corresponding to higher temperatures are "frozen in". The high hole concentration ($\sim 10^{20}$ cm^{-3}) reduces the charge carrier mobility. Attempts have been made to reduce the carrier density by incorporating excess tin /2/, doping with Cu /3/, In /4,5,6/ and other group III metals and also group V metals /7/. Excess tin always decreased the hole concentration and increased the mobility to a certain extent /2/. In the case of indium, as reported by different authors, indium acts as an acceptor and also as

a neutral element. The incorporation of indium always
produced a reduction in mobility. Copper and bismuth
act as donors in SnTe crystals and increase the mobility
/3/.

In trying to reduce the carrier concentration of
SnTe films, by removing tin vacancies, it was thought to
add trace quantities of a IVth group element itself.
Germanium was selected for this purpose as it is the
nearest element to tin in the IVth column of the periodic
table. Germanium has also got a smaller covalent radii
(1.22 Å) than tin (1.40 Å) which can possibly enhance its
diffusion coefficient in the SnTe matrix. Reported below
is the effect of doping SnTe with small quantities of
Germanium.

8.2. EXPERIMENTAL DETAILS

SnTe films were prepared by reactive evaporation
as described in chapter 7. Substrate temperature used
was 585 ± 3K. In the present work accurately known
quantities of tin and germanium were taken in the moly-
bdenum boat and the whole charge reactively evaporated
in the presence of tellurium vapour. Germanium has an
order of magnitude less vapour pressure than tin at the
evaporation temperature used (∼1500K). Because of the
very small percentage of germanium used in the evaporation,

the time taken for germanium to evaporate fully is approximately equal to the time taken for tin and hence more or less uniform dispersal of germanium in the SnTe matrix is possible. After deposition of the films, the films were annealed at the same temperature for three hours without breaking the vacuum. This annealing was found absolutely necessary for the reduction in carrier concentration and improvement in mobility.

5N purity tin and germanium were used for evaporation and weighed using a microbalance. Hall effect measurements were made using dc technique in an all metal evacuated cell (chapter 3) in the temperature range 125 to 400K. Satisfactory contacts to the samples were made using pressed indium. Weight percent indicated in the text and figures refer to that used for evaporation. No analysis was done to ascertain the actual germanium content in the films. All the films obtained were p-type.

8.3. RESULTS AND DISCUSSIONS

Fig.8.1 shows the dependence of carrier concentration on temperature for SnTe films together with that of SnTe:Ge films containing different weight percentages of Ge. It can be seen that the nature of variation of
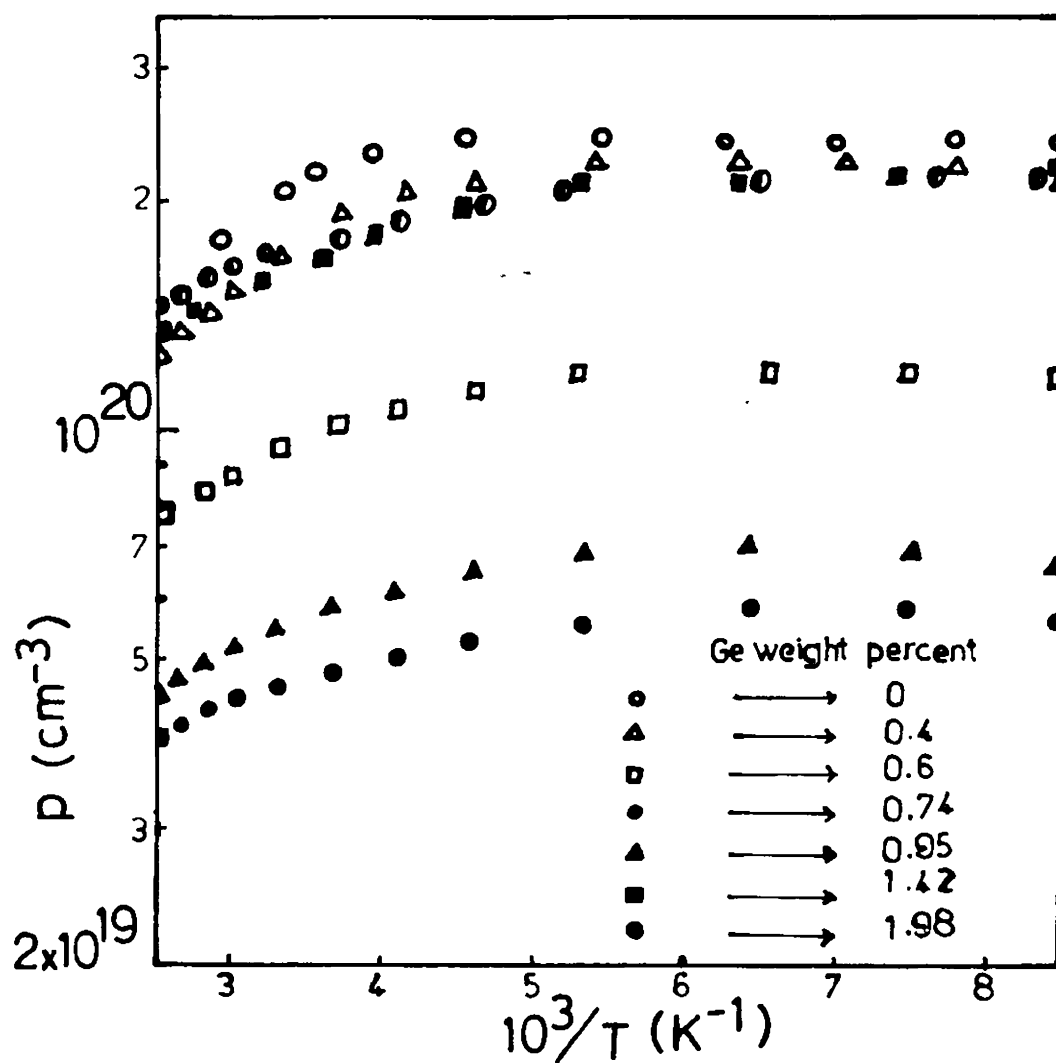
Fig.8.1 : Variation in the carrier concentration (P)
with temperature for different Ge weight
percentages of SnTe:Ge samples.

carrier concentration with temperature is almost the
same for all films. But for a particular temperature
carrier concentration decreases with increasing weight
percentage of Ge upto a certain doping level and then
increases. This dependence of carrier concentration at
room temperature on Ge weight percentage is shown in
fig.8.2. It can be observed from this figure that as
the concentration of Ge is increased from zero the carrier
concentration decreases after 0.4 weight percent and this
decrease continues till the weight percentage of Ge reached
a value of about 0.8 and thereafter for further increase in
Ge content the carrier concentration increases. The ini-
tial decrease in carrier concentration is obviously due
to the filling of tin vacancies by Ge atoms. It is possible
that for Ge content of about 0.8 weight percent the tin
vacancies have been filled by the Ge atoms to reach an
optimum minimum carrier concentration and the observed
further increase in carrier concentration with increase
in Ge content can possibly be explained by assuming that
these additional Ge atoms go to same positions where it
act as sources of holes. Beyond two weight percent the
added Ge has not much effect possibly because of the
formation of the ternary compound $Sn_{1-x} Ge_x Te$.

Fig.8.3 shows the variation of mobility with
temperature for different Ge weight percentages of
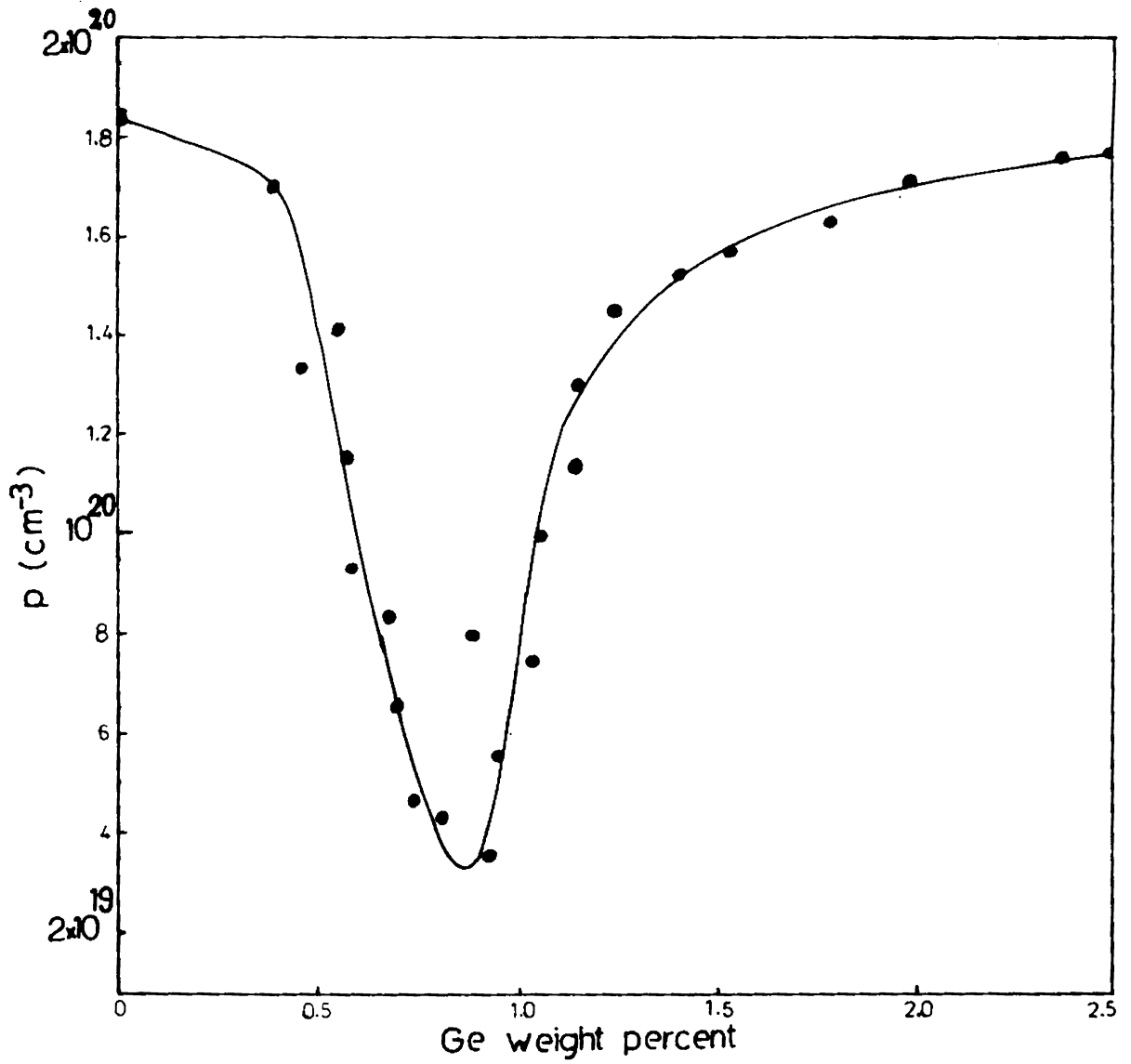
Fig.8.2 : Dependence of carrier concentration (P) at room
temperature on Ge weight percentage.
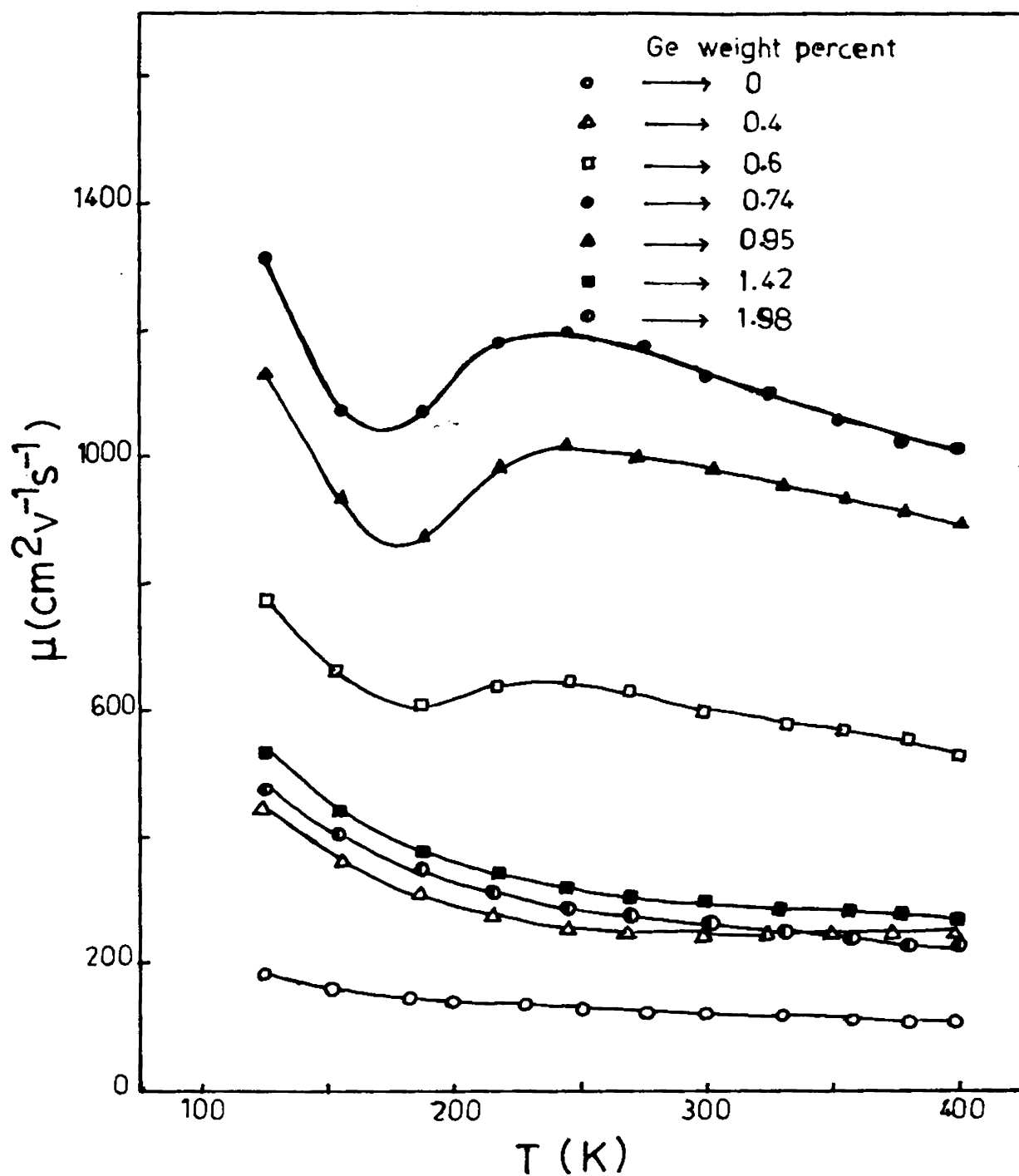
Fig.8.3 : Variation of mobility (μ) with temperature for different Ge weight percentages.

SnTe:Ge samples, together with that of undoped SnTe films. Fig.8.4 shows the dependence of mobility at room temperature on Ge weight percentage. From these two graphs it can be seen that at all temperatures mobility increases with increase in Ge weight percentage upto about 0.8 percent, where the mobility reaches the maximum value. The maximum room temperature mobility obtained is 1150 $cm^2v^{-1}s^{-1}$. After this maximum the mobility decreases with increasing Ge content. The contribution of defect scattering is higher in films with higher carrier concentration and so SnTe:Ge film with Ge weight percent around 0.8 having lesser carrier concentration shows a higher mobility. The dependence of mobility on carrier concentration at room temperature is shown in fig.8.5. It can also be seen from fig.8.3 that in the doped and undoped films the mobility increases with decrease in temperature in the range 250 to 400K. The graph $\mu^{2/3}$ versus T (fig.8.6) gives a straight line in this region indicating that this decrease in mobility is due to increase in carrier scattering. In the low temperature region (125-175K) the steep increase in mobility with decrease in temperature is because in this region the current is predominantly carried by light holes /8.9.10/. The reason for the increase in mobility with temperature
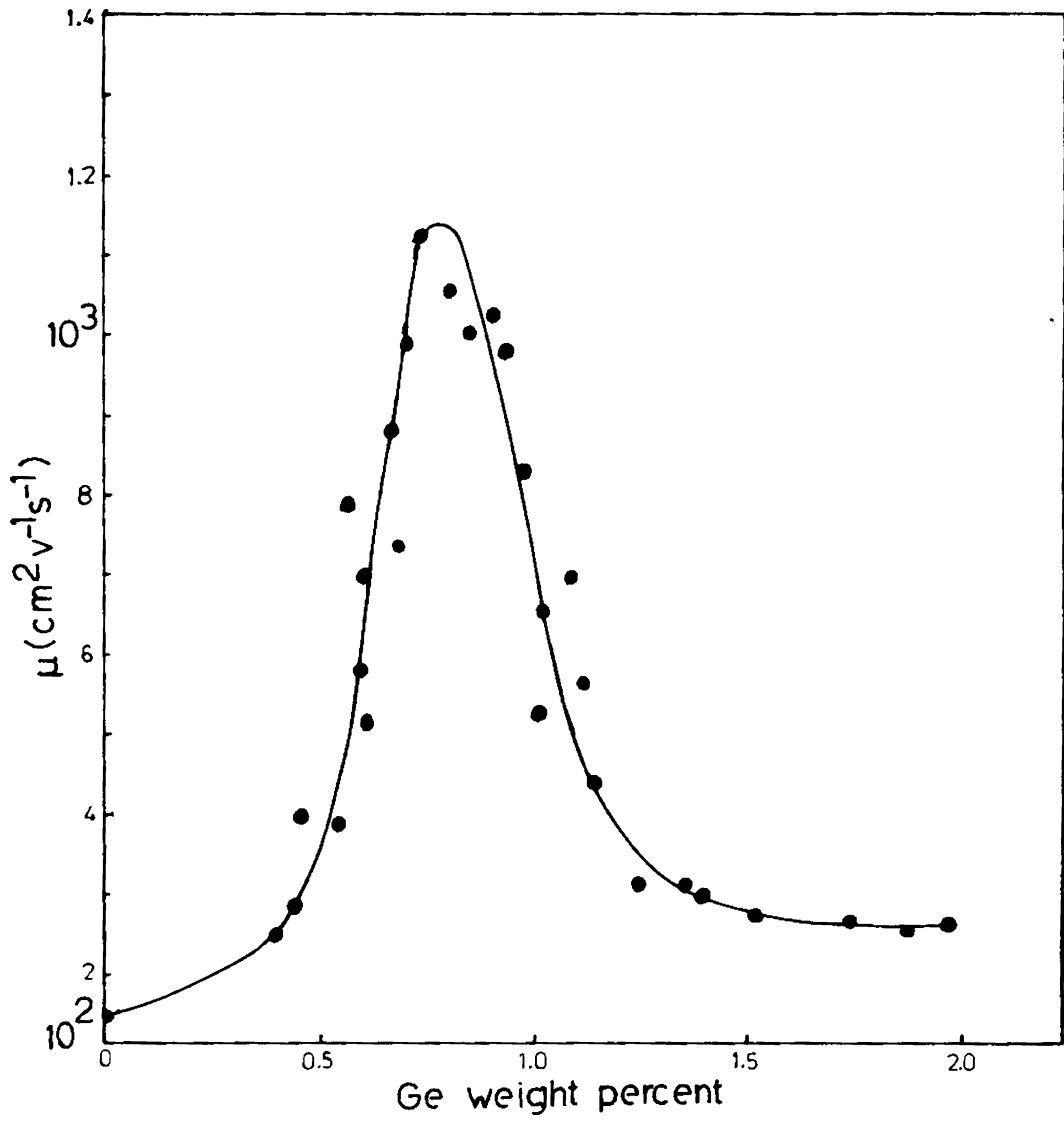
Fig.8.4 : Dependence of mobility (μ) at room temperature on
Ge weight percentage.

Fig.8.5 : Dependence of mobility (μ) on carrier
concentration at room temperature.
(p)

Fig.8.6 : $\mu^{2/3}$ versus T

between 175 and 250K observed in doped films having higher mobility is not clear at present.

8.4. CONCLUSIONS

High mobility polycrystalline SnTe:Ge films have been prepared by reactive evaporation of tin and germanium from a single source in an atmosphere of tellurium vapour for different weight percentages of germanium. It has been found that SnTe:Ge films with germanium content around 0.8 weight percent have got maximum mobility ($\sim$1150 $cm^2V^{-1}s^{-1}$ at room temperature) and minimum carrier concentration ($\sim$3 x 10^{19} cm^{-3} at room temperature). The reported values of room temperature mobility for undoped epitaxial SnTe films are below 500 $cm^2V^{-1}s^{-1}$. The maximum reported room temperature mobility for polycrystalline SnTe ingots is 400 $cm^2V^{-1}s^{-1}$ and is obtained by copper doping /3/. Thus it can be seen that by germanium doping, high mobility SnTe films can be obtained, the optimum value of germanium being around 0.8 weight percentage.

REFERENCES

1. H.T. Savage, B. Houston and J.R. Burke, Jr.
   Phys. Rev. B, 6 (1972) 2292.

2. A.L. Dawar, P.C. Mathur, A.O. Mohammed and O.P. Taneja,
   Thin Solid Films, 82 (1981) 273.

3. R.F. Brebrick, J. Phys. Chem. Solids, 24 (1963) 27.

4. G.S. Bushmarina, B.F. Grushinov, I.A. Drabkin, E. Ya.
   Lev, and V.M. Yuneev, Sov. Phys. Semicond., 18 (1984)
   1374.

5. E.I. Rogacheva, N.I. Dzyubenko, S.A. Laptev,
   V.M. Kosevich and A.G. Obedkov, Inorg. Mater. (USA),
   19 (1983) 515.

6. A.L. Dawar, A.O. Mohammed, P. Kumar, O.P. Taneja and
   P.C. Mathur, Phys. Stat. Solidi (a), 72 (1982) K83.

7. N.I. Dzyubenko, E.I. Rogachev, V.M.. Koserich, S.A.Laptev,
   and A.V. Arinkin, Inorg. Mater. (USA), 19 (1983) 1289.

8. R.S. Allgaier and B. Houstan, Phys. Rev. B, 5 (1972) 2186.

9. R.S. Allgaier, J. Appl. Phys. 32 (1961) 2185.

10. R.S. Allgaier and B.B. Houstan, Jr., J. Appl. Phys.
    37 (1966) 302.

CHAPTER IX

IR DETECTOR TEST SETUP

9.1. INTRODUCTION

The work reported in the earlier chapters of the thesis has been on the preparation and characterisation of PbS and SnTe thin films. These two, in the family of IV-VI compounds, have found applications as evaporated, polycrystalline film IR detectors and some preliminary work in IR detection such as the fabrication of a setup for the testing of IR detectors is reported in this chapter. The characteristics of an IR detector and how these quantities are measured are spelled out first and then the details of the fabrication are described.

Using IR detectors, the quantities of energy to be detected are usually very small either because the source is at a considerable distance and subtends a small solid angle, or because the band-width of spectrum being observed is very narrow, as in many spectroscopic applications. A detector converts an incident radiation signal into an electrical output. This output is made up of two parts, the response of the detector to the incident

radiation (called the signal) and random fluctuations known as 'noise'.

An IR detector is characterised mainly by its black body parameters, noise, and spectral response /1,2/. Blackbody parameters include blackbody response and blackbody detectivity. Blackbody response indicate how much voltage or current is obtained as output power for a given input blackbody spectral power in watts to the detector. The noise equivalent power (NEP)of a detector is the incident power required to produce a signal output equal to the rms noise output. Blackbody D* is a quantity which is the reciprocal of NEP normalized for detector area and noise bandwidth. This quantity allows comparison of different detectors having the same spectral response but different active areas and also measured at different noise bandwidths.

Measurement of rms noise power as a function of noise frequency is important as noise determines how small an incident power can be detected. Spectral response measurements indicate the wavelength region in which the detector has measurable response. This measurement is necessary when the detector should have specified response within a particular wavelength range.

9.2. BLACKBODY RESPONSE MEASUREMENT

Fig.9.1 shows the block-diagram of the setup for the measurement of blackbody response of the detector under test. This setup include a blackbody, a light chopper (the fabrication of which is described in 9.4), a specimen cell, a lock-in-amplifier etc. The specimen cell is a whole metallic cell provided with a cold finger to hold the IR detectors and has also been fabricated (fig.9.2) as part of this setup. This cell can be evacuated to 10^{-2} torr and the specimen can be cooled to liquid nitrogen temperature. The detector is properly biased using a current source and it is irradiated with a known amount of radiation from a 500K blackbody. The detector output signal is measured as a function of bias current and chopping frequency. Noise is also measured as a function of frequency (at constant band width) for different bias currents. These measurements, together with active area measurement, can be used to calculate responsivity and D* as a function of chopping frequency and bias current.

System Noise Measurement

The detector is replaced by a dummy low noise resistance of approximately the same value as that of the detector. The temperature of this low noise
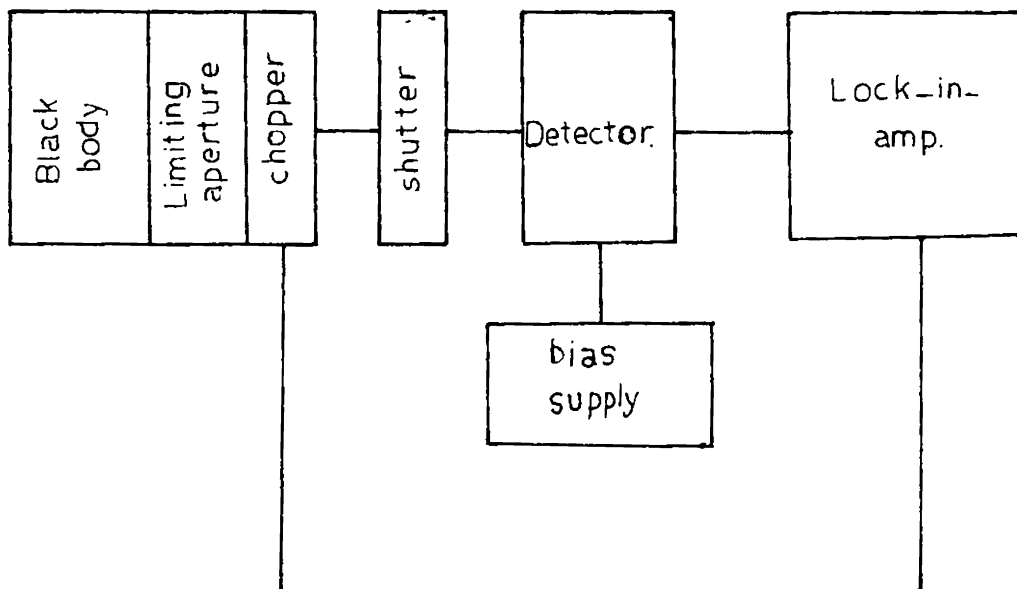
Fig.9.1 : Block diagram of the setup for the
measurement of blackbody response.
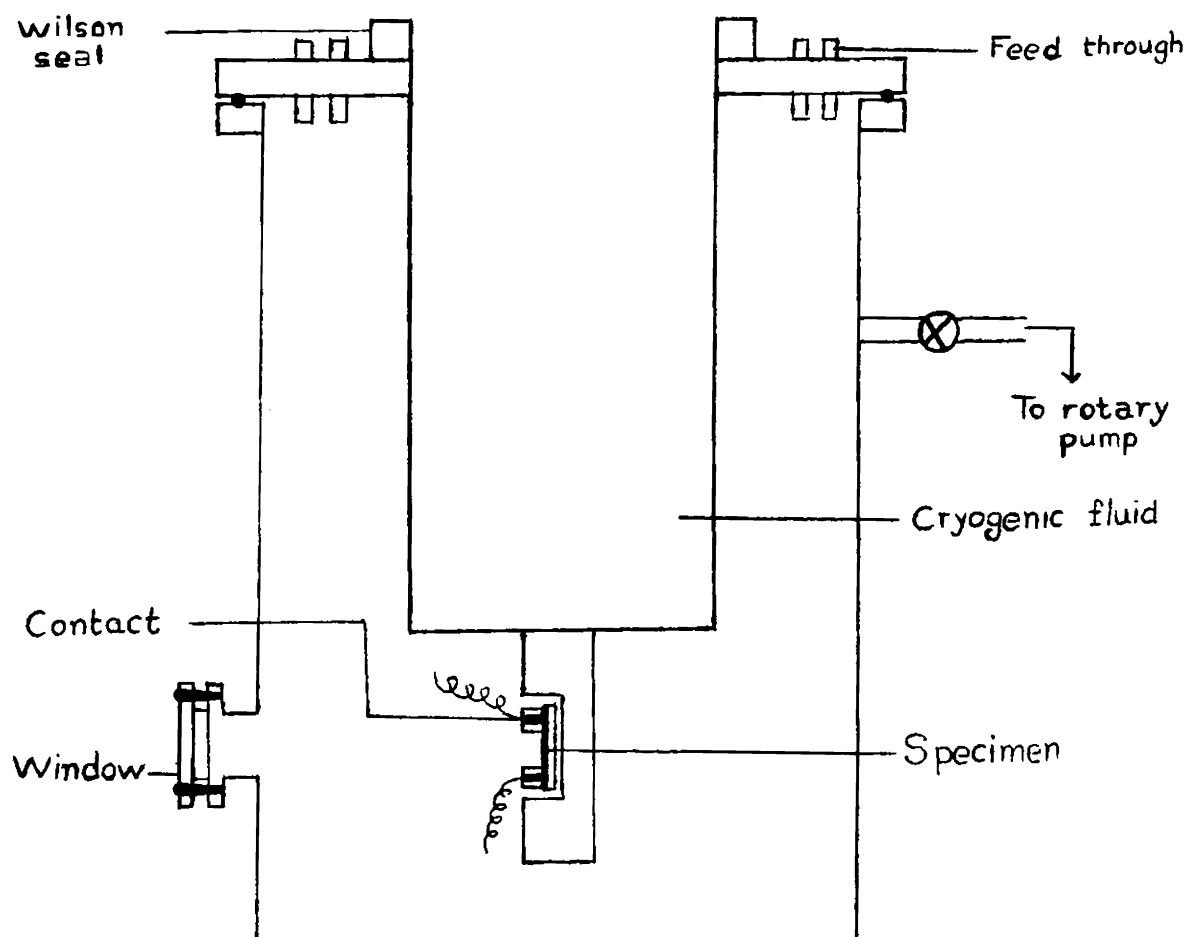
Fig.9.2 : Metallic cell to hold the IR detector.

resistance is maintained such that the thermal noise generated in the resistor is small compared to the noise generated in the amplifier. The rms noise voltage $V_{N_a}(f)$ is measured as a function of frequency.

System Gain Measurement

The system gain as a function of frequency $g(f)$ is then measured, with the dummy resistance in place of the detector, by injecting a signal of known amplitude from an audio oscillator.

Blackbody Measurement

500K blackbody radiation is allowed to fall on the detector and the detector output signal $V_s(f,b)$ is recorded as a function of chopping frequency (f) and bias current (I_B). Then the blackbody radiation is removed by closing the shutter and detector noise $V_{N_o}(b)$ as a function of frequency (at constant band width) for the same bias current as used in the blackbody measurement, is recorded.

Calculation of Responsivity

The responsivity is the ratio of output to the radiant input. The blackbody responsivity is given by

$$R(I_B, f, T) = \frac{V_s}{\phi_{BB}} \quad \text{volts Watt}^{-1} \qquad (9.2.1)$$

where V_s is the detector output in volts and ϕ_{BB} is the

incident blackbody power in watts.

Calculation of D*

The noise equivalent power (NEP) is the incident power required to produce a signal output equal to the rms noise output. It may be shown that

$$NEP = \frac{V_n}{R} \qquad (9.2.2)$$

where V_n is the rms noise voltage.

The detectivity D of a detector is the reciprocal of NEP. D* normalise the detector area and noise band width.

$$D^* = D \ (A_d \ \Delta f)^{1/2} = \frac{(A_d \ \Delta f)^{1/2}}{NEP} = \frac{R(A_d \ \Delta f)^{1/2}}{V_n} \qquad (9.2.3)$$

where A_d is the active detector area and Δf is the noise bandwidth.

9.3. SPECTRAL RESPONSE MEASUREMENT

Fig.9.3 shows the block-diagram of the setup to measure the spectral response of the detector. This includes a source, chopper, double monochromator, radiometer, a Lock-in-amplifier etc. The detector is illuminated with monochromatic radiations. The centre
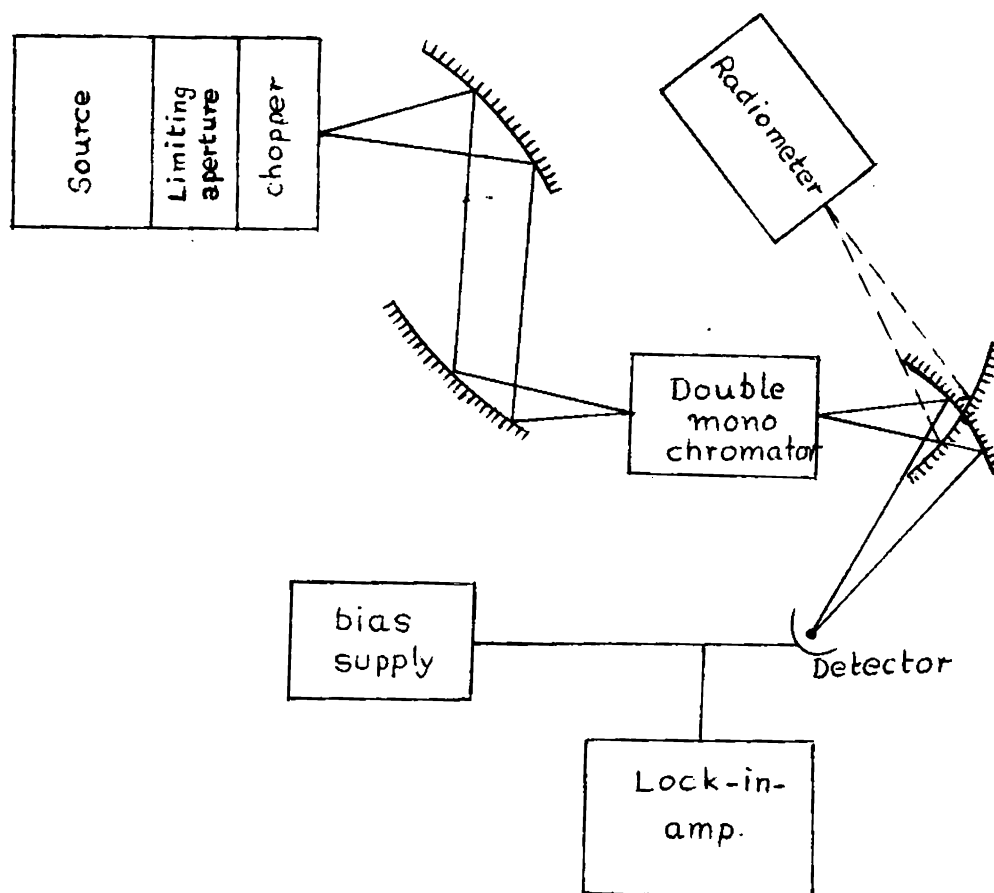
Fig.9.3 : Block diagram of the setup for the measurement
spectral response of the detector.

wavelength of the monochromator is varied over the
wavelength range of interest and the detector output
voltage is compared with the value obtained by the
radiometer.

9.4. A VARIABLE SPEED LIGHT CHOPPER FOR USE IN THE IR DETECTOR TEST SETUP

For use in the test setup described above a
simple mechanical light chopper has been designed and
fabricated. Although these may appear to be relatively
simple device, there are many problems associated with
them. Maintaining a constant frequency and eliminating
the transient noise spikes generated by motor speed
controllers are only two of the problems. Variable
speed motors have a speed stability of only about $\pm$ 1%
and in many applications this may not be sufficient,
especially when photon detectors are being tested. Many
motor speed controllers use silicon controlled rectifiers
as regulators which may generate all kinds of transients.
The simple light chopper described, below has been designed
to have a chopping frequency ranging from 10 to 2000 Hz,
using two chopping blades. The circuit is simple,
reliable and inexpensive. A small DC motor whose speed
can be varied ten fold is employed and its speed is main-
tained constant by feedback control.

Design of the chopping blade

In optical experiments the limiting apperture at the source is always circular. When a circular beam is chopped with a series of straight sided slots cut in the rim of a disc it gives excellent approximation to a square wave, provided that θ_b/θ_t is approximately equal to zero (fig.9.4) where θ_b and θ_t are the angles subtended by the light beam and a tooth-slot pair, respectively.

The maximum number of teeth in a chopper blade that will have an RMS conversion factor differing by less than 1% from that of a true square wave chopper is given by

$$ n = \frac{0.251 \ (D_c - D_b)}{D_b} \qquad (9.4.1) $$

where n is the number of teeth, D_c is the diameter of the chopper wheel and D_b is the beam width.

Description of the circuit

The speed of the motor is regulated by generating a square wave reference signal with a photodiode (SI 100, BEL, India) looking through the chopper blade, and sending this reference signal into a frequency to voltage converter to control the current through the motor.
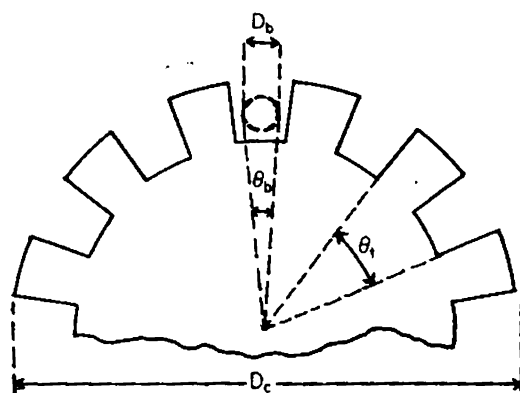
Fig.9.4 : Geometry of the square wave chopper.
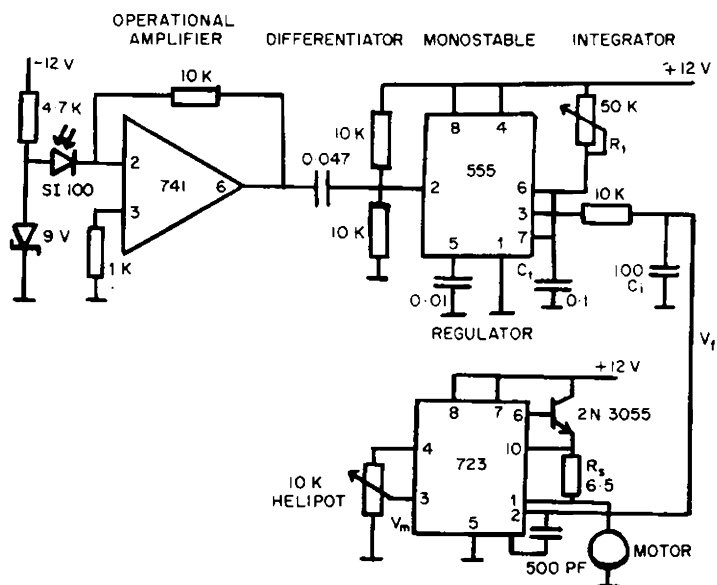
Fig.9.5 : Schematic diagram of speed control.

The photodiode is connected to an operational amplifier
and its output is differentiated and the negative going
pulses are used to trigger a monostable multivibrator.
The monostable pulses are integrated by feeding them into
a RC integrator. Thus the chopper frequency is converted
into a proportional analogue voltage.

The value of the timing capacitor and resistor
are selected such that for a given chopper blade when
the motor is running at its maximum rated speed, the RC
integrator develops 7V, which is the typical Zener
reference voltage of the 723 voltage regulator. The
feedback voltage is compared to the reference voltage
applied and depending on the speed, the motor current is
either increased or decreased to make it equal to the set
point value.

Analysis of the circuit

Let V_r be the reference voltage and V_f the
feedback voltage. The voltage applied to the motor is

$$V_s = (V_r - V_f) A \qquad\qquad (9.4.2)$$

where A is the amplification of the voltage regulator-
transistor combination. The feedback voltage V_f is
given by

$$V_f = 0.693 \; C_t R_t Vf \; = kf \qquad\qquad (9.4.3)$$

where C_t is the value of the timing capacitor, R_t is the value of the timing resistor, V is the pulse height of the monostable pulses and f is the frequency of the monostable pulses.

For a DC motor we have, neglecting the brush resistances

$$V_s = V_{back} + I \ (R_m + R_s) \qquad (9.4.4)$$

where V_{back} is the back EMF of the motor, R_m is the motor winding resistance and R_s is any series resistance associated with the motor.

The back EMF of the motor is given by

$$V_{back} = Kf \qquad (9.4.5)$$

where K is a constant which includes the magnetic flux density at the air gap, number of teeth in the chopper blade, etc.

$$Ak \ (f_r - f) - Kf = I \ (R_m + R_s) \qquad (9.4.6)$$

where f_r is the frequency corresponding to the reference voltage V_r and f is the actual chopping frequency.

Solving this, the steady state error is

$$E_s = f_r - f = \frac{Kf_r}{kA} + \frac{I(R_m + R_s)}{K + kA} \qquad (9.4.7)$$

Since $kA \gg Kf_r$, the first term in the right
hand side of (9.4.7) may be neglected giving,

$$E_s = \frac{I (R_m + R_s)}{K + kA}$$

(9.4.8)

This equation determines the steady state error
and since the voltage regulator-transistor combination
has an amplification factor of 10^4, it can be seen that
the steady error is a small quantity.

Performance of the chopper

A resistance R_s was put in series with the
motor and was used as a current sense for the 723 voltage
regulator to limit the maximum current through the motor
to what is necessary to just start the motor under load
conditions. This eliminated overshooting of the motor
for small errors. The effect of this limiting resistance
R_s on the accuracy of speed regulation is shown in
fig. 9.6. It can be seen that a proper selection of R_s
will give very high accuracies in speed regulation.
The chopper blade was not directly driven by the motor
but for increased transient stability it was driven
through a flywheel. This greatly reduced transient
instabilities associated with both line voltage trans-
ients and motor current variations.
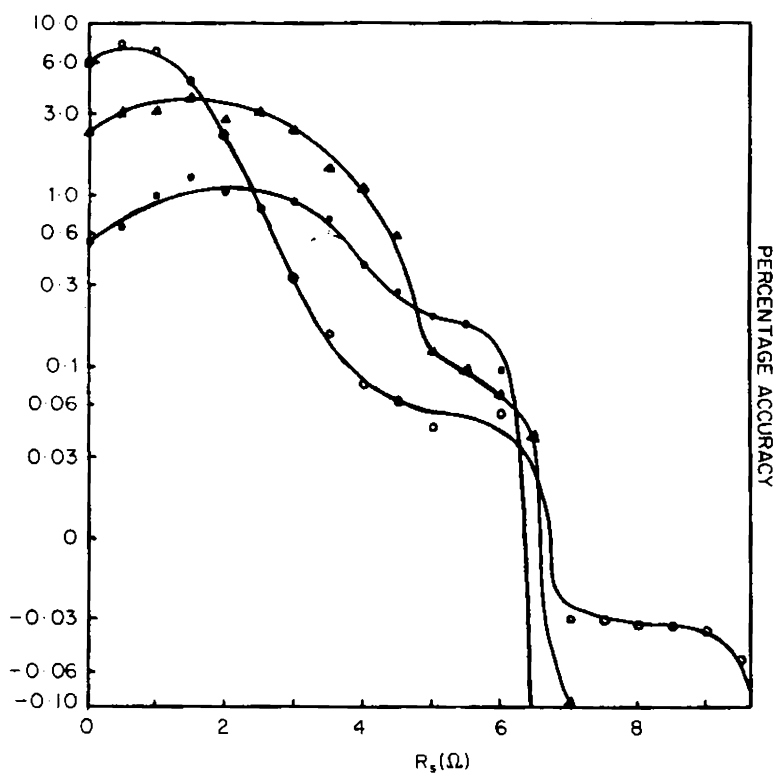
Fig.9.6 : Effect of the sensing resistance R_s, on percentage accuracy O-500Hz, Δ -1000 Hz, and ● -1500 Hz.

The regulation of the chopping speed was
excellent and was tested with a universal electronic
counter with 0.1 Hz resolution. After a warm up period
of half an hour it gave a frequency stability better
than 0.1%. This is better than commercially available
choppers. Drift due to temperature variation can be
made negligible by using a high stability resistor
and capacitor in the timing circuit.

REFERENCES

1. R.K. Willardson and A.C. Beer (eds.), Semiconductors and Semimetals, Vol.12 (Academic Press, New York, 1977).

2. R.H. Kingstan, Detection of Optical and Infrared radiations, Springer series in Optical Sciences, Vol.10, D.L. Mac Adam (ed.), (Springer-Verlag, Berlin, 1978).